NASA CONTRACTOR REPORT

NASA CR-1015

NASA CR-1015

GUIDANCE, FLIGHT MECHANICS AND TRAJECTORY OPTIMIZATION

Volume XVI - Mission Constraints and Trajectory Interfaces

by R. L. Robertson

Prepared by
NORTH AMERICAN AVIATION, INC.
Downey, Calif.
for George C. Marshall Space Flight Center

NATIONAL AERONAUTICS AND SPACE ADMINISTRATION • WASHINGTON, D. C. • APRIL 1968

NASA CR-1015

GUIDANCE, FLIGHT MECHANICS AND TRAJECTORY OPTIMIZATION

Volume XVI - Mission Constraints and Trajectory Interfaces

By R. L. Robertson

Distribution of this report is provided in the interest of information exchange. Responsibility for the contents resides in the author or organization that prepared it.

Issued by Originator as Report No. SID 66-1678-8

Prepared under Contract No. NAS 8-11495 by
NORTH AMERICAN AVIATION, INC.
Downey, Calif.

for George C. Marshall Space Flight Center

NATIONAL AERONAUTICS AND SPACE ADMINISTRATION

FOREWORD

This report was prepared under contract NAS 8-11495 and is one of a series intended to illustrate analytical methods used in the fields of Guidance, Flight Mechanics, and Trajectory Optimization. Derivations, mechanizations and recommended procedures are given. Below is a complete list of the reports in the series.

Volume I	Coordinate Systems and Time Measure
Volume II	Observation Theory and Sensors
Volume III	The Two Body Problem
Volume IV	The Calculus of Variations and Modern Applications
Volume V	State Determination and/or Estimation
Volume VI	The N-Body Problem and Special Perturbation Techniques
Volume VII	The Pontryagin Maximum Principle
Volume VIII	Boost Guidance Equations
Volume IX	General Perturbations Theory
Volume X	Dynamic Programming
Volume XI	Guidance Equations for Orbital Operations
Volume XII	Relative Motion, Guidance Equations for Terminal Rendezvous
Volume XIII	Numerical Optimization Methods
Volume XIV	Entry Guidance Equations
Volume XV	Application of Optimization Techniques
Volume XVI	Mission Constraints and Trajectory Interfaces
Volume XVII	Guidance System Performance Analysis

The work was conducted under the direction of C. D. Baker, J. W. Winch, and D. P. Chandler, Aero-Astro Dynamics Laboratory, George C. Marshall Space Flight Center. The North American program was conducted under the direction of H. A. McCarty and G. E. Townsend.

TABLE OF CONTENTS

SECTION PAGE

1.0 STATEMENT OF THE PROBLEM

The subject of this monograph is mission constraints and trajectory interfaces which result from imposing the physical limitations on a trajectory or earth orbit. The constraints considered in this document are those which reflect directly or indirectly on the characteristics of the various trajectories which constitute the mission. Each constraint limits, to a certain degree, the choice of the trajectory profile for a given mission phase. Mission constraints affecting trajectory profiles can be thought of as falling into two categories, those which are necessary for accomplishment of mission objectives and those which are due to crew or equipment limitations and capabilities. In the latter category would fall those necessary for crew safety or payload survival.

The type of mission constraints required for the accomplishment of mission objectives may be orbital lifetime, earth trace, surveillance patterns, tracking coverage, stationkeeping, lighting, launch window, launch site, and communications. Mission constraints imposed by crew and equipment limitations may be aerodynamic loading, acceleration/deceleration levels, tracking, recovery sites, lighting, radiation, aerodynamic heating and mission duration. As can be seen, many constraints overlap and conflict with each other in their interface with trajectory capabilities.

Trajectories are constrained first and foremost by physical laws governing their motion. Spatial orbit motion for example is described basically by two-body mechanics (except for small perturbations). Any deviation of the vehicle's path to accomplish a particular mission objective must be accounted for in the selection of the orbit or be accomplished by an expenditure of energy. Similarly, boost and entry trajectories are constrained to paths dictated by the summation of forces acting on the vehicle, whether they be thrust, aerodyanmic or some other. The set of constraints specified for any mission must be compatible with the physics of the trajectories constituting the mission.

It is the purpose of this monograph to formulate and examine the more important mission constraints and their relationship to trajectories in order to facilitate the synthesis of a realistic mission. The missions considered here will be earth orbital but will include parking orbits for lunar or planetary missions. The missions will be divided into the five trajectory phases which comprise most earth orbital missions. The phases are: launch, rendezvous, spatial, deorbit, and entry trajectories. The discussions will be limited primarily to first order detail except where it is necessary for understanding of the problem to include higher order effects. That is, the earth will be assumed either spherical or oblate to the first order in most cases. Maneuvers, except during boost, will generally be assumed to be impulsive. The atmospheric model will be assumed to be defined by an exponential density gradient. These assumptions are realistic during the preliminary mission design phase where extensive tradeoff analysis is necessary to integrate trajectory profiles and mission constraints but must be refined during the detailed design of a particular mission.

The constraints will first be discussed individually, in some detail, without regard to overlap areas. Then, the methodology for finding the best trajectory considering all mission constraints will be analyzed.

2.0 STATE-OF-THE-ART

2.1 INTRODUCTION

This section presents the formulation of various mission constraints and the relationship of the constraints to the various trajectory phases. The formulations are not intended to precisely define all of the relationships involved for any given constraint. The intent is to provide sufficient detail pertaining to the relationships which are necessary to evaluate mission constraint and trajectory interfaces. The discussions in this section attempt to identify the parameters which relate a mission constraint to a trajectory profile. Parametric data can be generated from the formulations in this section to aid in the synthesis of the best trajectory complying with a given set of mission constraints. Such analysis will, in many cases, identify mission constraints which are themselves incompatible.

Five trajectory phases which constitute most missions are discussed in this section. These are the launch, rendezvous, spatial, deorbit, and entry trajectories.

2.2 BOOST TRAJECTORIES

2.2.1 Introduction

Most of the major objectives of any orbital mission occur during the spatial phase since nearly all of the mission duration is occupied by the spatial phase. Obviously, however, without an efficient boost phase to insert the spacecraft into the desired orbit and the entry phase to return the payload safely to earth the mission could not be considered successful. The boost vehicle necessary to overcome the earth's gravitational field and pass through the atmosphere is usually a large sophisticated multi-stage vehicle whose performance is subjected to many constraints. Further, the launch and boost trajectory must satisfy constraints concerning launch window, range safety, and aerodynamic loading and achieve accurate orbital insertion conditions in a manner optimized to obtain maximum payload for minimum boost vehicle weight. The following sections will discuss and formulate these major constraints, present the equations of motion for the vehicle, and discuss the parameters of concern for evaluation of trajectory and mission interfaces.

2.2.2 Launch Window

The term "launch window" is broadly defined as the period of time during which, for a given mission, launch is possible from a particular launch site. A window may be a specific interval of time which is defined in terms of the day number or it may be a specific interval of time on each of several successive days, etc. Launch window considerations usually fall into three categories. In the first category the launch window is defined primarily by lighting and abort considerations as is generally the case for earth orbital missions for which no specific inertial orientation is required. The second category is more complex since it includes those missions for which specific inertial orientation of the orbit is required. Inertial orientation is a requirement for rendezvous missions but with an added launch window complication involving the target vehicle orbital position. The rendezvous problem including a rendezvous launch window is discussed in section 2.3. The requirement that a parking orbit contain a given inertially oriented vector comprises the third category. This is usually the case for lunar or planetary missions.

2.2.2.1 Missions Without Specific Inertial Orientation

Many types of missions (e.g., the Mercury flights, most Gemini flights, communication satellites, meterological satellites, surveillance satellites) are more concerned with orientation relative to the rotating earth than with inertial or spatial orientation. This is not to say that such missions are completely independent of orientation constraints since many of these missions require general spatial orientation for lighting, navigation or other purposes; however, the spatial orientation is not the primary concern. For missions in this category, primary constraints defining the launch window are that launch occur during daylight and that in the event of an abort during boost the vehicle reach the downrange emergency recovery site with enough daylight remaining to assure location and recovery. To evaluate the effect of these constraints on the launch window, the orientation of the orbit relative to the rotating earth is required.

The inclination (i) of the orbit plane to the earth's equator is a function of the launch azimuth and launch site latitude and is independent of the time of launch. From Figure 2-1 the inclination can be seen to be

$$i = \cos^{-1}(\cos \phi_L \sin \Sigma_L) \qquad (2.1)$$

where

ϕ_L = launch site latitude

Σ_L = launch azimuth

$\phi_L{}^\circ \leq i < 90^\circ$ for posigrade launches

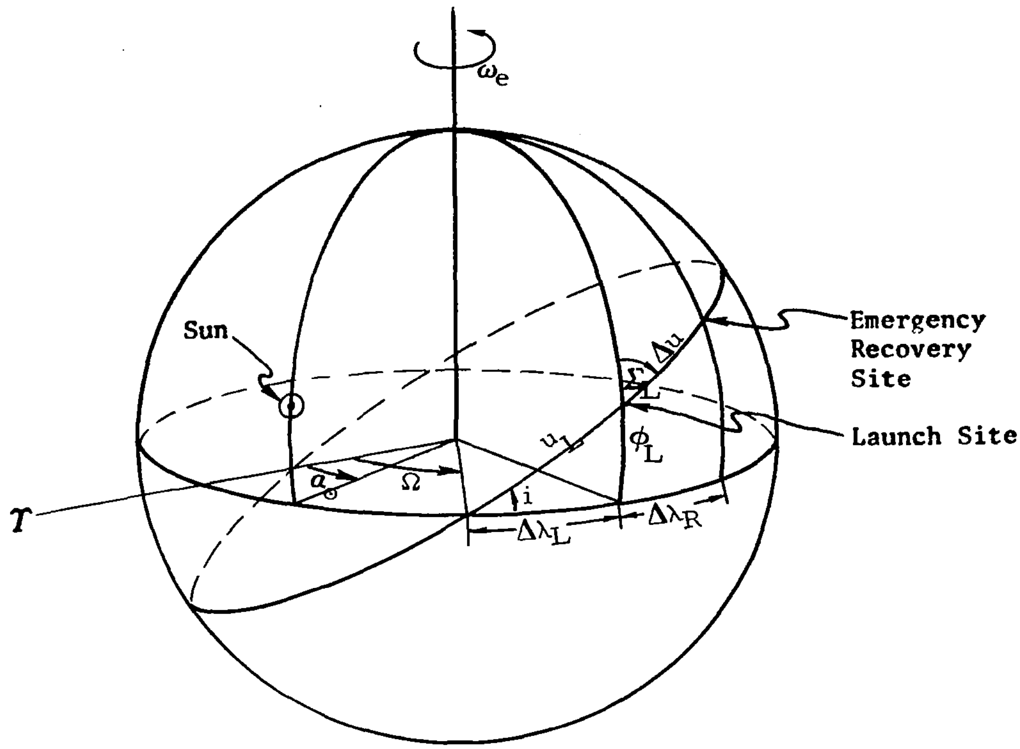

Figure 2-1

Similarly, the argument of latitude (u_L) of the launch site can be found from

$$u_L = \tan^{-1}\left(\frac{\tan \phi_L}{\cos \Sigma_L}\right) \tag{2.2}$$

where for launch sites in the northern hemisphere

$0 < u_L < 90°$ for northerly launches

$90 < u_L < 180°$ for southerly launches

and the projection ($\Delta\lambda_L$) of u_L on the earth's equator plane is

$$\begin{aligned} \sin \Delta\lambda_L &= \sin u_L \sin \Sigma_L \\ \cos \Delta\lambda_L &= \frac{\cos \Sigma_L}{\sin i} \\ \Delta\lambda_L &= \tan^{-1}\left(\frac{\sin \Delta\lambda_L}{\cos \Delta\lambda_L}\right) \end{aligned} \tag{2.3}$$

Thus, if the total range for an abort during boost and the subsequent entry trajectory range to impact in the emergency recovery site is given by Δu, the upper limit of the launch window can be evaluated. First, the projection ($\Delta\lambda_R$) of Δu on the earth's equator is obtained by (see Figure 2-1)

$$\Delta\lambda_R = \tan^{-1}[\cos i \tan(u_L + \Delta u)] - \Delta\lambda_L \tag{2.4}$$

where from northern hemisphere launch sites

$0 < \tan^{-1}[\cos i \tan(u_L + \Delta u)] < 180$ for northern hemisphere recovery sites

$180 < \tan^{-1}[\cos i \tan(u_L + \Delta u)] < 360$ for southern hemisphere recovery sites

Now, the Local Mean Time (LMT) at a particular point (e.g., the launch site) is defined as the hour angle of the fictitious mean sun plus 12 hours; that is,

$$LMT = HA_{\odot} + 12^h \tag{2.5}$$

where

$HA_{\odot}$ = angle measured along the equator clockwise from the local meridian to the fictitious mean sun's meridian (hour angle)

The LMT is, in turn, related to the Greenwich Mean Time (GMT) by

$$GMT = LMT + \frac{\lambda}{15\ deg/hr} \tag{2.6}$$

where

λ = the local longitude

Since the LMT of sunrise and sunset are available or can be easily determined from ephemeris data, the LMT is a convenient parameter for defining launch windows which depend on local lighting conditions.

To satisfy the constraint that launch occur during daylight the earliest time launch can occur is the LMT of sunrise at the launch site or

$$LMT_{L(MIN)} = LMT_{\text{sunrise at launch site}} \tag{2.7}$$

The latest time that launch can occur is determined by the constraint that N number of hours of daylight be available at the recovery site after impact to ensure location and recovery of the vehicle. This condition can be defined in terms of LMT at the recovery site by

$$LMT_{R(MAX)} = LMT_{\text{sunset at recovery site}} - N^{hrs} \tag{2.8}$$

or in terms of the LMT at the launch site

$$LMT_R = LMT_L + \frac{\Delta\lambda_R}{15 \text{ deg/hr}} \tag{2.9}$$

assuming negligible motion of the mean sun during the time from launch to emergency impact. Therefore, the latest time of launch which will satisfy recovery lighting constraints is

$$LMT_{L(MAX)} = LMT_{R(MAX)} - \frac{\Delta\lambda_R}{15 \text{ deg/hr}} \tag{2.10}$$

and the launch window is

$$LMT_{L(MIN)} \text{ to } LMT_{L(MAX)}$$

At this point, the inertial orientation as a function of the LMT_L can be defined by writing the expression for the ascending node as (see Figure 2-1)

$$\Omega = \alpha_{\odot} + 15 \text{ deg/hr } (LMT_L - 12^h) - \Delta\lambda_L \tag{2.11}$$

where

$\alpha_{\odot}$ = right ascension of the mean sun at the time of launch

2.2.2.2 Launch Into Specified Inertial Orientation

Many missions (e.g., earth orbital rendezvous missions) require launch and insertion into a specified inertial plane. However, launch and insertion into a given inertial plane without introducing a plane change requires a precise launch at one of the two times per day that the launch site is contained in the desired plane of motion (assuming the latitude of the launch site is less than the inclination of the desired orbit plane). This alternative cannot be surmounted in most missions because of the large amount of propellant required even for small plane changes at orbital velocities.

However, since it is impossible to launch precisely on time due to the finite burn time, a small amount of insertion delta-V must be allowed for plane change capability. This small plane change capability allows launch to be made within some launch window, the width of which is a function of the amount of delta-V reserved for plane changes. A complete development of the equations relating launch window width to plane change delta-V availability is given in the rendezvous section 2.3.2. The equations are developed in the rendezvous section because the launch of a shuttle vehicle into a direct ascent trajectory for rendezvous with a target in orbit represents one of the severest launch window constraints in mission design.

2.2.2.3 Orbit Plane Containing a Specific Inertial Vector

A parking orbit for an interplanetary mission is an example in which it is necessary for a specific inertially oriented vector to be contained in the orbit plane. The heliocentric interplanetary trajectory can be analyzed in terms of the earth's heliocentric velocity vector and the hyperbolic excess velocity vector ($\overline{V}_\infty$). The $\overline{V}_\infty$ vector, in turn, is defined by the spacecraft velocity and direction on the earth-centered hyperbola. The $\overline{V}_\infty$ is defined by its magnitude and direction in terms of right ascension (α_∞) and declination (δ_∞). For this type of mission, the spacecraft is inserted into a plane containing the required $\overline{V}_\infty$. At the proper point in the parking orbit, the spacecraft is inserted onto an escape hyperbola which will result in the desired $\overline{V}_\infty$ at the gravitational sphere of influence.

From a given launch site an orbit plane can be achieved at any time of day which will contain the desired $\overline{V}_\infty$ by proper selection of launch azimuth. Thus, the launch window is defined by the imposition of launch azimuth limits as may arise from range safety considerations (see section 2.2.3). The effect of launch azimuth limitations on the launch window is apparent from the following discussion. Assume the launch azimuth limitations are defined by

$\Sigma_{L\ MIN}$ = minimum allowable launch azimuth

$\Sigma_{L\ MAX}$ = maximum allowable launch azimuth

The earliest possible launch time is defined by Figure 2-2 (considering first a δ_∞ less than the latitude of the launch site [$\emptyset_L$]).

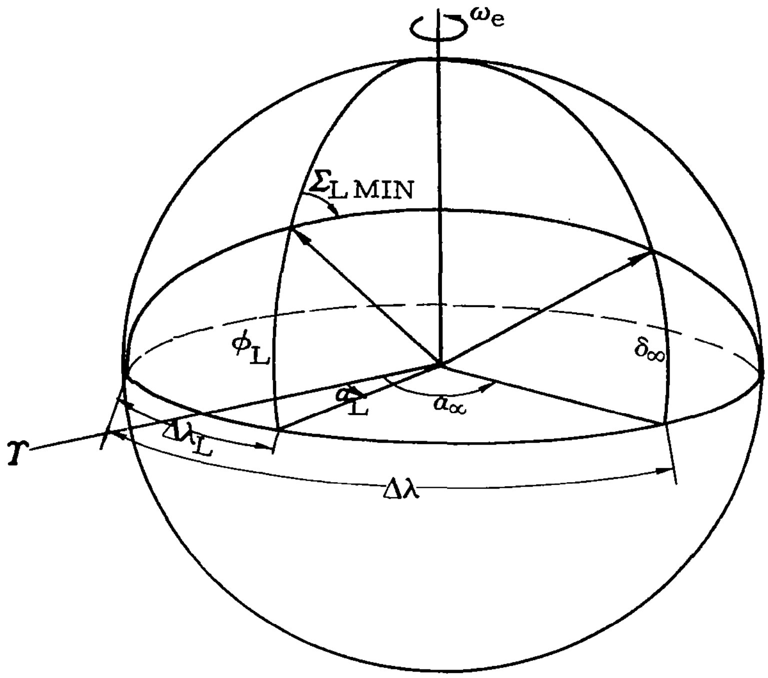

Figure 2-2

Now, the right ascension of the launch site (α_{LI}) for the earliest launch time can be determined from Figure 2-2 using spherical trigonometry. Further, the inclination of the orbit plane is seen to be

$$i = \cos^{-1}(\cos \phi_L \sin \Sigma_{L\ MIN}) \tag{2.12}$$

and the parameter $\Delta\lambda$ is

$$\Delta\lambda = \sin^{-1}\left(\frac{\tan \delta_\infty}{\tan i}\right) \tag{2.13}$$

where $90 < \Delta\lambda < 180$ for the early launch.

Similarly, the parameter $\Delta\lambda_L$ is

$$\sin \Delta\lambda_L = \left(\frac{\tan \phi_L}{\tan i}\right)$$

$$\cos \Delta\lambda_L = \frac{\cos \Sigma_{L\ MIN}}{\sin i} \tag{2.14}$$

$$\Delta\lambda_L = \tan^{-1}\left(\frac{\sin \Delta\lambda_L}{\cos \Delta\lambda_L}\right)$$

Thus,

$$\alpha_{LI} = \alpha_\infty - (\Delta\lambda - \Delta\lambda_L) \tag{2.15}$$

For a given launch site longitude (λ) and the right ascension of the fictitious mean sun ($\alpha_\odot$) on a particular day, the Greenwich Mean Time of launch corresponding to the computed launch site right ascension is

$$GMT_{LI} = \alpha_{LI} - \lambda - \alpha_\odot + 12^h \tag{2.16}$$

As the earth rotates through the launch window, the proper orbit plane orientation is achieved by increasing the launch azimuth as the earth rotates. The latest launch time allowable is defined by the maximum launch azimuth ($\Sigma_{L\ MAX}$) restriction. Following the procedure for the earliest launch,

$$i = \cos^{-1}(\cos \phi_L \sin \Sigma_{L\ MAX}) \tag{2.17}$$

$$\Delta\lambda = \sin^{-1}\left(\frac{\tan \delta_\infty}{\tan i}\right) \tag{2.18}$$

$$\sin \Delta\lambda_L = \frac{\tan \phi_L}{\tan i}$$

$$\cos \Delta\lambda_L = \frac{\cos \Sigma_{L\ MAX}}{\sin i} \tag{2.19}$$

$$\Delta\lambda_L = \tan^{-1}\left(\frac{\sin \Delta\lambda_L}{\cos \Delta\lambda_L}\right)$$

$$\alpha_{LF} = \alpha_\infty - (\Delta\lambda - \Delta\lambda_L) \tag{2.20}$$

and

$$GMT_{LF} = \alpha_{LF} - \lambda - \alpha_\odot + 12^h \tag{2.21}$$

The launch window is then the period during a given day from GMT_{LI} to GMT_{LF}. A slightly different effect occurs when the launch site latitude is less than the $\overline{V}_\infty$ declination, i.e.,

$$\phi_L < \delta_\infty$$

In this case, the initial launch time is defined as before by the minimum launch azimuth. However, instead of increasing the launch azimuth to the maximum as the earth rotates, the azimuth is increased to a maximum value less than 90° defined by the geometrical constraint

$$\Sigma_L = \sin^{-1}\left(\frac{\cos \delta_\infty}{\cos \phi_L}\right) \tag{2.22}$$

Then, the launch azimuth decreases with earth rotation back to $\Sigma_{L\ MIN}$ to define the launch window limit. The same basic equations with suitable quadrant adjustments are used to compute the window. Because of the geometrical symmetry of the problem, two launch periods per day exist and are easily obtained from the previous equations. A typical family of launch time curves as a function of launch azimuth is presented in Figure 2-3 for δ_∞ values less than, equal to, and greater than the launch site latitude ϕ_L.

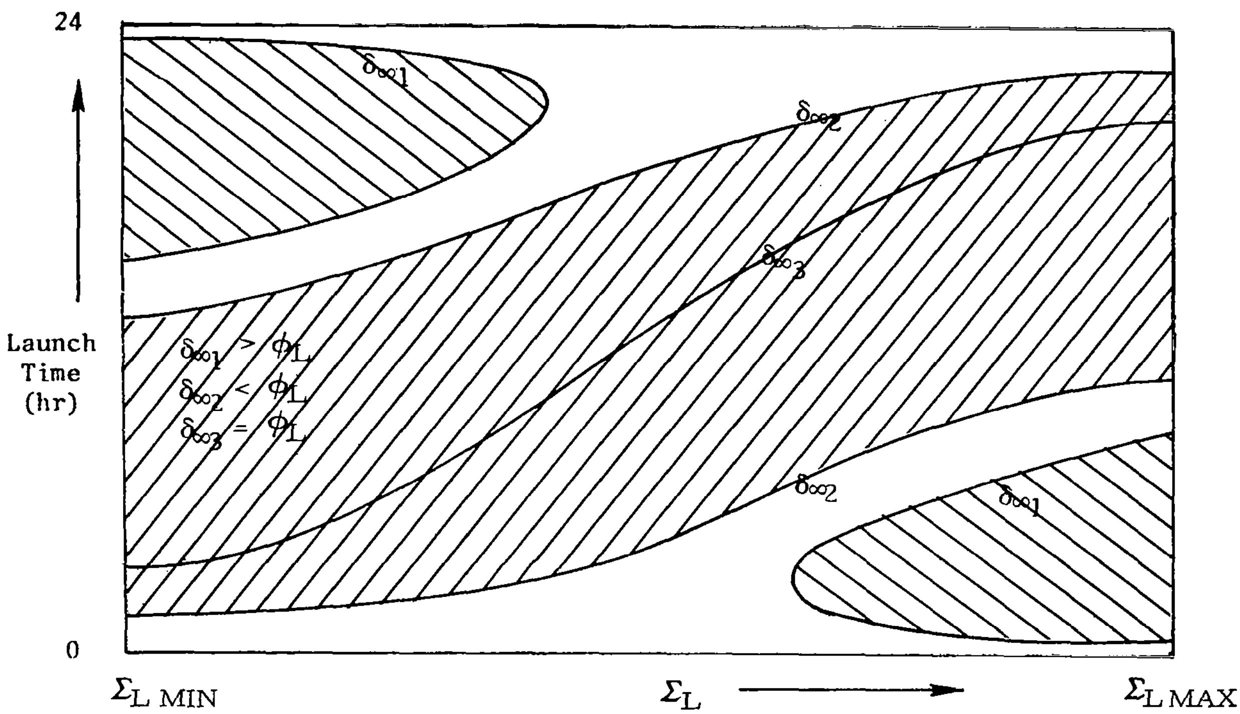

Figure 2-3

The launch window defined by launch azimuth restrictions may, of course, be further restricted by lighting considerations or other factors. All such considerations must be evaluated in order to finally determine the launch window.

2.2.3 Range Safety

The range safety interface with the boost trajectory is primarily concerned with the possibility of vehicle or booster stage impact on populated areas or on heavily traveled transportation routes. The usual approach to this problem is to impose launch azimuth limits for launches from a given site. For boost trajectories within these limits the probability of stage or vehicle impact in populated areas is very low. If, during boost, the vehicle drifts over the range safety limits for any reason the vehicle is usually destroyed.

Range safety limits on launch azimuth result in limitations on orbital inclinations which may be achieved for launches from a given site. Equation (2.1) in section 2.2.2.1 gives the relationship between inclination and launch azimuth, i.e.,

$$i = \cos^{-1}(\cos \phi_L \sin \Sigma_L)$$

where

ϕ_L = launch site latitude

Σ_L = launch azimuth

The launch azimuth nearest 90° defines the minimum inclination achievable from a given site (Σ_L = 90° defines absolute minimum inclination achievable from a given site) while the launch azimuth limit furthest from 90° defines the maximum possible inclination. If orbital inclinations outside of the range safety limits are desirable, it is necessary to insert into an intermediate orbit within range safety limits and make a subsequent plane change into the desired orbit. This plane change must be made at the node of the intermediate orbit and the desired orbit unless other elements of the intermediate orbit are to be altered. In this latter case, optimization of a two-impulse maneuver is required.

2.2.4 Ascent Trajectories

There are two general categories of boost trajectory profiles for orbital missions:

1. Powered ascent plus coasting

2. Direct ascent (continuous burn)

The powered ascent plus coasting technique is basically a launch similar to a short or medium range ballistic missile. Following the main powered ascent, the vehicle coasts along a free flight elliptical path to apogee where a short impulse is applied to provide orbital velocity. A special version of this technique which is used for high altitude orbit insertion involves burnout at perigee of the coasting ellipse, with a subsequent Hohmann transfer to apogee where circularization occurs.

The direct ascent without coasting category consists of a continuous burn (except during staging) with guidance from launch to the insertion conditions at which time the thrusting is terminated. Generally, the vehicle is launched vertically and after a few seconds is pitched in the direction of the preselected azimuth. The tilting is accomplished by the application of a programmed thrust attitude. Then, when the aerodynamic forces are small, a thrust vector program can be applied to obtain the insertion conditions with minimum cost (fuel, time, etc.).

The ascent trajectory and its flight parameters for each category are obtained from numerical integration of the equations of motion, with respect to time, from launch to the insertion point. The detailed trajectory shaping, within each category, is a complex subject and requires advanced numerical techniques for solution. Techniques used in trajectory shaping are the subject of other reports in this series (References 24, 27, 28, 29). Such trajectory shaping techniques are employed for specific vehicles with specific mission requirements. However, to aid in the understanding of the trajectory relationships involved in boost and insertion into earth orbits, the equations of motion for the ascent trajectory will be discussed in the next section.

2.2.4.1 Equations of Motion

The equations of motion can be written directly from Newtonian Mechanics by equating the product of the mass and acceleration and the sum of all of the forces acting on the vehicle, i.e.,

$$m \dot{\overline{V}} = \Sigma \overline{F} \tag{2.23}$$

Evaluation of all of the forces acting on the vehicle and the definition of a suitable coordinate system will require considerable expansion, however.

The major forces acting on the vehicle are thrust, aerodynamic, gravitational, coriolis and centrifugal. (These latter forces are fictitious and result from the fact that the equations of motion will be written in a rotating coordinate system.) The first of these forces, the thrust provided by a rocket, may be written as

$$F = \dot{m}\, v_e + A_e(p_e - p) \tag{2.24}$$

or

$$F = F_o + A_e(p_e - p)$$

where

F = thrust
$\dot{m}$ = mass flow rate of propellant
v_e = velocity of nozzle exit gases
A_e = nozzle exhaust area
p_e = pressure of nozzle exhaust gases
p = atmospheric pressure
F_o = initial or design value of thrust

If the thrust is integrated over the total burning time, the total impulse is obtained. Then, the impulse provided per pound of propellant or the thrust per pound of propellant burned per second [the specific impulse (I_{sp})] may be written as

$$I_{sp} = \frac{I_T}{W_P} \tag{2.25}$$

or

$$I_{sp} = \frac{F}{\dot{W}}$$

where

I_{sp} = specific impulse

I_T = total impulse

W_P = total propellant burned

$\dot{W}$ = propellant flow rate

The specific impulse is useful in computing the ideal velocity (neglecting gravitational, drag, and other losses) which may be attained from an impulse. This velocity gain is the familiar

$$\Delta V_I = I_{sp}\, g\, \ell n\, u_V \tag{2.26}$$

where

ΔV_I = ideal velocity gain

g = acceleration of gravity

u_V = propellant mass ratio

$= \dfrac{\text{vehicle weight + initial propellant weight}}{\text{vehicle weight + propellant weight after burn}}$

Aerodynamic forces during the early phases of boost are very significant. These aerodynamic forces are dependent on the vehicle shape, the atmospheric density, the air velocity relative to the vehicle, and the reference area of the vehicle. The aerodynamic forces are usually expressed in terms of the dynamic pressure (q) which is defined as

$$q = \frac{1}{2} \rho v^2 \tag{2.27}$$

where

ρ = atmospheric mass density

v = vehicle velocity relative to the wind

The aerodynamic force parallel to the relative velocity vector is defined as the drag force (D), while that which is perpendicular to the relative velocity vector is defined as the lift force (L). (If these forces are expressed in body coordinates, parallel and perpendicular to the vehicle axes, the resultant forces are the axial force and the normal force, respectively.) The drag and lift force can be written as a function of the dynamic pressure as

$$\begin{aligned} D &= q\, A_m\, C_D \\ L &= q\, A_m\, C_L = q\, A_m\, C_L'\, \alpha \end{aligned} \tag{2.28}$$

and the axial (X) and normal (F) force expressions are

$$\begin{aligned} X &= q\, A_m\, C_X \\ N &= q\, A_m\, C_N = q\, A_m\, C_N'\, \alpha \end{aligned} \tag{2.29}$$

where

A_m = vehicle reference area

C_D = drag coefficient

C_L = lift coefficient

C_L' = derivative of lift coefficient with respect to angle of attack

α = angle of attack

C_X = axial force coefficient

C_N = normal force coefficient

C_N' = derivative of normal force coefficient with respect to angle of attack

The weight of the vehicle is the gravitational force exerted on the vehicle by the earth. Since propellant is being consumed during boost, weight decreases as a function of burn time according to

$$W = W_o - \dot{W}(t - t_o) \tag{2.30}$$

The vehicle mass is given by a similar equation

$$m = m_o - \dot{m}(t - t_o) \tag{2.31}$$

where

W_o = initial vehicle weight

$\dot{W}$ = propellant flow rate

t = time

t_o = initial time

m_o = initial mass

$\dot{m}$ = propellant mass flow rate (constant)

In addition to weight variation due to burning, the vehicle weight is also a function of altitude according to Newton's law of gravitation

$$W = m\ g = \frac{m\ \mu}{r^2} \tag{2.32}$$

where

μ = GM, the gravitational constant for the earth

r = vehicle radius

As mentioned before, coriolis and centrifugal forces are fictitious forces resulting when the equations of motion are written with reference to a rotating coordinate system. These forces may be expressed in vector notation by

coriolis force

$$\overline{C} = -\ 2m\ \overline{\omega} \times \overline{V} \tag{2.33}$$

centrifugal force

$$\overline{CF} = - m \, \overline{\omega} \times (\overline{\omega} \times \overline{r}) \tag{2.34}$$

where

$\overline{\omega}$ = rotational velocity vector of earth or coordinate system

$\overline{r}$ = radius vector

$\overline{V}$ = velocity vector

m = vehicle mass

Various perturbative forces due to thrust misalignment, unsymmetrical aerodynamic shape, earth oblateness, gravitational forces due to the moon and sun, etc., are relatively small and will not be considered in this section.

Writing the equations in vector notation using the forces acting on the vehicle discussed above, the following expression is obtained.

$$m \, \dot{\overline{V}} = \overline{F} + \overline{D} + \overline{L} + \overline{W} - 2 \, m \, \overline{\omega} \times \overline{V} - m \, \overline{\omega} \times (\overline{\omega} \times \overline{r}) \tag{2.35}$$

Figure 2-4 defines the major forces acting on the vehicle.

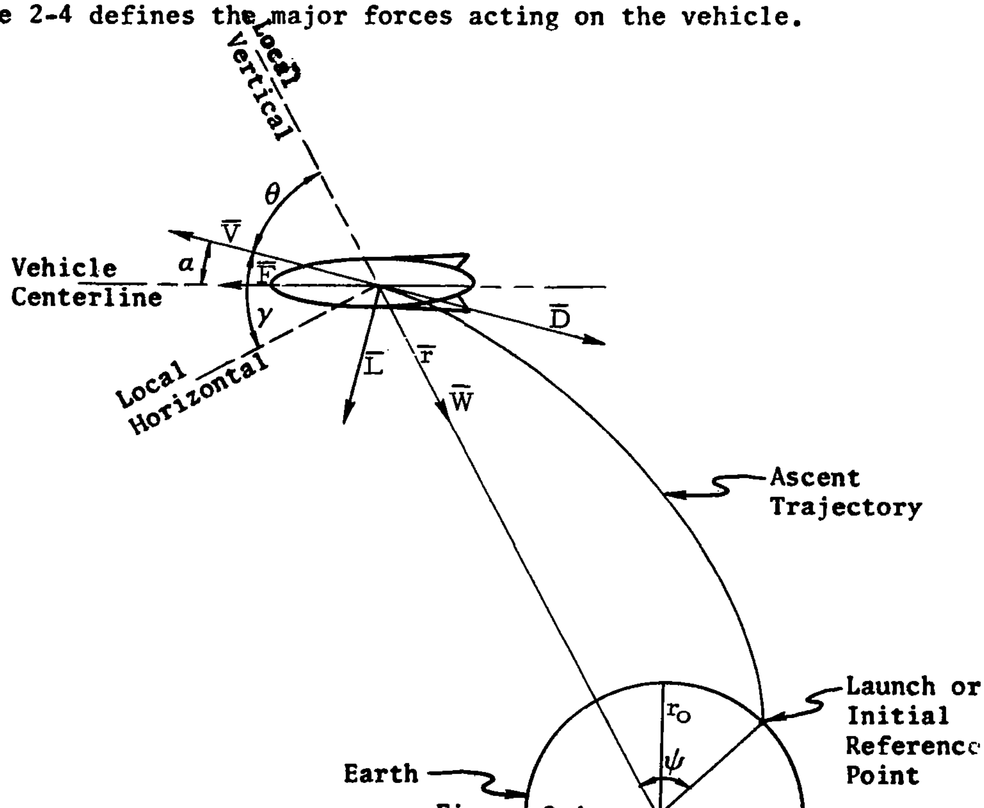

Figure 2-4

To solve equation (2.35), it must be expressed in terms of a convenient coordinate system. The equations of motion can be written in several different coordinate systems with various degrees of complexity; however, a local coordinate system in the tangential and normal flight directions is useful for simple trajectory equations in two dimensions. Since this system is useful in flight performance calculations and for vehicle design, it will be used in this section to illustrate the relationships and parameters involved in ascent trajectories.

The equations of motion in this system are written in two degrees of freedom with the summation of forces given with respect to the tangential direction, or vehicle velocity vector direction, and the normal direction, or perpendicular to the velocity vector. During the ascent through the heavy atmospheric layers a stationary earth is assumed. The contribution due to the rotation of the earth is made after some point in the upper atmosphere where the aerodynamic forces become negligible in their affect on the trajectory. The rotating earth correction will be covered after the discussion of the differential equations of motion in tangential and normal coordinates.

The equations of motion in the tangential and normal system are written

$$m\,\dot{v} = F \cos\alpha - D - W \cos\theta$$

$$m\,v\,\dot{\theta} = F \sin\alpha + L + W \sin\theta - m\,v\,\dot{\psi} \qquad (2.36)$$

The angle θ, which has not previously been defined, is shown in Figure 2-4 to be the flight path angle from the local vertical to the velocity vector. The angle ψ is the angle between the launch or initial radius and the vehicle radius at time t. The term in equation (2.36) containing the time derivative of ψ is the fictitious centrifugal force added to compensate for the curvature of the spherical earth. The time derivative of ψ can be determined from

$$d\psi = \frac{v\,dt\,\sin\theta}{r} \qquad (2.37)$$

as

$$\dot{\psi} = \frac{v\,\sin\theta}{r} \qquad (2.38)$$

Substituting (2.38) into (2.36) and rewriting, the equations of motion become

$$\dot{v} = \frac{F \cos \alpha}{m} - \frac{D}{m} - g \cos \theta \tag{2.39}$$

$$\dot{\theta} = \frac{F \sin \alpha}{m\ v} + \frac{L}{m\ v} + \left(\frac{g}{v} - \frac{v}{r}\right)\sin \theta \tag{2.40}$$

Integration of equations (2.39) and (2.40) gives the flight path angle and velocity as functions of time

$$v = \int_0^t \dot{v}\ dt \tag{2.41}$$

$$\theta = \int_0^t \dot{\theta}\ dt \tag{2.42}$$

The altitude and ground range are then obtained via a second integration

$$h = \int_0^t v \cos \theta\ dt \tag{2.43}$$

$$s = r_o \int_0^t \frac{v \sin \theta}{r}\ dt \tag{2.44}$$

As can be seen, numerical methods are generally necessary to perform these integrations.

Integration of equation (2.39) can be accomplished if the drag term is neglected and certain other simplifying assumptions are made. This result is useful because it expresses the velocity in terms of the ideal velocity (equation (2.26) and gravity losses. As such, these parameters can be employed in the evaluation of thrusting maneuvers near the earth. To perform the integration, assume a constant or mean value for the thrust (F), acceleration due to gravity (g) and flight path angle (θ). The angle of attack α is assumed to be zero. These conditions define a rectilinear trajectory.

$$v = \int_{t_o}^{t} \frac{F}{m}\, dt - \int_{t_o}^{t} g \cos \theta \, dt \tag{2.45}$$

Thus, substituting

$$F = I_{sp} \dot{W} \tag{2.46}$$

$$m = \frac{1}{g_o}[W_o - \dot{W}(t - t_o)] \tag{2.47}$$

$$u_v = \frac{W_o}{W_o - \dot{W}(t - t_o)} \tag{2.48}$$

into equation (2.45) and integrating yields

$$v = v_o + I_{sp}\, g_o\, \ell n\, u_v - g \cos \theta (t - t_o) \tag{2.49}$$

where

F = assumed average thrust

I_{sp} = assumed average specific impulse

m = vehicle mass at time t

g_o = initial acceleration due to gravity

W_o = initial total vehicle weight

$\dot{W}$ = propellant flow rate

t_o = initial time

t = time

g = assumed average acceleration due to gravity

v_o = initial velocity

The second term in equation (2.49) is the ideal velocity and the third term is the gravity loss term. It should be noted that the total ideal velocity of a multi-stage vehicle can be computed by adding the ideal velocities for each thrusting stage with adjustments to the mass ratio for staging. That is,

$$V_{ideal} = I_{sp_1} g_o \ln u_{v_1} + I_{sp_2} g_o \ln u_{v_2} + \ldots + \text{etc.} \tag{2.50}$$

The preceding discussion has been limited to a non-rotating earth. The earth's rotational velocity must be accounted for in the total ascent trajectory. Actually a significant advantage is gained from the component of the earth's rotation which is in the desired plane (a function of the launch latitude and the launch azimuth). To account for the earth's rotation, the earth's rotational velocity vector can be added to the vehicle velocity vector at injection or at some point during the ascent trajectory after passage through the more dense atmospheric layers. This vector addition converts the velocity from earth-fixed to space-fixed values. The conversion is accomplished by the following relations.

$$v_s = \sqrt{v^2 + 2\omega r v \cos \phi \sin \theta \sin \Sigma + \omega_e{}^2 r^2 \cos^2 \phi_L}$$

$$\theta_s = \cos^{-1}\left(\frac{v \cos \theta}{v_s}\right) \tag{2.51}$$

where

v_s = inertial velocity

v = earth relative velocity (equation (2.41)

ω_e = earth rotation rate

r = vehicle radius

ϕ = vehicle latitude

θ = flight path angle from local vertical to the velocity vector (earth relative)

Σ = vehicle trajectory azimuth

θ_s = inertial flight path angle

This is a simplified approach to the adjustment for the earth's rotational velocity but is adequate for making vehicle performance and optimization studies.

2.2.4.2 Velocity Requirements

The boost vehicle cutoff velocity required for orbit insertion is an important parameter in the estimation of boost vehicle design requirements. Equation (2.50) expresses the relationship between ideal velocity requirements and vehicle configuration. However, the nature of the adjustments will not be presented.

For insertion into a circular orbit, the insertion velocity is equal to the circular orbit velocity at the desired altitude.

$$V_I = \sqrt{\frac{\mu}{(R_E + h)}} \tag{2.51}$$

where

h = altitude

V_I = insertion velocity

μ = gravitational constant (GM)

R_E = radius of earth

A generalization of this case for insertion into an elliptical orbit (assuming perigee insertion) yields the required velocity as a function of perigee and apogee radius as

$$V_I = \left[\frac{2\ \mu\ r_a}{r_p(r_p + r_a)}\right]^{1/2} \tag{2.52}$$

where

r_a = apogee radius

$= R_E + h_a$

r_p = perigee radius

$= R_E + h_p$

For high altitude orbits, ascent via an elliptical transfer orbit is usually necessary. For a Hohmann type transfer orbit, the transfer orbit insertion velocity can be determined from equation (2.52). However, if insertion into the transfer is made at some point other than perigee, the insertion velocity as a function of insertion radius, flight path, and apogee radius is

$$V_I = \left[\frac{2\,\mu(r_a - r_I)\,r_a}{r_I(r_a^2 - r_I^2\,\sin^2\theta_I)}\right]^{1/2} \tag{2.53}$$

where

r_I = transfer orbit insertion radius

θ_I = transfer orbit insertion flight path angle from local vertical

The total velocity for insertion into the high altitude orbit is provided by equation (2.53) and the difference between the apogee velocity of the transfer ellipse and the final orbit velocity. The apogee velocity of the transfer orbit is given by

$$V_a = \frac{V_I\,r_I\,\sin\theta_I}{r_a} \tag{2.54}$$

so that the total insertion velocity for a circular target orbit is given by

$$V_T = V_I + \sqrt{\frac{\mu}{r_a}} - \frac{V_I\,r_I\,\sin\theta_I}{r_a} \tag{2.55}$$

since the radius of the final orbit is equal to the transfer orbit apogee radius.

Generalizations of these relationships to include injection at arbitrary points on the trajectory and for transfer between arbitrary trajectories can be readily obtained by matching the velocity on the various arcs (as defined by two-body mechanics) with that of the vehicle.

2.3 RENDEZVOUS

2.3.1 Introduction

The rendezvous of two vehicles in orbit poses several unique problems in mission design since this requirement means that the position and velocity vectors at an instant in time for both vehicles must be matched. Thus, rendezvous is more than a simple transfer from one orbit to another since it requires that the transfer be performed under a severe time constraint. There are many rendezvous techniques but in general they may be placed in two categories. The first is rendezvous with a target vehicle in orbit by a vehicle ascending directly from the ground. This mode includes direct ascent and ascent via specifically selected orbits. The second general category is the rendezvous of two vehicles in two arbitrary orbits. Included in this category may be the rendezvous of two vehicles in the same orbit but at different positions in the orbit. In order to understand the interface between the rendezvous requirement and trajectory design, the various aspects of the rendezvous problem will be discussed in the following sections.

2.3.2 Direct Ascent

Direct ascent is the technique whereby the shuttle vehicle is launched into the plane of the target vehicle orbit and ascends to rendezvous without the benefit of an intermediate phasing orbit. Direct ascents require rather severe constraints on the time of launch. Not only are the launches broadly restricted to the two times per day that the launch site will be in the target orbit plane, but for any particular planar launch opportunity, the target vehicle must be in the proper position in orbit at the time of launch. Thus, it is probable that, for an arbitrary target orbit and arbitrary launch site, the target vehicle location will not be favorable for planar launch opportunities within a given time constraint. Thus, successful direct ascents require the design of the target orbit such that a number of rendezvous opportunities will exist within the time limitations which are imposed. One technique for assuring that a number of direct ascent rendezvous opportunities will exist is to insert the target vehicle in a "rendezvous compatible orbit"; that is, an orbit for which the earth track is periodically repeating. In a rendezvous compatible orbit, the target vehicle can be made to pass over the launch site once or twice per day to afford many direct ascent rendezvous opportunities during the mission duration. The design of rendezvous compatible orbits will be examined in more detail in following sections. Another method which increases the flexibility of direct ascent rendezvous is to allow a plane change capability in the shuttle vehicle. Out-of-plane launches can then be made and a subsequent plane change maneuver performed in order to place the shuttle vehicle in the target orbit plane. However, since plane change maneuvers are expensive in terms of delta-V requirements, the usual method is to allow just enough plane change capability to enable some flexibility in launch time for a particular launch opportunity. This launch flexibility affords a "launch window" during which a direct ascent and rendezvous can be accomplished. In this section the equations defining launch time requirements, launch windows, and the gross rendezvous maneuver will be discussed.

The launch time constraint can be defined by comparing the geometrical relationships for planar launches and the time requirements imposed by the orbital maneuvers required for rendezvous. Figure 3-1 illustrates the geometrical relationships required for launch into the target orbit plane without a plane change.

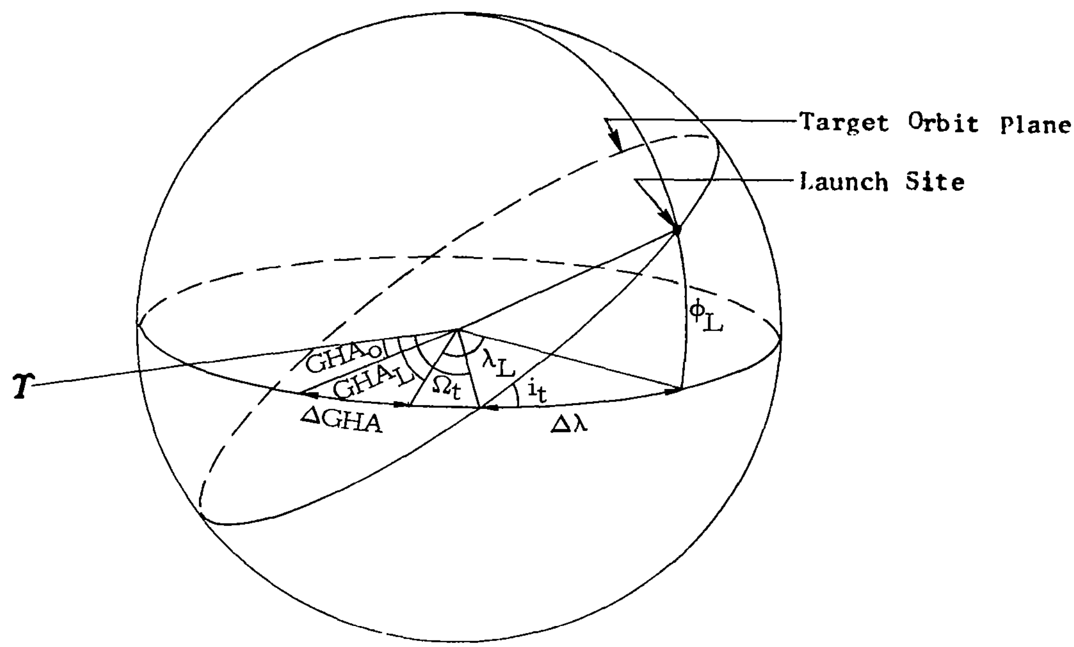

Figure 3-1

The Greenwich Hour Angle (GHA) required for the launch site to be in the target orbit plane is determined with the aid of Figure 3-1 to be

$$GHA_L = \Omega_t + \Delta\lambda - \lambda_L \tag{3.1}$$

where

$$\Delta\lambda = \sin^{-1}\left(\frac{\tan \phi_L}{\tan i_t}\right) \tag{3.2}$$

assuming launch sites in northern hemisphere

$0° \leq \Delta\lambda \leq 90°$ for northerly launches

$90° < \Delta\lambda < 180°$ for southerly launches

ϕ_L = launch site geocentric latitude

i_t = inclination of target orbit plane

λ = launch site longitude

Ω_t = current value of target orbit ascending node
$= \Omega_{t_o} + T_D \dot{\Omega}_t$ including earth oblateness correction

Ω_{to} = target orbit ascending node at target insertion into orbit

$\dot{\Omega}_t$ = nodal regression rate

$$\approx - \frac{3}{2} J_2 \pi \left(\frac{R_e}{a_t}\right)^2 \frac{\cos i_t}{(1 - e_t{}^2)^2}$$

R_e = radius of the earth

a_t = target orbit semi-major axis

e_t = target orbit eccentricity

T_D = time since target insertion

Utilizing the Greenwich Hour Angle (GHA_o) at some epoch, which for convenience can be taken at the time of initial perigee passage in the target orbit, the times of launch with respect to the epoch are given by

$$t_L = \frac{GHA_L - GHA_o + 2 M \pi}{\omega_e} \qquad (3.3)$$

where

M = integer number of days since epoch

ω_e = angular velocity of earth rotation

These relationships define the times with respect to the epoch that a vehicle may be launched into the target orbit plane. These relationships do not define the relative positions of the target in its orbit or that of the shuttle launch point. Additional relationships are required to determine whether a rendezvous can be affected for a particular planar shuttle launch opportunity. The shuttle launch time with respect to the epoch can also be written

$$t_L = \Delta t_R - t_{ascent} - t_{boost} + N \tau_t \qquad (3.4)$$

where

Δt_R = time from target perigee passage to the rendezvous point in the target orbit

t_{ascent} = time from shuttle boost trajectory burnout until rendezvous

t_{boost} = shuttle boost trajectory burning time

N = integer number of revolutions in target orbit from the epoch to perigee in the revolution just prior to rendezvous

$\tau = \frac{2\pi}{\sqrt{\mu}} a_t^{3/2}$ = period of target orbit

Examination of equations (3.3) and (3.4) is in order to determine the conditions necessary for a successful direct ascent rendezvous. Obviously, the launch times computed from equations (3.3) and (3.4) must be equal to achieve rendezvous. Also, the launch time computed from equation (3.3) is a fixed set of values for any given launch site and target orbit. Equation (3.4), however, contains independent variables which may be varied within limits to achieve a launch time compatible with equation (3.3). The parameter t_{boost} is a relatively fixed quantity depending on the booster vehicle and the boost guidance techniques. The quantity $N \tau_t$ is defined by the number of revolution in which rendezvous is being attempted. Therefore, the parameters t_{ascent} and Δt_R will be analyzed in an attempt to achieve an acceptable rendezvous. The time since the last perigee passage of the target to the rendezvous point (Δt_R) may be considered a function of the time from shuttle vehicle booster burnout to the rendezvous point (t_{ascent}) by the following argument. Since the time of launch for a particular opportunity is specified by equation (3.3) and since the efficient use of propellant requires the insertion of the shuttle into the ascent trajectory near perigee of the ascent trajectory, orientation of the semi-major axis of the ascent trajectory can be considered defined. (See Figure 3-2 for the geometric configuration at the time of launch.) Thus, considering the family of possible in-plane ascent trajectories indicated in Figure 3-2, it is apparent that the intercept point of the ascent trajectory and the target orbit is a function of the ascent trajectory injection delta-V. Therefore, the time of intercept (Δt_R) can be considered a function of the time of ascent (t_{ascent}) and, in turn, can be used as the independent variable in an iteration scheme to match equations (3.3) and (3.4). The evaluation of a trial ascent trajectory to determine if equations (3.3) and (3.4) are satisfied can be accomplished by equations which are developed as follows.

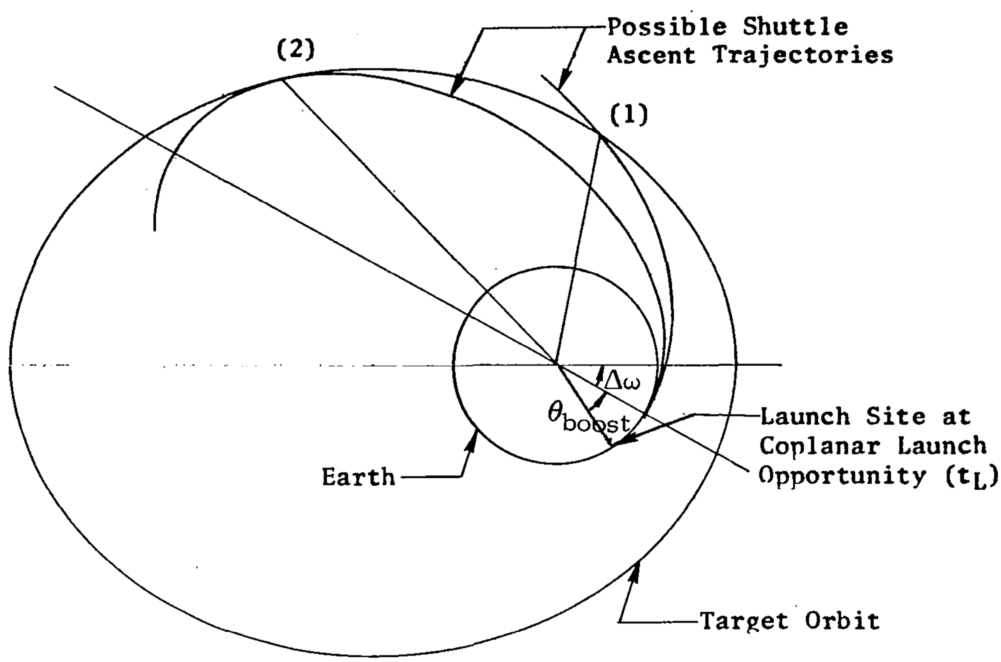

Figure 3-2

Assuming the injection velocity (V_I) is known, the semi-major axis (a_s) may be obtained from

$$a_s = \frac{\mu\,(R_e + h_I)}{2\mu - (R_e + h_I)V_I^2} \tag{3.5}$$

where

h_I = injection altitude

R_e = radius of the earth

μ = (GM) earth gravitational constant

V_I = injection velocity

Similarly, the eccentricity (e_s) of the ascent trajectory is given by

$$e_s = \sqrt{1 - \frac{(\bar{r} \cdot \bar{v})^2}{\mu\, a_s}} \tag{3.6}$$

and the argument of perigee of the ascent trajectory (ω_s) can be seen to be

$$\omega_s = \sin^{-1}\left(\frac{\sin \phi_L}{\sin i_t}\right) + \theta_{boost} \tag{3.7}$$

where (assuming a launch site in the northern hemisphere)

$0 < \omega_s < 90°$ for northerly launches

$90 < \omega_s < 180°$ for southerly launches

θ_{boost} = boost angular range

Note that the semi-major axis of the target orbit and the ascent trajectory are displaced by (see Figure 3-2)

$$\Delta\omega = \omega_t - \omega_s \tag{3.8}$$

where

ω_t = argument of perigee of the target orbit

Thus, the true anomaly of the intercept point in the target orbit is

$$\theta_t = \theta_s - \Delta\omega \tag{3.9}$$

where θ_s = true anomaly of the intercept point in the ascent trajectory, and the radius of the intercept point is given by the expression

$$r = \frac{a_t(1 - e_t^2)}{1 + e_t \cos\theta_t} = \frac{a_s(1 - e_s^2)}{1 + e_s \cos\theta_s} \tag{3.10}$$

Therefore, substituting (3.8) and (3.9) into (3.10) and expanding yields

$$(e_t \cos \Delta\omega - e_s \frac{p_t}{p_s}) \cos \theta_s + e_t \sin \Delta\omega \sin \theta_s = \frac{p_t}{p_s} - 1 \tag{3.11}$$

where

$p_t = a_t(1 - e_t^2)$

$p_s = a_s(1 - e_s^2)$

So that if

$$A \equiv e_t \cos \Delta\omega - e_s \frac{p_t}{p_s}$$

$$B \equiv e_t \sin \Delta\omega \tag{3.12}$$

$$C \equiv \frac{p_t}{p_s} - 1$$

Then,

$$A \cos \theta_s + B \sin \theta_s = C \tag{3.13}$$

and since

$$\sin \theta_s = [1 - \cos^2\theta_s]^{1/2} \tag{3.14}$$

$$(A^2 + B^2) \cos^2\theta_s - 2 A C \cos \theta_s + C^2 - B^2 = 0 \tag{3.15}$$

or

$$\cos \theta_s = \frac{A C \pm B \sqrt{A^2 + B^2 - C^2}}{A^2 + B^2} \tag{3.16}$$

Equation (3.16) yields two solutions for $\cos \theta_s$ corresponding to the plus or minus sign in front of the radical. Finally, substituting each version of (3.16) into equation (3.13) and solving for $\sin \theta_s$ will completely define the two intersection solutions.

For

$$\cos \theta_s = \frac{A C + B \sqrt{A^2 + B^2 - C^2}}{A^2 + B^2}$$

$$\sin \theta_s = \frac{C B - A \sqrt{A^2 + B^2 - C^2}}{A^2 + B^2} \tag{3.17}$$

and for

$$\cos \theta_s = \frac{A\,C - B\sqrt{A^2 + B^2 - C^2}}{A^2 + B^2}$$

$$\sin \theta_s = \frac{C\,B + A\sqrt{A^2 + B^2 - C^2}}{A^2 + B^2} \tag{3.18}$$

There are at most two points at which two elliptical orbits will intersect. However, it is possible to have no intersections or one intersection. These possibilities will result in imaginary or zero values respectively for the radical in equations (3.17) and (3.18). For each solution of the true anomaly (θ_s) of the intersection of the ascent trajectory and the target orbit, the intercept time can be computed and substituted into equation (3.4). The time from ascent trajectory insertion to intercept can then be computed from the following.

$$\cos E_s = \frac{\cos \theta_s + e_s}{1 + e_s \cos \theta_s} \tag{3.19}$$

$$\sin E_s = \frac{\sqrt{1 - e_s^2}\ \sin \theta_s}{1 + e_s \cos \theta_s} \tag{3.20}$$

$$E_s = \tan^{-1}\left(\frac{\sin E_s}{\cos E_s}\right) \tag{3.21}$$

$$M_s = E_s - e_s \sin E_s \tag{3.22}$$

$$t_{ascent} = \frac{M_s}{\sqrt{\mu}}\, a_s^{3/2} \tag{3.23}$$

After obtaining the true anomaly of the intercept point in the target orbit plane from equation (3.9), the time from perigee to intercept in the target orbit (Δt_R) is computed from

$$\cos E_t = \frac{\cos \theta_t + e_t}{1 + e_t \cos \theta_t} \tag{3.24}$$

$$\sin E_t = \frac{\sqrt{1 - e_t^2}\ \sin \theta_t}{1 + e_t \cos \theta_t} \tag{3.25}$$

$$E_t = \tan^{-1}\left(\frac{\sin E_t}{\cos E_t}\right) \tag{3.26}$$

$$M_t = E_t - e_t \sin E_t \tag{3.27}$$

$$\Delta t_R = \frac{M_t}{\sqrt{\mu}} a_t^{3/2} \tag{3.28}$$

Summarizing, the ascent trajectory injection velocity (V_I) can be used as the independent variable in the iteration loop and equations (3.5) through (3.28) solved and substituted into equation (3.4) to determine whether a successful rendezvous is obtained. However, for any given opportunity for a launch into the target orbit plane [described by equation (3.3)], it may not be possible to find an ascent trajectory within booster constraints for which a rendezvous is possible.

Obviously, the determination of a suitable ascent trajectory to affect rendezvous with a target vehicle in an arbitrary orbit is a difficult and involved process. A far more suitable arrangement would be to place the target in a rendezvous compatible orbit prior to the rendezvous attempt. A rendezvous compatible orbit suitable for rendezvous using a given boost vehicle can be easily predetermined and the target placed in this orbit either directly or at some time prior to the rendezvous maneuver.

Another very important factor which should be considered while iterating on a solution to equations (3.3) and (3.4) is the launch window. It is not necessary, or in some cases possible, to find a perfect launch time and ascent trajectory combination which will completely satisfy equations (3.3) and (3.4). Rather, the criticality produced by the time constraint is relaxed by including a plane change capability in the shuttle vehicle. This plane change capability can be translated into a launch window or a launch time tolerance within which insertion into the target orbit and rendezvous is still possible and can be interpreted as an additional term in equation (3.3) as

$$t_L = \frac{GHA_L - GHA_o + 2\ M\ \pi}{\omega_e} + \Delta T_{LW} \tag{3.29}$$

where the term ΔT_{LW} is the launch window width defined from the following.

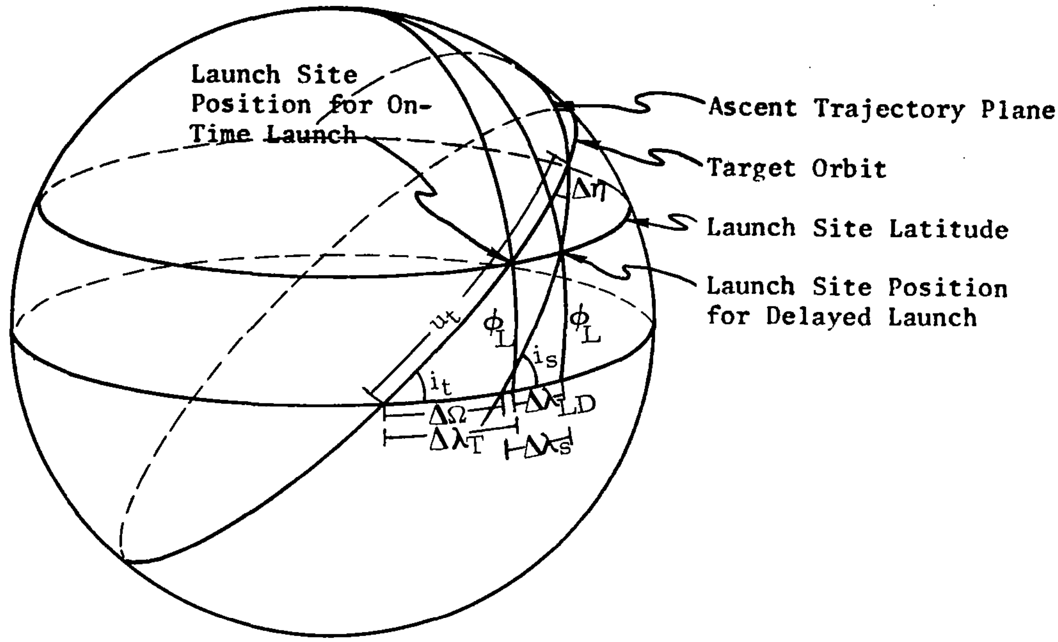

Figure 3-3

The plane change capability is indicated by the angle $\Delta\eta$ in Figure 3-3 assuming the plane change is made at the rendezvous point defined by the argument of latitude (u_t) in the target orbit. But, $\Delta\eta$ will be small (for propellant budget reasons); thus, the ascent trajectory profile, for the delayed launch, will be approximately the same as for a nominal launch. For this reason, the true anomaly (θ_s) of the intercept point in the ascent trajectory and the flight path angle (γ_s) can then be approximated from nominal ascent trajectory calculations. The delta-V required to produce a plane change of $\Delta\eta$ can be written with the aid of Figure 3-4 as

$$\Delta V = [2V_s^2 \cos^2\gamma_s(1 - \cos \Delta\eta)]^{1/2} \qquad (3.30)$$

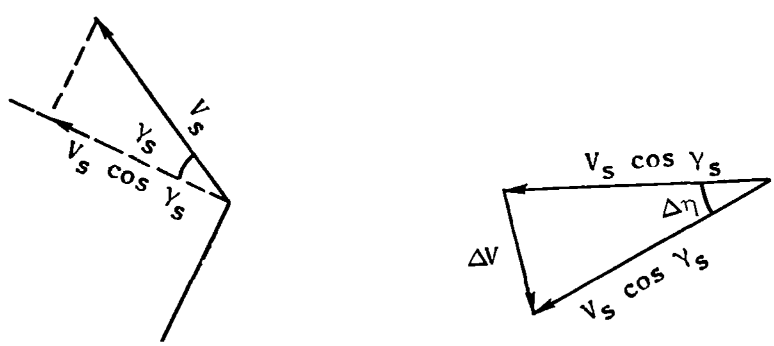

Figure 3-4

$$\Delta\eta = \cos^{-1}\left(1 - \frac{\Delta V^2}{2V_s^2 \cos \gamma_s}\right) \tag{3.31}$$

Returning to Figure 3-3, the inclination of the ascent trajectory plane for a delayed launch can be written

$$i_s = \cos^{-1}(\cos \Delta\eta \cos i_t - \sin \Delta\eta \sin i_t \cos u_t) \tag{3.32}$$

where

$$0 < i_s < 180 \quad \text{for posigrade orbits}$$

and the difference in nodes ($\Delta\Omega$) of the target orbit and the ascent trajectory is given by

$$\cos \Delta\Omega = \frac{\cos \Delta\eta - \cos i_t \cos i_s}{\sin i_t \sin i_s}$$

$$\sin \Delta\Omega = \frac{\sin \Delta\eta \sin u_t}{\sin i_s} \tag{3.33}$$

$$\Delta\Omega = \tan^{-1}\left(\frac{\sin \Delta\Omega}{\cos \Delta\Omega}\right) \tag{3.34}$$

Finally, the computation of the parameters $\Delta\lambda_t$ and $\Delta\lambda_s$ complete the required information

$$\Delta\lambda_t = \sin^{-1}\left(\frac{\tan \phi_L}{\tan i_t}\right) \tag{3.35}$$

where from northern hemisphere launch sites

$$0 < \Delta\lambda_t < 90 \quad \text{for northerly launches}$$

$$90 < \Delta\lambda_t < 180 \quad \text{for southerly launches}$$

$$\Delta\lambda_s = \sin^{-1}\left(\frac{\tan \phi_L}{\tan i_s}\right) \; * \tag{3.36}$$

---

* Constraints for $\Delta\lambda_s$ are the same as for $\Delta\lambda_t$

Thus, for a given plane change delta-V capability, the landing site may rotate

$$\Delta\lambda_{LD} = \Delta\Omega + \Delta\lambda_s - \Delta\lambda_t \tag{3.37}$$

past the nominal launch point. Considering the width of a launch window, it is also possible to launch early by an amount defined by the plane change capability. For an early launch the inclination of the ascent trajectory plane is given by

$$i_s = \cos^{-1}(\cos i_t \cos \Delta\eta + \sin i_t \sin \Delta\eta \cos u_t) \tag{3.38}$$

Then computing $\Delta\Omega$, $\Delta\lambda_t$, and $\Delta\lambda_s$ using equation 3.38) in equations (3.33) through (3.36) the early launch parameter ($\Delta\lambda_{LE}$) becomes

$$\Delta\lambda_{LE} = \Delta\Omega_E + \Delta\lambda_{E_t} - \Delta\lambda_{E_s} \tag{3.39}$$

At this point, the total launch window corresponding to the plane change delta-V capability, that is, the time required for the earth to rotate through the angles $\Delta\lambda_{LD}$ and $\Delta\lambda_{LE}$, is

$$\frac{\Delta\lambda_L}{\omega_e} = \frac{\Delta\lambda_{LD} + \Delta\lambda_{LE}}{\omega_e}$$

The launch window limits are, for a delayed launch,

$$\Delta T_{LW} = \frac{\Delta\lambda_{LD}}{\omega_e}$$

and for an early launch (3.40)

$$\Delta T_{LW} = \frac{\Delta\lambda_{LE}}{\omega_e}$$

Equations (3.40) define the term required in equation (3.29). As was mentioned before, this term is necessary to compensate for actual liftoff time errors and to aid in the determination of an acceptable rendezvous solution of equations (3.3) and (3.4).

The preceding discussion listed equations governing the relationships between launch from a specific site, and direct ascent to a rendezvous with a target in an arbitrary earth orbit. It is not intended that these equations be used in defining precision rendezvous maneuvers. The intent is simply to point out the interfaces between the mission constraints of direct ascent to rendezvous and the trajectory requirements necessary to accomplish this task. The equations can, however, be used to obtain initial profiles upon which refinements can be made to obtain a realistic rendezvous mission.

2.3.3 Rendezvous Compatible Orbits

As mentioned in the previous section, placing the target in a rendezvous compatible orbit (RCO) greatly simplifies the direct ascent and rendezvous problem. In cases such as the assembly of a vehicle in orbit where many rendezvous are necessary, an RCO is almost a necessity. Thus, this section will discuss the trajectory constraints for a rendezvous compatible orbit and formulate the structure of the problem.

In order for the target to pass over the launch site every nth revolution after launch, the following relationship must hold.

$$n \ \tau_{oblate} = \frac{2\pi \ M + \dot{\Omega} \ n}{\omega_e} - t_{ascent} \tag{3.41}$$

where

n = integer number of revolutions

τ_{oblate} = nodal period over an oblate earth

$$\simeq \frac{2\pi}{\sqrt{\mu}} a^{3/2} \left\{ 1 - \frac{3 \ J_2 \ R_e^2}{a^2} \left(\frac{7 \cos^2 i - 1}{8} \right) \right\}$$

a = semi-major axis of target orbit

μ = gravitational constant (GM)

e = eccentricity of target orbit

J_2 = zonal harmonic coefficient

i_t = target orbit inclination

R_e = equatorial radius of earth

M = integer number of days between passes

$\dot{\Omega}$ = nodal regression per revolution

$$\simeq -3\pi \ J_2 \left[\frac{R_e}{a(1 - e^2)} \right]^2 \cos i_t \ \text{rad/rev}$$

t_{ascent} = time from launch to target orbit insertion

ω_e = angular rotation rate of the earth

Thus, rewriting equation (3.41) yields the required period for an RCO orbit which passes over the launch site every n revolutions as

$$\tau_{oblate} = \frac{2\pi + \dot{\Omega}\eta - t_{ascent} + \omega_e}{\eta . \omega_e} \tag{3.42}$$

Note that inclination terms are included in the oblate earth relationships for $\dot{\Omega}$ and τ_{oblate} (however, equation (3.42) is independent of the orientation (inclination) of the RCO to the first order); thus, if it is desired to take advantage of the two launch opportunities per day it is necessary to specify an inclination. That is, if it is desired to make a southerly pass over the launch site Q revolutions after the northerly pass during a 24 hour period, the inclination of the RCO can be determined from the following relationship, assuming a circular RCO. See Figure 3-5.

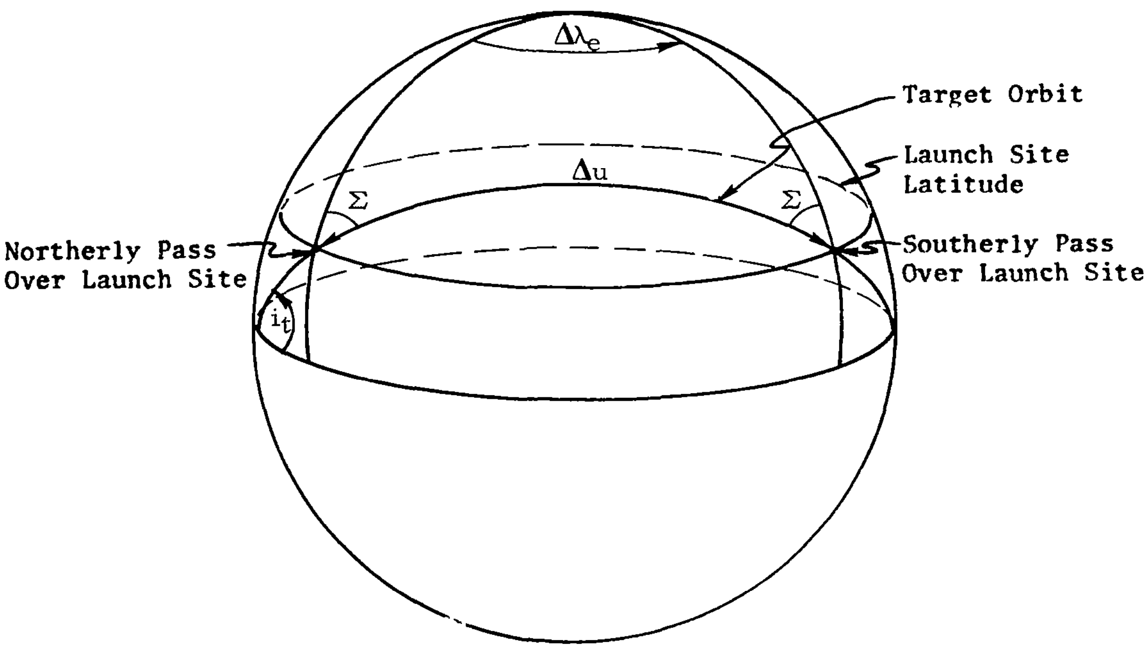

Figure 3-5

$$Q\ \tau_{oblate} + \frac{\Delta u}{n_m} - \frac{\Delta\lambda_e}{\omega_e} = 0 \tag{3.43}$$

where

Q = number of revolution in target orbit between northerly pass over launch site and southerly pass over launch site

n_m = target mean motion

$$= \frac{\sqrt{\mu}}{a^{3/2}}$$

$\Delta u = 2 \tan^{-1}(\cot \phi_L \cos \Sigma)$

$\Delta \lambda_e = 2 \cot^{-1}(\tan \Sigma \sin \phi_L)$

$\Sigma = \sin^{-1} \dfrac{\cos i_t}{\cos \phi_L}$

$0° < \Sigma < 90°$ for northern hemisphere launch sites

ϕ_L = launch site latitude

It is necessary to solve equations (3.42) and (3.43) numerically because of the interdependence of the inclination in $\dot{\Omega}$ and τ_{oblate}. However, this solution can be expedited by neglecting the oblate earth effects in equation (3.42) to obtain an initial estimate of τ_{oblate} with which to begin the numerical solution of (3.43).

2.3.4 Intermediate Orbit Rendezvous Techniques

2.3.4.1 General

The insertion of the shuttle or chase vehicle into an intermediate parking or phasing orbit prior to the final transfer and rendezvous has one major advantage. This advantage arises from the fact that the use of an intermediate orbit will allow the launch of the shuttle vehicle at virtually any time the launch site crosses the target orbit plane regardless of the phasing conditions since the proper phasing for the final rendezvous maneuver can be accomplished by coasting in the intermediate orbit. In this method, the altitude of the intermediate orbit may be preselected so as to result in optimized phasing for a particular case. It is also possible to absorb part of the phasing problem by proper timing of the launch and insertion into the intermediate orbit but this is not really necessary. Some delta-V savings may be realized by launch timing but for illustration of the interfaces involved in the use of an intermediate orbit technique it will be assumed that the shuttle vehicle is inserted into an intermediate orbit at some arbitrary phasing relationship with the target vehicle in its orbit. It will also be assumed that the intermediate and target orbit are circular. The discussion can be extended to elliptical orbits but because of the nature of the transcendental time equation for elliptical orbits numerical solutions are usually required.

Several intermediate orbit techniques will be discussed in order to illustrate the trajectory interfaces involved.

2.3.4.2 Concentric Orbits

In this rendezvous technique, concentric circular target and intermediate orbits are established such that the relative sizes of the two orbits satisfy the phasing relationships between the target and the shuttle craft. Then the rendezvous maneuver profile is determine from the following sketch.

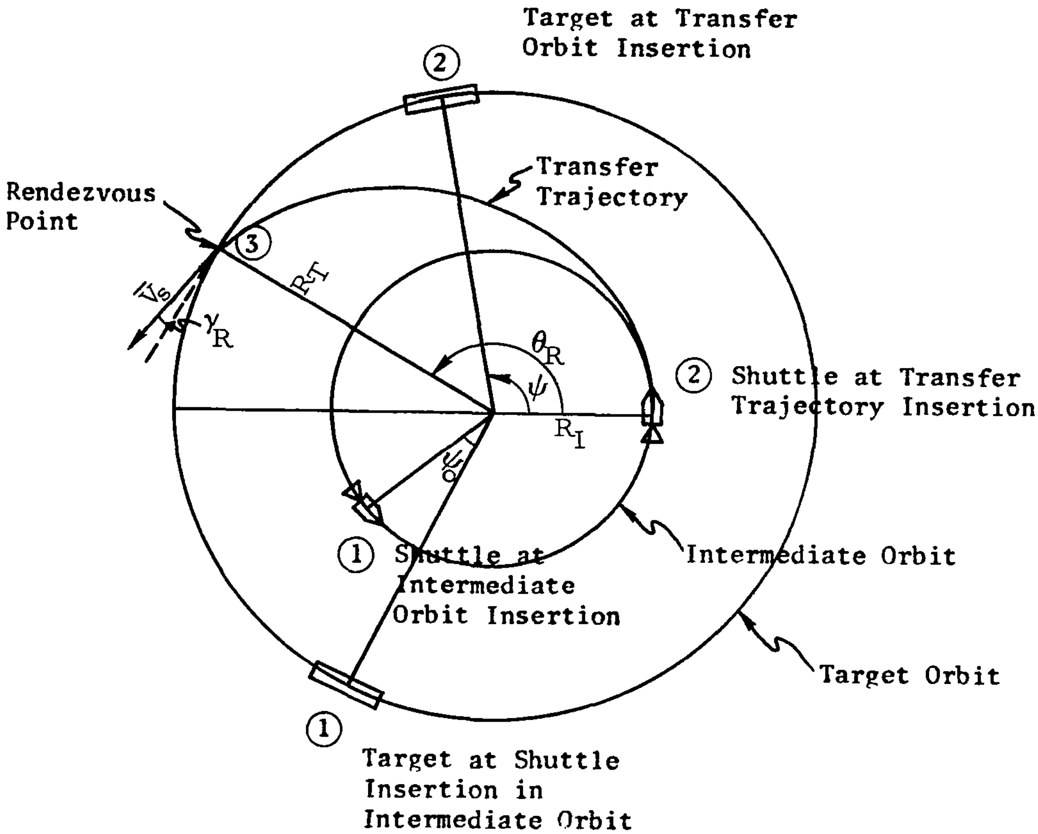

Figure 3-6

Figure 3-6 illustrates the geometry of the rendezvous maneuver profile for the case where injection occurs at periapse and where the flight path angle in the transfer orbit is some value (γ_R) at the target intercept point.(If it is required that the transfer orbit be tangent to the target orbit at intercept, the problem reduces to a simple Hohmann transfer.) Thus, the semi-major axis of the transfer orbit can now be determined from the conservation of angular momentum and the energy equation and shown to be

$$a_{TR} = \frac{R_T^2 \cos^2\gamma_R - R_I^2}{2(R_T \cos^2\gamma_R - R_I)} \tag{3.44}$$

where

R_I = radius of the intermediate orbit

γ_R = flight path angle in the transfer orbit at rendezvous

R_T = radius of the target orbit

The eccentricity of the transfer orbit can then be determined from the perifocal distance

$$e_{TR} = 1 - \frac{R_I}{a_{TR}} \tag{3.45}$$

Thus, the true anomaly (θ_R) in the transfer orbit at the intercept point is

$$\cos \theta_R = \frac{p_{TR} - R_T}{R_T\ e_{TR}}$$

$$\sin \theta_R = \frac{p_{TR} \tan \gamma_R}{R_T\ e_{TR}} \tag{3.46}$$

$$\theta_R = \tan^{-1}\left(\frac{\sin \theta_R}{\cos \theta_R}\right)$$

where

$$p_{TR} = a_{TR}(1 - e_{TR}{}^2)$$

and the eccentric anomaly at the rendezvous point (E_R) in the transfer orbit can be found from

$$\cos E_R = \frac{\cos \theta_R + e_{TR}}{1 + e_{TR} \cos \theta_R}$$

$$\sin E_R = \frac{\sqrt{1 - e_{TR}{}^2}\ \sin \theta_R}{1 + e_{TR} \cos \theta_R} \tag{3.47}$$

$$E_R = \tan^{-1}\left(\frac{\sin E_R}{\cos E_R}\right)$$

Finally, the mean anomaly (M_R) at the rendezvous point in the transfer is

$$M_R = E_R - e_{TR} \sin E_R \tag{3.48}$$

and the time (ΔT_R) from transfer orbit insertion to rendezvous can be computed as

$$\Delta T_R = \frac{M_R}{\sqrt{\mu}} (a_{TR})^{3/2} \tag{3.49}$$

The lead angle (ψ), required for proper phasing, is measured from the shuttle to the target at transfer orbit insertion and is given by

$$\psi = \theta_R - n_T \, \Delta T_R \tag{3.50}$$

where

$$n_T = \text{target mean motion}$$

$$= \frac{\sqrt{\mu}}{a_T{}^{3/2}}$$

Thus, the coasting time (t_{coast}) in the intermediate orbit (the time from insertion) is given by

$$t_{coast} = \frac{\psi - \psi_o}{n_T - n_I} \tag{3.51}$$

where

ψ_o = target lead angle at the time of intermediate orbit insertion

n_I = intermediate orbit mean motion

$$= \frac{\sqrt{\mu}}{a_I{}^{3/2}}$$

The cost of the total maneuver can now be assessed in terms of the propulsive effort required since for the assumptions given the delta-V requirement for insertion into the transfer orbit is

$$\Delta V_{TR} = \sqrt{\mu\left(\frac{2}{R_I} - \frac{1}{a_{TR}}\right)} - \sqrt{\frac{\mu}{R_I}} \tag{3.52}$$

Similarly, at rendezvous the velocity in the transfer orbit is

$$V_R = \sqrt{\mu \left(\frac{2}{R_T} - \frac{1}{a_{TR}}\right)} \tag{3.53}$$

and the target orbit circular velocity is

$$V_T = \sqrt{\frac{\mu}{R_T}} \tag{3.54}$$

Therefore, the rendezvous delta-V is

$$\Delta V_R = \sqrt{V_R^2 + V_T^2 - 2\, V_R\, V_T \cos \gamma_R} \tag{3.55}$$

2.3.4.3 Co-Orbital

The co-orbital technique employs insertion of the shuttle craft into an orbit which intersects or is tangent to that of the target but with the shuttle either leading or behind the target. In this scheme, the period of the orbit for the shuttle is selected so that after n orbits the position error has been cancelled. The basic advantage of the co-orbital technique is the simplicity of the phasing maneuver. The shuttle craft is merely inserted into an elliptical orbit with a period sufficient to catch up with the target in one or more revolutions. The chief disadvantage of the co-orbital method is that the shuttle must be inserted into the target orbit close enough to the target to keep the elliptical catchup orbits within reasonable bounds.

The equations expressing the relationships for co-orbital rendezvous are developed as follows.

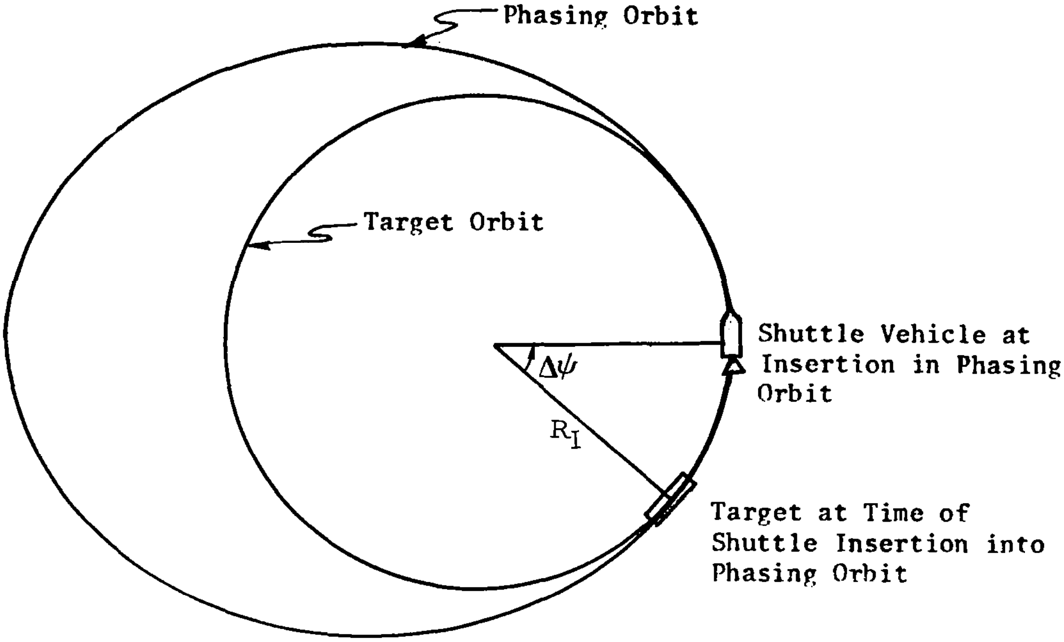

Figure 3-7

As illustrated in Figure 3-7 the shuttle vehicle is inserted into a phasing orbit with a period sufficient to allow the target to arrive at perigee of the phasing orbit after one or more revolutions of the shuttle in the phasing orbit. If the target is lagging the shuttle vehicle by an angle $\Delta\psi$ at the time of phasing orbit insertion, the timing difference which must be corrected is

$$\Delta t = \frac{\Delta\psi}{n_T} \tag{3.56}$$

where

$$n_T = \text{target mean motion}$$
$$= \frac{\sqrt{\mu}}{a_T^{3/2}}$$

If the rendezvous is to occur after N revolutions in the phasing orbit, the period of the phasing orbit must be

$$\tau_{ph} = \tau_T + \frac{\Delta t}{N} \tag{3.57}$$

Therefore, the semi-major axis of the phasing orbit is

$$a_{ph} = \left[\frac{\sqrt{\mu}}{2\pi}\tau_{ph}\right]^{2/3} \tag{3.58}$$

and the difference between the required velocity and that of the target is

$$\Delta V = \sqrt{\mu\left(\frac{2}{R_T} - \frac{1}{a_{ph}}\right)} - \sqrt{\frac{\mu}{R_T}} \tag{3.59}$$

(Note: Under some conditions it is possible to offset rendezvous without imposing a delta-V penalty. In others, two impulses of this magnitude are required.) Finally, the time required for rendezvous is

$$T_{rendezvous} = N\,\tau_{ph} \tag{3.60}$$

2.3.4.4 LOS Delta-V Rendezvous

A technique which holds promise for manual backup control during the rendezvous maneuver is a method in which thrusting for insertion into the final transfer orbit is along the line-of-sight vector from the shuttle to the target.* This technique is actually a special case of the concentric orbit technique. The shuttle is inserted into an intermediate orbit below the target orbit; then, when the line-of-sight between the shuttle and the target reaches a predetermined elevation angle, the spacecraft centerline having already been aligned along this elevation, an impulse is applied in the line-of-sight direction. Thus, the shuttle is inserted into a transfer trajectory from which the target is visible from insertion to rendezvous. See Figure 3-8 for the geometry of the maneuver.

---

* It can be readily established that thrusting in this manner for a time which is large compared to the total transfer time will not produce rendezvous. However, if the burning time is short, an intercept can be produced.

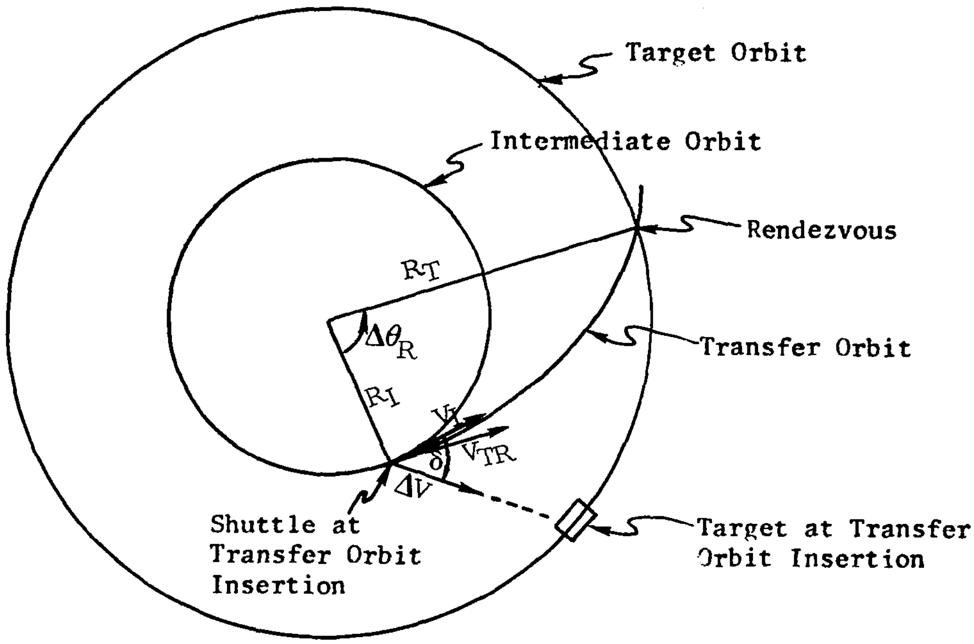

Figure 3-8

A rendezvous maneuver solution can usually be found for any positive line-of-sight elevation angle δ. However, it is necessary to determine the required delta-V for a given δ by iteration of the following equations.

Assume an arbitrary value of δ and an estimate of delta-V (ΔV_{est}) are available. Then, the velocity in the transfer orbit after insertion is

$$V_{TR} = (\Delta V_{est}{}^2 + V_I{}^2 + 2\Delta V_{est}\, V_I \cos\delta)^{1/2} \tag{3.61}$$

and the flight path angle at insertion into the transfer orbit is

$$\gamma_{TR} = \sin^{-1}\left(\frac{\Delta V_{est} \sin\delta}{V_{TR}}\right) \tag{3.62}$$

Now,the angular momentum of the transfer orbit can be computed as

$$h_{TR} = R_I\, V_{TR} \cos\gamma_{TR} \tag{3.63}$$

so that the semi-latus rectum (p_{TR}) is given by

$$p_{TR} = \frac{h_{TR}^2}{\mu} \tag{3.64}$$

and the semi-major axis of the transfer orbit is

$$a_{TR} = \frac{\mu \ R_I}{2\mu - R_I \ V_{TR}^2} \tag{3.65}$$

Thus, both the energy and angular momentum of the orbit are known and the eccentricity can be computed.

$$e_{TR} = \sqrt{1 - p/a_{TR}} \tag{3.66}$$

Having computed the elements of the transfer orbit, the phasing calculations can be made. First, the true anomaly (θ_{TR}) in the transfer orbit at insertion is given by

$$\cos \theta_{TR} = \frac{p_{TR} - R_I}{R_I \ e_{TR}}$$

$$\sin \theta_{TR} = \frac{p_{TR} \tan \gamma_{TR}}{R_I \ e_{TR}} \tag{3.67}$$

$$\theta_{TR} = \tan^{-1}\left(\frac{\sin \theta_{TR}}{\cos \theta_{TR}}\right)$$

Then, the eccentric anomaly at insertion becomes

$$\cos E_{TR} = \frac{\cos \theta_{TR} + e_{TR}}{1 + e_{TR} \cos \theta_{TR}}$$

$$\sin E_{TR} = \frac{\sqrt{1 - e_{TR}^2} \sin \theta_{TR}}{1 + e_{TR} \ \cos \theta_{TR}} \tag{3.68}$$

$$E_{TR} = \tan^{-1}\left(\frac{\sin E_{TR}}{\cos E_{TR}}\right)$$

Finally, the mean anomaly at insertion is

$$M_{TR} = E_{TR} - e_{TR} \sin E_{TR} \tag{3.69}$$

At the target orbit interception point where rendezvous would occur, if the phasing were correct, the velocity in the transfer orbit is

$$V_R = \sqrt{\mu\left(\frac{2}{R_T} - \frac{1}{a_{TR}}\right)} \tag{3.70}$$

The flight path angle at intercept is given by

$$\gamma_R = \cos^{-1}\left(\frac{h_{TR}}{R_T V_R}\right) \tag{3.71}$$

Then the true anomaly at intercept can be found from

$$\cos \theta_R = \frac{p_{TR} - R_T}{R_T e_{TR}}$$

$$\sin \theta_R = \frac{p_{TR} \tan \gamma_R}{R_T e_{TR}} \tag{3.72}$$

$$\theta_R = \tan^{-1}\left(\frac{\sin \theta_R}{\cos \theta_R}\right)$$

and the eccentric anomaly E_R from

$$\cos E_R = \frac{\cos \theta_R + e_{TR}}{1 + e_{TR} \cos \theta_R}$$

$$\sin E_R = \frac{\sqrt{1 - e_{TR}^2}\,\sin \theta_R}{1 + e_{TR} \cos \theta_R} \tag{3.73}$$

$$E_R = \tan^{-1}\left(\frac{\sin E_R}{\cos E_R}\right)$$

Thus, the mean anomaly (M_R) at intercept becomes

$$M_R = E_R - e_{TR} \sin E_R \tag{3.74}$$

and the time in the transfer orbit from insertion to intercept is

$$\Delta t_R = \frac{M_R - M_{TR}}{\sqrt{\mu}} (a_{TR})^{3/2} \tag{3.75}$$

These computations define the central angle traversed by the shuttle craft from insertion to intercept as

$$\Delta\theta_R = \theta_R - \theta_{TR} \tag{3.76}$$

However, from Figure 3-9 it can be seen that the central angle the target must cover during Δt_R for rendezvous to occur is

$$\Delta\theta_T = \Delta\theta_R - \beta \tag{3.77}$$

where β is computed as follows.

$$\alpha = \sin^{-1}\left(\frac{R_I \cos \delta}{R_T}\right) \tag{3.78}$$

$$\beta = 90° - \delta - \alpha \tag{3.79}$$

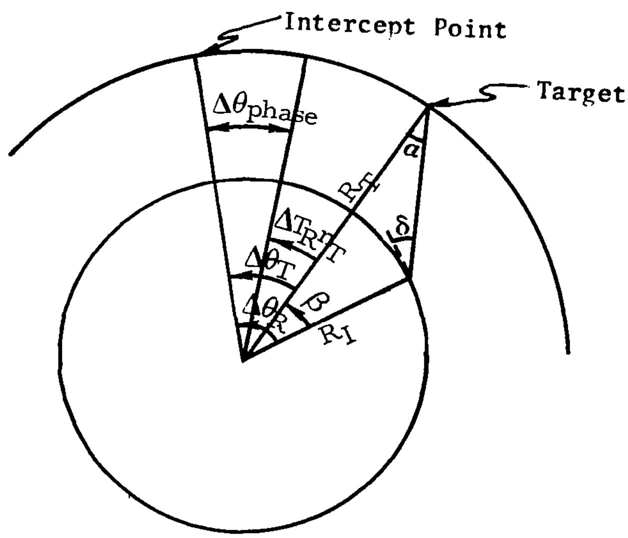

Figure 3-9

To this point, no consideration has been given to the motion of the target. Again for simplicity, assuming circular orbits, this motion is given by the quantity

$$\Delta T_R \; n_T$$

where

$$n_T = \frac{\sqrt{\mu}}{a_T^{3/2}}$$

The phase angle error at the time the shuttle reaches the target orbit is therefore

$$\Delta\theta_{phase} = \Delta\theta_R - \Delta T \; n_T$$

An iteration using delta-V as the independent variable can now be performed until the phase angle error is reduced to an acceptable level.

The delta-V vector requirements for insertion into the target orbit from the transfer orbit are computed in a straightforward manner from standard equations and will not be repeated here.

2.3.5 Terminal Maneuver

The previous sections (2.3.1 through 2.3.4) have been concerned with the placing of the shuttle craft in the vicinity of the target in a manner such that a rendezvous may be accomplished. Various tradeoffs between mission constraints and trajectory requirements were discussed. Another area, fully as important as the rendezvous trajectory profile is the terminal maneuver. The terminal maneuver includes the complex guidance and thrusting requirements for the final closing and joining of the two vehicles once the shuttle vehicle has been placed in the vicinity of the target. This aspect of the problem has been treated in another monograph in the series (Reference 30).

2.4 SPATIAL

2.4.1 Introduction

A discussion of the interfaces between mission objectives or constraints and the orbit selection for the mission requires the evaluation of many factors. The first category of these constraints arises from the type of mission (e.g., reconnaissance, navigational, communication). However, most missions also have many constraints not necessarily associated with the mission; this type of constraint results from range safety limitations, delta-V budgets, environmental control (for example, all manned flights would have similar environmental control problems), lifetime requirements, orbital perturbation specifications, etc. Generally, the constraints conflict with each other or with physical limitations of spatial orbits. In these cases, it is necessary to tradeoff the various constraints and trajectory profiles in order to arrive at a workable mission. This section will explore several of the major spatial mission constraints and their trajectory interfaces.

2.4.2 Perturbations and Lifetime

2.4.2.1 Variation-of-Parameters General Perturbation Technique

A number of affects cause perturbations of a satellite orbit around the earth; these affects cause the motion to deviate from Keplerian two-body motion. The major sources of perturbations are the earth's oblateness, luni-solar gravitational effects, solar radiation pressure, and atmospheric drag. A number of techniques using both special perturbation and general perturbation theory have been developed by numerous authors (Reference 31). In this section, the variation-of-parameters general perturbations technique will be summarized and applied to these perturbative influences. It is not the purpose of this section to attempt to reproduce the works as presented in Reference 31 but rather to summarize some of the most important conclusions for use in this application.

The presentation here is generally as given in Reference 1, sections 8.31-8.36, except that for this discussion the perturbation effects will be limited to the first order.

The conventional elements

a semi-major axis

e eccentricity

i inclination

Ω right ascension of the ascending node

ω argument of perigee

T_p time of periapse passage

will be used in the development of the variation-of-parameters method presented in this section.

In the variation-of-parameters technique, the parameters of an osculating orbit are determined by the actual position and velocity at a given instant. These parameters completely describe the two-body orbit that the vehicle would follow if all subsequent perturbations were removed. Then, since these vectors can be readily determined from the elements, a solution can be obtained if the elements are known as a function of time. This concept of time dependent "constant" leads to the general equation

$$\frac{df}{d\tau} = \dot{f} + f^{\grave{}} \qquad (4.1)$$

where the notation used is defined as

$\frac{df}{d\tau}$ the time rate of change of an element

f any element function

$\dot{f}$ the two-body variation in the absence of any perturbation

$f^{\grave{}}$ (f grave) the part of the variation due to the presence of perturbations

τ $K_e(t - t_o)$

K_e quasi-gaussian gravitational constant

But, if the conventional elements are employed (recall they are constant in a two-body orbit) the variations are due to the perturbations alone. Thus for a, e, i, Ω, ω, and T_p

$$\frac{da}{d\tau} = a^{\grave{}} \qquad \dot{a} = 0$$

$$\frac{de}{d\tau} = e^{\grave{}} \qquad \dot{e} = 0$$

$$\frac{di}{d\tau} = i^{\grave{}} \qquad \frac{di}{dt} = 0 \qquad (4.2)$$

$$\frac{d\Omega}{d\tau} = \Omega^{\grave{}} \qquad \dot{\Omega} = 0$$

$$\frac{d\omega}{d\tau} = \omega^{\grave{}} \qquad \dot{\omega} = 0$$

and

$$\frac{dT_p}{d\tau} = T_p^{\grave{}} \qquad \dot{T}_p = 0$$

The anomalies ν, E, and M (true, eccentric and mean, respectively) each have both kinds of variation. Therefore,

$$\frac{d\nu}{d\tau} = \dot{\nu} + \nu^{\backprime} \tag{4.4}$$

$$\frac{dE}{d\tau} = \dot{E} + E^{\backprime} \tag{4.5}$$

$$\frac{dM}{d\tau} = \dot{M} + M^{\backprime} \tag{4.6}$$

If it is now assumed that the perturbing accelerations are given in a radial, transverse, and normal coordinate system, and are denoted $\dot{r}^{\backprime}$, $r\dot{\nu}^{\backprime}$, and $r\dot{b}^{\backprime}$, then

$$a^{\backprime} = -\frac{2}{3}\, a\, \frac{n^{\backprime}}{n} \tag{4.7}$$

$$e^{\backprime} = \frac{r\,\dot{r}^{\backprime}}{\sqrt{\mu\,p}} \left(\frac{p}{r}\sin\nu\right) + \frac{r^2\,\dot{\nu}^{\backprime}}{\sqrt{\mu\,p}} \left[\left(\frac{p}{r}+1\right)\cos\nu + e\right] \tag{4.8}$$

$$i^{\backprime} = \frac{r^2\,\dot{b}^{\backprime}}{\sqrt{\mu\,p}} \cos u \tag{4.9}$$

$$\Omega^{\backprime} = \frac{r^2\,\dot{b}^{\backprime}}{\sqrt{\mu\,p}}\, \frac{\sin u}{\sin i} \tag{4.10}$$

$$\omega^{\backprime} = u^{\backprime} - \nu^{\backprime} \tag{4.11}$$

$$M^{\backprime} = \sqrt{1-e^2}\,\nu^{\backprime} - \frac{2\,r\,\dot{r}^{\backprime}}{\sqrt{\mu\,a}} \tag{4.12}$$

$$\frac{n^{\backprime}}{n} = \frac{-3}{1-e^2}\left[\frac{r\,\dot{r}^{\backprime}}{\sqrt{\mu\,p}}\left(\frac{e\,p}{r}\sin\nu\right) + \frac{r^2\,\dot{\nu}^{\backprime}}{\sqrt{\mu\,p}}\left(\frac{p}{r}\right)^2\right] \tag{4.13}$$

$$u^{\backprime} = -\,\Omega^{\backprime}\cos i \tag{4.14}$$

$$e\nu^{\backprime} = \frac{r\,\dot{r}^{\backprime}}{\sqrt{\mu\,p}}\left(\frac{p}{r}\cos\nu\right) - \frac{r^2\,\dot{\nu}^{\backprime}}{\sqrt{\mu\,p}}\left(\frac{p}{r}+1\right)\sin\nu \tag{4.15}$$

where

$$p = a(1 - e^2) \tag{4.16}$$

$$\mu = \nu + \omega \tag{4.17}$$

$$M^{\backprime} = -n\, T_p^{\backprime}$$

These equations can now be solved providing the disturbances can be expressed as functions of the time or one of the anomalistic variables. However, a discussion of this solution must be deferred until a discussion of the cause of the disturbance is presented. Before leaving this brief review, however, it is considered advisable to also summarize some of the basic two-body relations required to solve equations (4.4) through (4.6). First,

$$\dot{\nu} = \frac{\sqrt{\mu\, p}}{r^2} \tag{4.18}$$

and

$$\dot{E} = \frac{\sqrt{\mu / a}}{r} \tag{4.19}$$

Thus, time can be eliminated in favor of true anomaly (ν) or eccentric anomaly (E) for integration purposes by introducing

$$\frac{df}{d\nu} = \frac{\frac{df}{d\tau}}{\frac{d\nu}{d\tau}} \tag{4.20}$$

or

$$\frac{df}{dE} = \frac{\frac{df}{d\tau}}{\frac{dE}{d\tau}} \tag{4.21}$$

Then, since

$$\frac{df}{d\tau} = \dot{f} + f^{\backprime} \tag{4.22}$$

Equations(4.4) and (4.18) can be used to obtain the variation in any element with respect to true anomaly as

$$\frac{df}{d\nu} = (\dot{f} + f^{\backprime}) \frac{r^2}{\sqrt{\mu p}} \left(1 - \frac{r^2}{\sqrt{\mu\, p}} \nu^{\backprime}\right) \tag{4.23}$$

if the term

$$\left(\frac{r^2 \nu^{\backprime}}{\sqrt{\mu\ p}}\right)^2$$

is neglected.

Equation (4.23) can be integrated to determine the change in any element due to perturbative accelerations. If the integration limits are 0 to 360°, the changes in the elements will be per anomalistic period. Depending on the element of interest, one of the equations (4.7 through 4.15) is substituted into equation (4.23) for $f^{\backprime}$ along with functions for the radial, transverse, and normal components of perturbative acceleration ($\dot{r}^{\backprime}$, $r\dot{\nu}^{\backprime}$, and $r\dot{b}^{\backprime}$) as determined by the type of perturbative force being considered. Equation (4.25) is then integrated to determine the "delta-element." In some cases, the resulting equation after substitutions is very complex and the integration of equation (4.23) requires sophisticated integration techniques. In such cases, the preciseness of the results is a function of the investment in analysis.

2.4.2.2 Perturbative Acceleration Components

This section lists the perturbative acceleration components due to several sources which are used in conjunction with equations (4.7) through (4.15) and (4.23) to compute the changes in the orbital elements.

2.4.2.2.1 Asphericity of the Earth. From the equations of motion, it can be shown that (as a function of the earth's geopotential Φ) the perturbative acceleration components are

$$\dot{r}^{\backprime} = \frac{1}{K_e^2}\frac{\partial\Phi}{\partial r} + \frac{\mu}{r^2} \tag{4.24}$$

$$r\dot{\nu}^{\backprime} = r\dot{\ell}^{\backprime} = \frac{1}{K_e^2}\frac{1}{r}\frac{\partial\Phi}{\partial\ell} \tag{4.25}$$

$$r\dot{b}^{\backprime} = \frac{1}{K_e^2}\frac{1}{r}\frac{\partial\Phi}{\partial b} \tag{4.26}$$

where an adaptation of the Laplacian expression given by Tesserand gives

$$\Phi = \frac{K_e^2 m}{r}\left[1 + \frac{J_2}{2}\left(\frac{R_e}{r}\right)^2(1 - 3U_z^2) + \frac{J_3}{2}\left(\frac{R_e}{r}\right)^3(3 - 5U_z^2)\right.$$
$$\left. - \frac{J_4}{8}\left(\frac{R_e}{r}\right)^4(3 - 30U_z^2 + 35U_z^2) + \ldots\right] \tag{4.27}$$

with

U_z sin δ

δ geocentric latitude

R_e equatorial radius of the earth

J_p coefficients of zonal harmonics

K_e quasi-gaussian constant

m mass of the earth

Thus, the partials $\partial\Phi/\partial r$, $\partial\Phi/\partial\ell$, and $\partial\Phi/\partial b$ can be evaluated by recognizing, with the aid of Figure 4-1, that

$$\frac{\partial r}{\partial r} = 1 , \quad \frac{\partial r}{\partial \ell} = 0 , \quad \frac{\partial r}{\partial b} = 0, \quad \frac{\partial U_z}{\partial r} = 0 \qquad (4.28)$$

and

$$\Delta\overline{U} = \Delta\ell\overline{V} + \Delta b\overline{W} \qquad (4.29)$$

so that

$$\frac{\partial U_z}{\partial \ell} = V_z \quad ; \quad \frac{\partial U_z}{\partial b} = W_z \qquad (4.30)$$

where

$$\begin{aligned} U_z &= \sin i \sin u \\ V_z &= \sin i \cos u \\ W_z &= \cos i \\ U_z^2 &= 1/2 \sin^2 i(1 - \cos 2u) \\ U_z V_z &= 1/2 \sin^2 i \sin 2u \\ U_z W_z &= \sin i \cos i \sin u \end{aligned} \qquad (4.31$$

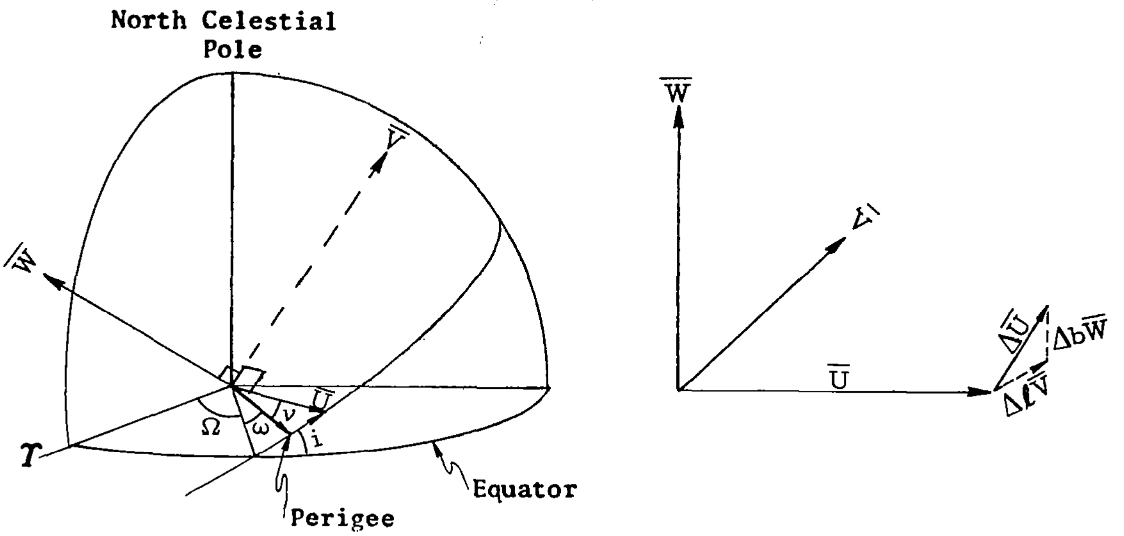

Figure 4-1

When these partials are evaluated, substituted into the equations of motion truncated after the terms J_2, and integrated under the assumptions that the cross-coupling between elements is negligible for one anomalistic period, the following first order secular variations may be obtained.

$$\Omega = \Omega_o - \left[\frac{3}{2} J_2 \left(\frac{R_e}{p}\right)^2 \cos i\right] n\ t \tag{4.32}$$

$$\omega = \omega_o + \left[\frac{3}{4} J_2 \left(\frac{R_e}{p}\right)^2 (4 - 5 \sin^2 i)\right] n\ t \tag{4.33}$$

and

$$M = M_o + nt \left[1 + \frac{3}{2} J_2 \left(\frac{Re}{p}\right)^2 (1 - \frac{3}{2} \sin^2 i)\sqrt{1 - e^2}\right] \tag{4.34}$$

There are no first order secular variations in a, e, and i.

2.4.2.2.2 Luni-Solar Perturbations. The perturbative acceleration components due to a third body such as the moon or the sun may also be defined in terms of a disturbing function (R) since the forces are conservative. Thus,

$$\dot{r}^{\backprime} = \frac{\partial R}{\partial r} \tag{4.35}$$

$$r\dot{\ell}^{\backprime} = \frac{1}{r} \frac{\partial R}{\partial \ell} \tag{4.36}$$

$$r\dot{b}^{\backprime} = \frac{1}{r} \frac{\partial R}{\partial b} \tag{4.37}$$

where for lunar perturbations on a close earth satellite the disturbing function is

$$R = k_e^2 \frac{M_m}{r_m} \left(\frac{r_m}{|\bar{r}_m - \bar{r}|} - \frac{r}{r_m} S \right) \tag{4.38}$$

or

$$R = k_e^2 \frac{M_m}{r_m} \left[\left(1 - 2 \frac{r}{r_m} S + \frac{r^2}{r_m^2} \right)^{-1/2} - \frac{r}{r_m} S \right] \tag{4.39}$$

where

M_m mass of the moon in earth masses

$\bar{r}_m$ geocentric radius vector of moon

$\bar{r}$ geocentric radius vector of satellite

$$S = \frac{\bar{r} \cdot \bar{r}_m}{r \, r_m} = \hat{r} \cdot \hat{r}_m$$

But, since both of the unit vectors required to define S can be represented as

$$\begin{aligned} & r_x = \cos u \cos \Omega - \sin u \sin \Omega \cos i \\ \hat{r} = & r_y = \cos u \sin \Omega + \sin u \cos \Omega \cos i \\ & r_z = \sin u \sin i \end{aligned} \tag{4.40}$$

S can be expressed as

$$\begin{aligned} S = & 1/4(1 - \cos i)(1 - \cos i_m) \cos(\Omega - \Omega_m - u + u_m) \\ & + 1/4(1 + \cos i)(1 + \cos i_m) \cos(\Omega +- \Omega_m + u - u_m) \\ & + 1/4(1 + \cos i)(1 - \cos i_m) \cos(\Omega - \Omega_m + u + u_c) \\ & + 1/4(1 + \cos i)(1 + \cos i_m) \cos(\Omega - \Omega_m - u - u_c) \\ & + 1/2(\sin i \sin i_c \, [\cos(u - u_c) - \cos(u + u_c)] \end{aligned} \tag{4.41}$$

After evaluation and substitution of (4.35), (4.36), and (4.37) into (4.7) through (4.15) and (4.23) the changes in the elements due to a third body can be determined if cross-couplings and motions of the disturbing body during the period of integration are neglected. Once again, it is found that the a, e, a and i have only periodic variations. The secular variations in Ω, ω, and M are given by

$$\frac{d\Omega}{dt} = \frac{-3}{4} \frac{n_m^2}{n} M_m \frac{\cos i}{\sqrt{1 - e^2}} (1 + \frac{3}{2} e^2)(1 - \frac{3}{2} \sin^2 i_m) \qquad (4.42)$$

$$\frac{d\omega}{dt} = \frac{3}{4} \frac{n_m^2}{n} M_m \frac{1}{\sqrt{1 - e^2}} (2 - \frac{5}{2} \sin^2 i + \frac{1}{2} e^2)(1 - \frac{3}{2} \sin^2 i_m) \qquad (4.43)$$

and

$$\frac{dM}{dt} = - \frac{1}{4} \frac{n_m^2}{n} M_m (7 + 3e^2)(1 - \frac{3}{2} \sin^2 i)(1 - \frac{3}{2} \sin^2 i_m) \qquad (4.44)$$

For close earth satellites, lunar and solar perturbations are several magnitudes less than those due to the asphericity of the earth and the effects can generally be neglected. However, for highly eccentric geocentric satellite orbits, or for orbits of high energy, both the periodic solar and lunar perturbations can become substantial.

2.4.2.2.3 Solar Radiation Pressure. Though small (except for satellites of low mass to area ratio), radiation pressure perturbations become more significant than the atmospheric drag for orbits over about 300 NM altitude. These perturbative accelerations are given by

$$\dot{r}' = \frac{\overline{F}_\odot \cdot \overline{U}}{m} \qquad (4.45)$$

$$r\dot{\nu}' = r\dot{\ell}' = \frac{\overline{F}_\odot \cdot \overline{V}}{m} \qquad (4.46)$$

$$r\dot{b}' = \frac{\overline{F} \cdot \overline{W}}{m} \qquad (4.47)$$

where the components of the force $\overline{F}_\odot$ acting on a spherical satellite * due to radiation pressure from the sun can be expressed in an equatorial coordinate system as

$$F_{x_\odot} = -A\, P_\odot\, \gamma\, \nu \cos \ell_\odot \qquad (4.48)$$

$$F_{y_\odot} = -A\, P_\odot\, \gamma\, \nu \cos \varepsilon \sin \ell_\odot \qquad (4.49)$$

$$F_{z_\odot} = -A\, P_\odot\, \gamma\, \nu \sin \varepsilon \sin \ell_\odot \qquad (4.50)$$

---

* If the satellite is irregular, the force must be obtained by integrating the pressure over the illuminated surface.

where

A	effective cross-sectional area of the satellite
$P_{\odot}$	solar radiation pressure in the vicinity of the earth (4.5×10^{-5} dynes/cm^2)
γ	factor depending on the reflective charateristics of the satellite
ν	eclipse factor
ε	obliquity of the ecliptic
$\ell_{\odot}$	true longitude of the sun

The equatorial components of the radial, transverse, and normal unit vectors $\overline{U}$, $\overline{V}$, and $\overline{W}$, respectively are

$$
\begin{aligned}
U_x &= \cos u \cos \Omega - \sin u \sin \Omega \cos i \\
U_y &= \cos u \sin \Omega + \sin u \cos \Omega \cos i \\
U_z &= \sin u \sin i
\end{aligned}
\tag{4.51}
$$

$$
\begin{aligned}
V_x &= - \sin u \cos \Omega - \cos u \sin \Omega \cos i \\
V_y &= - \sin u \sin \Omega + \cos u \cos \Omega \cos i \\
V_z &= \cos u \sin i
\end{aligned}
\tag{4.52}
$$

$$
\begin{aligned}
W_x &= \sin \Omega \sin i \\
W_y &= - \cos \Omega \sin i \\
W_z &= \cos i
\end{aligned}
\tag{4.53}
$$

When the effect of earth's shadow is neglected, there are no secular variations; all elements except a have long period variations which are strong functions of the area to mass ratio. However, the inclusion of the shadow drastically alters the nature of the solution.

2.4.2.2.4 Atmospheric Drag. Formulation of the differential equations for the atmospheric drag perturbations to a satellite orbit is a relatively straightforward problem. The integration and evaluation of the resulting differential equations, however, have been attempted but not rigorously accomplished by numerous investigators using various techniques. The principal difference in these works is the manner in which the exponential density function is developed; there is no evidence that any particular technique is superior for all purposes.

In this section, the basic perturbation expressions will be developed and the major effects of atmospheric decay on the orbit will be discussed under the assumption that the atmosphere is non-rotating and spherically symmetric. A detailed analysis of a much more complete problem is presented in Reference 31.

The components of acceleration due to drag are

$$\dot{r}` = -\frac{\rho_o C_D A}{2 m_s} \frac{\rho}{\rho_o} \dot{r} \dot{s} \tag{4.54}$$

$$r\dot{\nu}` = -\frac{\rho_o C_D A}{2 m_s} \frac{\rho}{\rho_o} r \dot{\nu} \dot{s} \tag{4.55}$$

$$r\dot{b}` = 0 \tag{4.56}$$

where

$\frac{\rho}{\rho_o}$	the density ratio
ρ_o	the density at some reference altitude
C_D	drag coefficient
A	cross-section area of satellite perpendicular to the direction of motion
m_s	satellite mass
$\dot{r}$	radial velocity of satellite
$r\dot{\nu}$	radial velocity of satellite
$\dot{s}$	tangential velocity of satellite

In the literature of this type of analysis, the density ratio appearing in equations (4.54) through (4.56) is inevitably expressed in terms of the exponential function

$$\frac{\rho}{\rho_o} = e^{-K(r-ro)} \tag{4.57}$$

where 1/K is the atmospheric scale height.

If the perigee radius (q) is used as the reference altitude, equation (4.57) becomes

$$\frac{\rho}{\rho_o} = \frac{\rho q}{\rho_o} \; e^{-K(r-q)} \tag{4.58}$$

The perigee radius (q) changes very slowly (Reference 31) in comparison with apogee radius; thus, the exponent (r-q) can be expressed in terms of the true anomaly as

$$(r-q) = a(1 - e)\left\{\frac{1}{1 - \frac{e}{1 + e}\,(1 - \cos \nu)}\right\} \tag{4.59}$$

or in terms of eccentric anomaly as

$$(r - q) = ae(1 - \cos E) \tag{4.60}$$

Therefore, the components of acceleration due to drag can be substituted into equations (4.7) through (4.15) and then into (4.23) to obtain the variations in the elements with respect to the anomalistic variable. The first step in this process is the transformation of the independent variable from time to eccentric anomaly and is accomplished as

$$\frac{df}{dE} = r \sqrt{\frac{a}{\mu}} \; f^{\backprime} \tag{4.61}$$

Equation (4.61) yields the following equations:

$$\frac{da}{dE} = - \frac{C_D \; A \; \rho_o}{m} \frac{\rho}{\rho_o} \, a^2 \, \frac{(1 + e \cos E)^{3/2}}{(1 - e \cos E)^{1/2}} \tag{4.62}$$

$$\frac{de}{dE} = - \frac{C_D \; A \; \rho_o}{m} \frac{\rho}{\rho_o} \; p \cos E \; \frac{(1 + e \cos E)^{1/2}}{(1 - e \cos E)^{1/2}} \tag{4.63}$$

$$e\frac{dM}{dE} = \frac{C_D \; A \; \rho_o}{m} \frac{\rho}{\rho_o} \; a \sin E(1 - e^3 \cos E)\left(\frac{1 + e \cos E}{1 - e \cos E}\right)^{1/2} \tag{4.64}$$

$$\frac{di}{dE} = 0$$

$$\frac{d\Omega}{dE} = 0$$

$$e \frac{d\omega}{dE} = - \frac{C_D A \rho_o}{m} \frac{\rho}{\rho_o} a \sqrt{1 - e^2} \sin E \left(\frac{1 + e \cos E}{1 - e \cos E}\right)^{1/2} \tag{4.65}$$

$$\frac{dp}{dE} = - \frac{C_D A \rho_o}{m} \frac{\rho}{\rho_o} p(1 - e \cos E)^{1/2} (1 + e \cos E)^{1/2} \tag{4.66}$$

$$\frac{dq}{dE} = - \frac{C_D A \rho_o}{m} \frac{\rho}{\rho_o} a\, q(1 - \cos E) \frac{(1 + e \cos E)^{1/2}}{(1 - e \cos E)^{1/2}} \tag{4.67}$$

It is at this point that various techniques have been used by the analysts to integrate the equations (4.62) through (4.67) to determine the lifetime of an earth satellite. Sterne (Reference 12) integrates the rates, defined by equations (4.62) through (4.67), by introducing the new variable

$$y^2 = \nu(1 - \cos E)$$

where

$$\nu = Kae$$

and defining the density ratio ρ/ρ_o in terms of the new variables as follows,

$$\frac{\rho}{\rho_o} = \frac{\rho_q}{\rho_o} e^{-K(r-r_q)} = \frac{\rho_q}{\rho_o} e^{-Kae(1-\cos E)} = \frac{\rho_q}{\rho_o} e^{-\nu(1-\cos E)} = \frac{\rho_q}{\rho_o} e^{-y^2}$$

Now, introducing this definition for the density ratio and the new variable y in equations (4.62) through (4.67) yields, after expansion of the resulting expressions in series truncated to the y^4 power, a sequence of integrals of the form,

$$\int_0^{\sqrt{2\nu}} e^{-y^2} y^n \, dy \qquad n = 0, 2, 4 \tag{4.68}$$

At this point, it should be mentioned that the value of the parameter $\nu = Kae$ is of primary importance. If $\nu \geq 3$, the above integrals can be integrated by letting the upper limit of integration approach ∞ and, for this reason, the solutions are called asymptotic. Thus,

$$\int_0^{\infty} e^{-y^2} y^n \, dy = \frac{\lfloor n - 1 \rfloor}{2^{n/2}} \frac{\sqrt{\pi}}{2} \qquad n = 0, 2, 4 \tag{4.69}$$

However, when $\nu < 3$, no solutions can be obtained by this technique. For such cases, the Bessel function approach must be used, and the respective solutions are called general or standard solutions.

It should be emphasized that the Bessel function technique can be used for both cases; that is, both for $\nu \geq 3$ and $\nu < 3$. The technique itself is simple and elegant. It consists in expanding the integrands of the definitions (4.62) through (4.67) directly in powers of (cos E), resulting in expressions (for the secular rates of the orbital elements) of the general form,

$$\dot{\psi}_{sec} = -\left(\frac{\text{CONST}}{P}\right)\rho_q\, e^{-\nu} \int_0^{2\pi} e^{\nu\cos E} [\alpha_0 + \alpha_1 \cos E + \alpha_2 \cos^2 E$$

$$+ \alpha_3 \cos^3 E + \alpha_4 \cos^4 E + \ldots]\, dE \tag{4.70}$$

where $\dot{\psi}_{sec}$ denotes the secular rate of any orbital element and P the orbital period.

Next, the modified Bessel functions of the first kind of the first and second orders, $I_0(\nu)$ and $I_1(\nu)$, of the parameter ν are introduced through the following well-known definitions for the case of $\nu < 3$; that is, for the general or standard case,

$$\frac{1}{2\pi}\int_0^{2\pi} e^{\nu\cos E}\, dE = I_o(\nu)$$

$$\frac{1}{2\pi}\int_0^{2\pi} e^{\nu\cos E} \cos E\, dE = I_1(\nu)$$

$$\frac{1}{2\pi}\int_0^{2\pi} e^{\nu\cos E} \cos^2 E\, dE = I_0(\nu) - \frac{I_1(\nu)}{\nu}$$

$$\frac{1}{2\pi}\int_0^{2\pi} e^{\nu\cos E} \cos^3 E\, dE = -\frac{I_0(\nu)}{\nu} + \left(1 + \frac{2}{\nu^2}\right) I_1(\nu)$$

$$\frac{1}{2\pi}\int_0^{2\pi} e^{\nu\cos E} \cos^4 E\, dE = \left(1 + \frac{3}{\nu^2}\right) I_o(\nu) - \frac{2}{\nu}\left(1 + \frac{3}{\nu^2}\right) I_1(\nu)$$

Substitution of these definitions in the expressions for $\dot{\psi}_{sec}$ yields the general or standard solutions ($\nu < 3$) in the following form,

$$\dot{\psi}_{sec} = -\left(\frac{CONST}{P}\right) 2\pi\ \rho_q\ e^{-\nu} \left[\left(\alpha_o + \alpha_2 + \alpha_4 - \frac{\alpha_3}{\nu} + \frac{3\alpha_4}{\nu^2}\right) I_o(\nu) + \left(\alpha_o - \frac{4\alpha_1}{\nu} - \frac{16\alpha_o\ e}{\nu}\right) I_1(\nu) \right] \tag{4.71}$$

In order to obtain the asymptotic solutions for eccentric orbits (that is, when $\nu \geq 3$), the general modified Bessel functions $I_o(\nu)$ and $I_1(\nu)$ must be replaced by their respective asymptotic definitions as follows.

$$I_o(\nu) = \frac{e}{\sqrt{2\pi\nu}} \left(1 + \frac{1}{8\nu} + \frac{9}{128\nu^2} + \frac{75}{1024\nu^3} + \ldots\right) = \frac{e^{\nu}}{\sqrt{2\pi\nu}} G_o(\nu)$$

$$I_1(\nu) = \frac{e}{\sqrt{2\pi\nu}} \left(1 - \frac{3}{8\nu} - \frac{15}{128\nu^2} - \frac{105}{1024\nu^3} + \ldots\right) = \frac{e^{\nu}}{\sqrt{2\pi\nu}} G_1(\nu)$$

Thus, substitution of these asymptotic definitions yields

$$\dot{\psi}_{sec} = -\left(\frac{CONST}{P}\right) \rho_q \sqrt{\frac{2\pi}{\nu}} \left[\left(\alpha_o + \alpha_2 + \alpha_4 - \frac{\alpha_3}{\nu} + \frac{3\alpha_4}{\nu^2}\ G_o(\nu)\right) + \left(\alpha_o - \frac{4\alpha_1}{\nu} - \frac{16\alpha_o\ e}{\nu}\right) G_1\ (\nu) \right] \tag{4.72}$$

The method just reported is presented in detail in the original reference and in Reference 31. There is, however, one major failing arising from the fact that an analytic solution was sought at the expense of precision in the model. It is true that values of ρ_o can be obtained from very sophisticated atmospheric models to improve the degree of approximation, but the model error cannot be removed without revising the formulation of the problem by including more terms in the expansions of the density and of the orbital parameters.

Several standard atmospheric models have been developed in the past by various agencies which are suited for use in the previous section. The list includes the ARDC Standard Atmospheres of 1959, 1962, etc., the 1963 Patrick AFB Reference atmosphere model and others which have been adopted for special cases. Such atmospheres are of doubtful value in predicting satellite lifetimes unless dynamic atmospheric corrections are made for the influence of the sun.

At altitudes above 200 KM (656,000 ft) significant fluctuations in atmospheric density are produced by solar ultraviolet and corpuscular emissions which, in turn, considerably affect the lifetime of a satellite by producing non-uniform drag, even when the projected drag area is constant.

The ultraviolet solar emissions are: diurnal, seasonal, and 27-day periodic. The last one corresponds to the period of the sun's rotation.

1. The diurnal ultraviolet radiation heats the upper atmosphere by conduction, which then expands producing fluctuations in atmospheric density proportional to the degree of heating. The maximum heating occurs on the side of the earth facing the sun at the latitude of the subsolar point and about 30° east from the point itself. The 30° or 2 hour lag in time with the sun is due to the rotation of the earth and the time required for the atmosphere to reflect the new conditions.

The diurnal effect of solar ultraviolet radiation increases with altitude and at 270 NM (500 KM) may affect lifetime by as much as 20 percent.

2. The seasonal fluctuations of atmospheric density occur as a result of variation in latitude of the subsolar point during the year.

The functional dependence of both diurnal and seasonal atmospheric density fluctuations, on the position of the subsolar point relative to the orbital plane (more precisely the perigee direction), is analytically expressed by the angle ψ subtended by the respective two directions, allowing for the 30° lag in the right ascension of the sun,

$$\cos \psi = \sin \Phi_s \sin \Phi_p + \cos \Phi_s \cos \Phi_p \cos[(\alpha_s - \Omega) - (\alpha_p - \Omega) + 30^\circ]$$

where the subscript p stands for perigee and s for the sun.

The effect of diurnal and seasonal atmospheric density fluctuations on orbital lifetime can be minimized by orienting the orbital plane so that it is normal to the vector from the center of the earth to the atmosphere bulge produced by solar radiation.

The maximum lifetime loss occurs when the orbital plane lies in the ecliptic.

3. The periodic 27-day solar ultraviolet emissions, corresponding to the period of the sun's rotation about its axis, are more intense in nature than the diurnal and seasonal emissions. Their effect is fairly well represented by the smoothed monthly average of the decimetric solar flux daily indices of 10.7 cm wave radiation in units of 10^{-22} watt/m^2/cps bandwidth. The values of these smoothed monthly indices, denoted by $\overline{F}_{10}$, typically range between 70 (during the period of quiet solar activity) to 220 (during the period of intense solar activity).

The corpuscular solar emissions inject particles into the upper atmosphere producing an increase in atmospheric density. This type of solar activity has a cyclic period of 11 years, which is directly related to the sunspot rate. Its effect on orbital lifetime is far greater than the diurnal and seasonal ultraviolet solar radiation effects.

Comparison of its effect with that of the 27-day solar ultraviolet activity indicates a strong correlation between the 11-year cycle corpuscular emissions and the smoothed monthly solar flux indices $\overline{F}_{10}$. Therefore, the smoothed monthly indices may be used to represent both the 27-day ultraviolet and the 11-year corpuscular solar radiation effects.

2.4.3 Earth Trace

Precision earth trace computation for orbits around an oblate earth requires numerical integration techniques because of the many perturbations on the orbit. The expressions developed below, however, will enable computation of a first order ground track over an oblate earth since first order secular perturbations arising from the effects discussed on the previous pages can be considered.

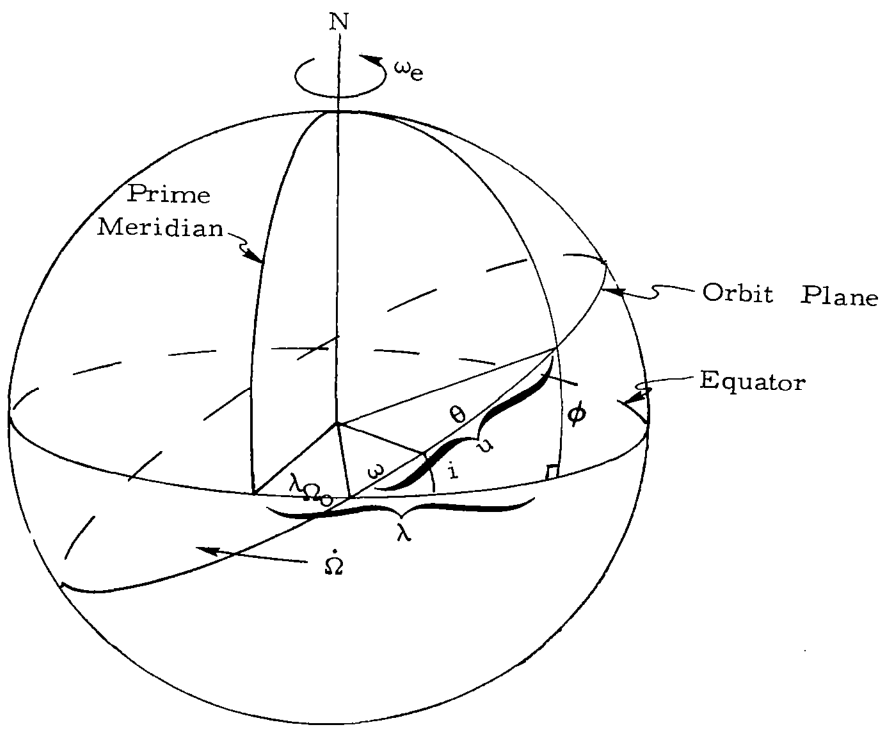

Figure 4-2

Referring to Figure 4-2, the expressions for geocentric latitude and longitude at some time (t) are seen to be

$$\phi = \sin^{-1}[\sin(i + \Delta i)\ \sin(u + \Delta u)] \tag{4.73}$$

$$\lambda = \tan^{-1}[\cos(i + \Delta i)\ \tan(u + \Delta u)] + \lambda_{\Omega_o} - \omega_e\ \Delta t + \Delta\Omega \tag{4.74}$$

where the terms Δi, Δu, and $\Delta\Omega$ are the result of the previously defined perturbations, i.e.,

$$\Delta i = \sum_{j=1}^{n} \Delta i_j \tag{4.75}$$

$$\Delta\Omega = \sum_{j=1}^{n} \Delta\Omega_j \tag{4.76}$$

$$\Delta u = \sum_{j=1}^{n} \Delta u_j \tag{4.77}$$

In order to utilize (4.73) and (4.74) to obtain the earth trace it is necessary to obtain $u = f(t)$. This is no problem for circular orbits but for elliptical orbits the procedure is complicated by the fact that iteration of a transcendental equation is required. However, for elliptical orbits u can be found from a Fourier-Bessel series* expansion as

$$u = \omega + 2e \sin n\ t + \frac{5}{4} e^2 \sin^2 n\ t + \ . \ . \ . \tag{4.78}$$

The argument of perigee (ω) in this solution is not a constant as in two-body mechanics since there are secular affects produced by the perturbing influences. Thus, this variability must be modeled by evaluating the change produced by all influences. The computation of the earth trace can now proceed using equations (4.73)and (4.74).

2.4.4 Earth Coverage

The previous section described a technique for computing the latitude and longitude at any time during the orbit. This section will describe the area on the surface of the earth that is visible at any given time in the orbit for the purpose of relating visibility constraints to the dynamics of the problem.

---

* retaining terms through order e^2

At any instant of time, the maximum half width of the area which is visible from a given altitude as can be seen in Figure 4-3* is

$$d = R_e \theta = R_e \cos^{-1}\left(\frac{R_e}{R_e + h}\right) \tag{4.79}$$

where

$\cos^{-1}\left(\frac{R_e}{R_e + h}\right)$ is in radians

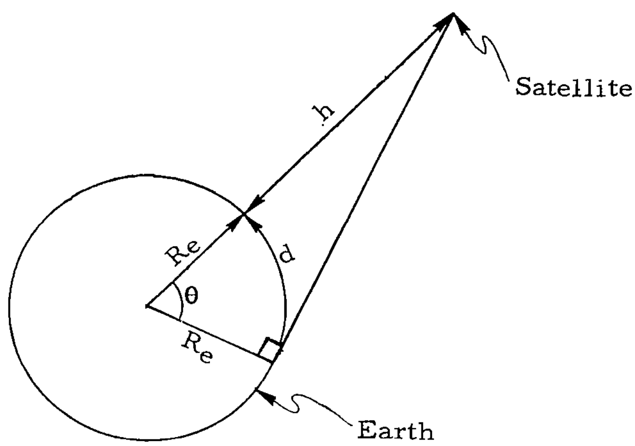

Figure 4-3

If the sensor viewing half angle is restricted to α , it can be shown from Figure 4-3 that the half-width visible from the satellite is given by

$$d = R_e \theta = R_e \left[\sin^{-1}\left(\frac{R_e + h}{R_e} \sin\alpha\right) - \alpha\right] \tag{4.80}$$

where the angle in the brackets is in radians and

$$0 \leq \sin^{-1}\left(\frac{R_e + h}{R_e} \sin \alpha\right) \leq \frac{\pi}{2} .$$

* The analysis will concern itself with a spherical earth. The error is not large and is generally neglected for most preliminary studies; however, if desired, this error can be eliminated at the expense of considerable complexity.

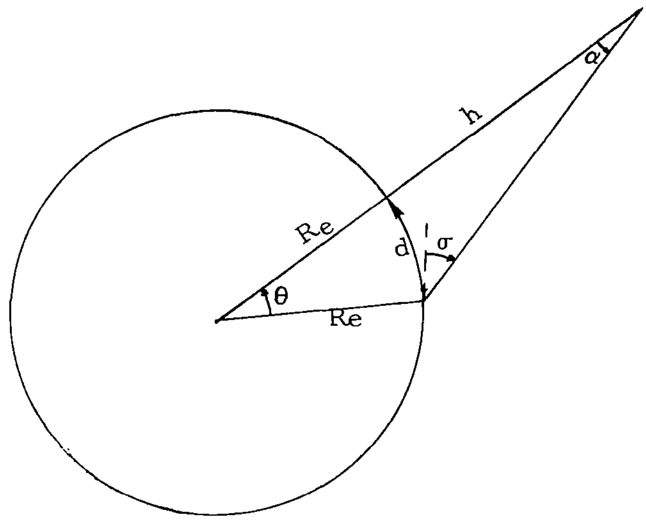

Figure 4-4

or alternately if the minimum angle of incidence at the earth (σ) is specified, the half-width is given by

$$d = R_e\ \theta = R_e \left[\cos^{-1}\left(\frac{R_e \cos \sigma}{R_e + h}\right) - \sigma\right] \tag{4.81}$$

where

$$0 < \cos^{-1}\left(\frac{R_e \cos \sigma}{R_e + h}\right) \leq \frac{\pi}{2}$$

Thus, the latitude and longitudes of the perimeter points of the area of visibility described in equations (4.79), (4.80), and (4.81) can be determined as follows.

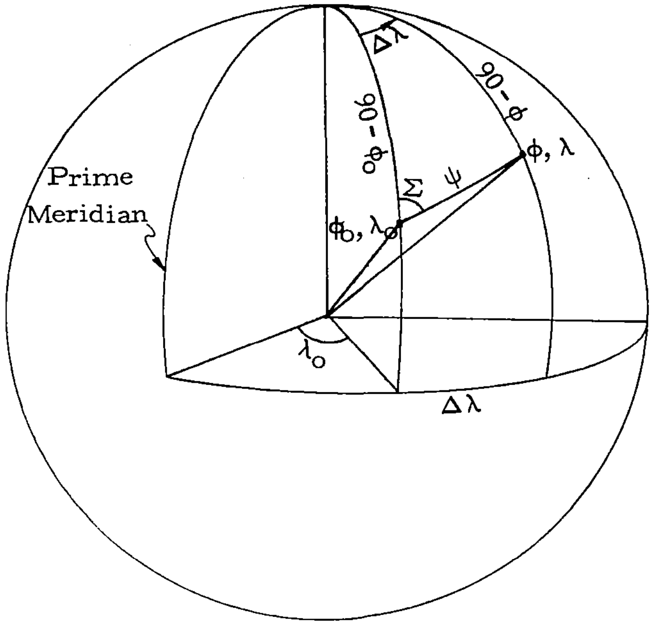

Figure 4-5

In Figure 4-5 assume ϕ_o and λ_o are the instantaneous latitude and longitude, respectively, of the satellite. Then, the latitude and longitude of an arbitrary point on the perimeter of the visible area of angular radius θ are given by ϕ and λ where

$$\lambda = \lambda_o + \Delta\lambda \tag{4.82}$$

but from the law of cosines

$$\cos(90 - \phi) = \cos(90 - \phi_o) \cos \psi + \sin(90 - \phi_o) \sin \psi \cos \Sigma \tag{4.83}$$

or

$$\sin \phi = \sin \phi_o \cos \psi + \cos \phi_o \sin \psi \sin \Sigma \tag{4.84}$$

where Σ is the azimuth of the radial arc θ and is the independent variable used to generate the perimeter.

Then

$$\sin \Delta\lambda = \frac{\sin \psi \sin \Sigma}{\sin(90 - \phi)} = \frac{\sin \psi \sin \Sigma}{\cos \phi} \tag{4.85}$$

Equations (4.82), (4.83), and (4.85) can now be used to generate the latitude, longitude locus of the area visible from an instantaneous satellite position with a visibility arc on the earth's surface of θ.

As a satellite moves along its orbit, the perimeter of the ground area covered for each point sweeps out a swath all points within which are visible from the satellite at some time during the orbit. The edges of this swath may be computed from equations (4.84) and (4.85) by setting

$$\Sigma = \Sigma_o \pm 90^\circ \tag{4.86}$$

where Σ_o is the orbit azimuth relative to the rotating earth at point ϕ_o, λ_o, and where the relative azimuth Σ_o may be computed as follows. Consider the component of velocity parallel to the earth surface (V_T) as given by

$$V_T = V_o \cos \gamma_o \tag{4.87}$$

where V_o is the orbital velocity at the point ϕ_o, λ_o

γ_o is the flight path angle at ϕ_o, λ_o

Now consider the components of velocity due to the earth's rotation as given by

$$V_e = R_e \, \omega_e \cos \phi_o \tag{4.88}$$

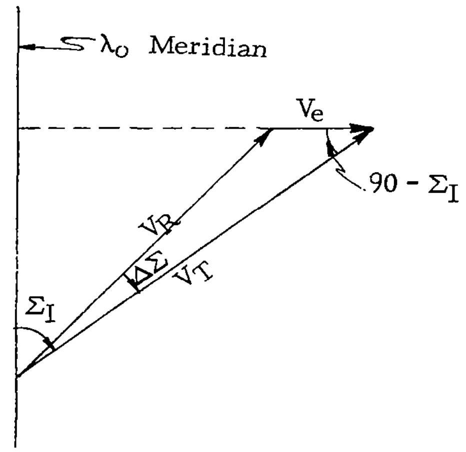

Figure 4-6

Finally, consider Figure 4.6 and observe that Σ_I is the inertial azimuth at ϕ_o, λ_o and that

$$\Delta\Sigma = \Sigma_I - \Sigma_o \tag{4.89}$$

But since

$$V_R^2 = V_e^2 + V_T^2 - 2V_e V_T \sin \Sigma_I \tag{4.90}$$

and since

$$\Delta\Sigma = \sin^{-1}\left(\frac{V_e}{V_R} \cos \Sigma_I\right) \tag{4.91}$$

the desired result is

$$\Sigma_O = \Sigma_I - \Delta\Sigma \tag{4.92}$$

From the equations of the previous sections it is possible to compute earth coverage conditions for a rotating oblate earth for as many points as desired. However, in some cases satisfactory results involving far fewer calculations may be obtained by computing an earth coverage swath for one satellite revolution and then shifting this pattern from revolution to revolution. In this process, the longitudinal shift of the ground track and, therefore, of the swath is defined by

$$\Delta\lambda_\tau = \omega_e \tau_{nodal} + \Delta\Omega \tag{4.93}$$

where τ_{nodal} is the nodal period of the satellite orbit. This nodal period is not be to be confused with the anomalistic period or with an "inertial" period since they are all slightly different if perturbations are being included. A discussion of this aspect of the problem is presented in Reference 31.

2.4.5 Tracking

One of the basic aspects of the tracking problem is the determination of the tracking station coverage as a function of the spatial trajectory since after tracking station coverage has been ascertained, detailed trajectory predictions in an observer centered coordinate system can be determined. Thus, it is of interest that a simplified technique exists which can be used either to determine for a particular orbit the tracking coverage available from an existing set of stations or to determine the optimum locations of tracking stations for the coverage requirements of an orbit. This technique is described in subsequent paragraphs.

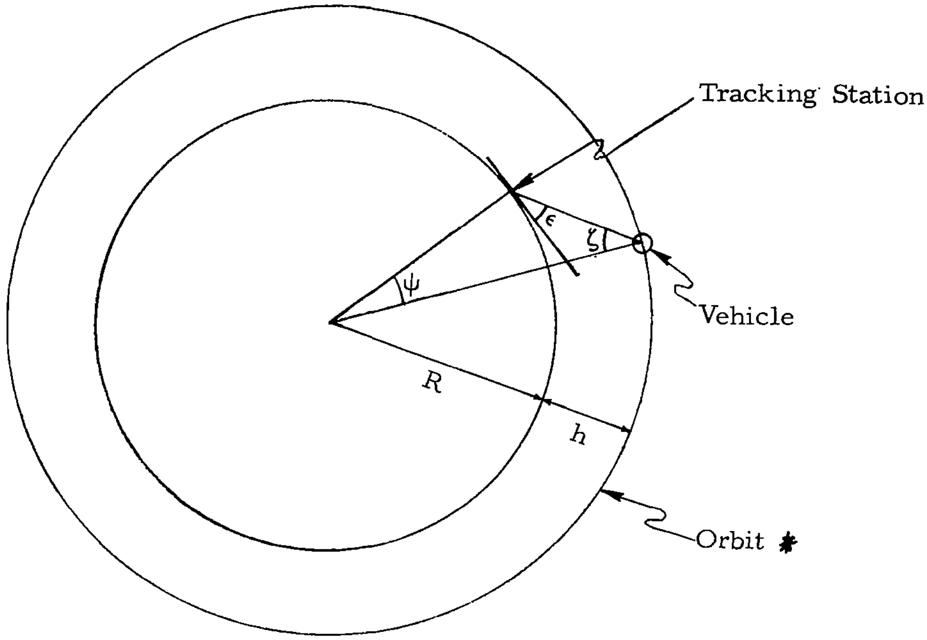

Figure 4-7

Consider Figure 4-7 showing the relationship between the elevation angle (ε) from the station to the vehicle, the altitude (h) of the vehicle and the great circle angle ψ between the station and the vehicle. It can be seen that

$$\zeta = \sin^{-1}\left[\frac{R \sin(90 + \varepsilon)}{R + h}\right] \tag{4.94}$$

and

$$\psi = 90 - (\varepsilon + \zeta) \tag{4.95}$$

Thus, if a minimum elevation angle ε_M(mask angle) is specified, the maximum great circle arc between the station and the vehicle is

$$\psi_{max} = 90 - (\varepsilon_M + \zeta) \tag{4.96}$$

The angle ψ_{max} can then be used to define the locus of subsatellite points around any tracking station within which the satellite will be visible at an elevation > ε_M. The geographic locus of subsatellite points is computed in a similar manner as the earth coverage calculations given in the section on satellite surveillance. That is, from Figure 4-8

* The orbit illustrated is circular; however, the results can be applied to other conic sections provided h is expressed as a f(t).

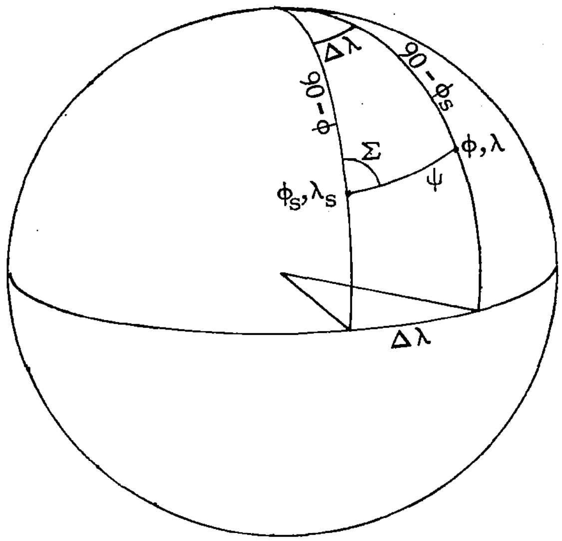

Figure 4-8

$$\sin \phi = \sin \phi_s \cos \psi + \cos \phi_s \sin \psi \cos \Sigma \tag{4.97}$$

and

$$\sin \Delta\lambda = \frac{\sin \Sigma \sin \psi}{\cos \phi} \tag{4.98}$$

$$\lambda = \lambda_o + \Delta\lambda \tag{4.99}$$

where

ϕ_s station latitude

λ_s station longitude

ϕ latitude of arbitrary point on perimeter of coverage area

λ longitude of arbitrary point on perimeter of coverage area

Σ azimuth from north to point on perimeter of coverage area along arc ψ (independent variable)

$\Delta\lambda$ delta-longitude between station and perimeter point

These equations yield the areas of visibility around given stations as a simple function of orbit altitudes for circular orbits. Then using the techniques of section 2.4.3, the earth trace of the orbit can be superimposed and the tracking station coverage ascertained. This technique can be used to determine coverage or optimize tracking station locations for a given orbit. However, after coverage by a particular station has been affirmed, the predicted position history in station centered coordinates is of interest to aid in the tracking of the vehicle as it passes over the station. The topocentric coordinates of the vehicle can be calculated as follows.

Figure 4-9 illustrates the geometry of a vehicle position in terms of the inclination and node of the orbit a plane, the argument of latitude (u) at some time (t) and the radius (r).

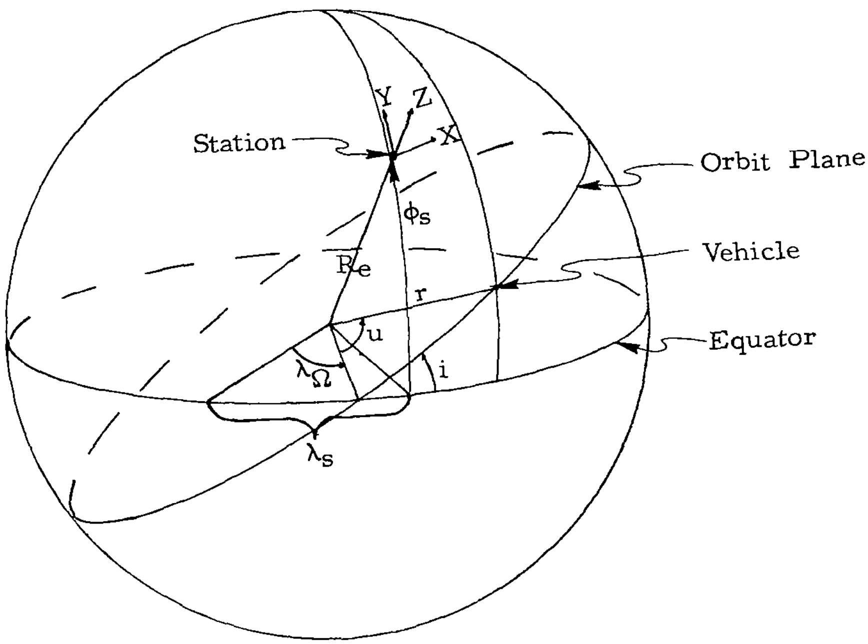

Figure 4-9

Figure 4-9 also illustrates a topocentric coordinate system with the Z axis normal to the surface, the X axis due east, and the Y axis due north. This system is described by the latitude (ϕ_s) and longitude (λ_s) of the station.* Now, the difference in longitudes of the satellite node and the station at time (t) is given by

$$\Delta\lambda_s = (\omega_e + \dot{\Omega})t + \lambda_1 \tag{4.100}$$

where

ω_e angular rotation of the earth

$\dot{\Omega}$ nodal regression rate

t time since t_o

λ_1 longitude of station at t_o - longitude of node at t_o

Thus, the coordinates of the satellite in the topocentric coordinate system are

$$x = r(\cos i \sin u \cos \Delta\lambda_s - \cos u \sin \Delta\lambda_s) \tag{4.101}$$

$$\begin{aligned} y = r[&\cos \phi_s \sin i \sin u - \sin \phi_s(\cos u \cos \Delta\lambda_s \\ &+ \cos i \sin u \sin \Delta\lambda_s)] \end{aligned} \tag{4.102}$$

$$\begin{aligned} z = r[&\sin \phi_s \sin i \sin u + \cos \phi(\cos u \cos \Delta\lambda_s \\ &+ \cos i \sin u \sin \Delta\lambda_s)] - R_e \end{aligned} \tag{4.103}$$

These equations yield the range (ρ) from the station to the satellite as

$$\rho = \sqrt{x^2 + y^2 + z^2} = \sqrt{r^2 + R_e - 2r\, R_e \cos \psi} \tag{4.104}$$

and the direction cosine (ℓz) of the zenith angle (the angle from the Z axis to the station satellite line) as

$$\ell_z = \frac{Z}{\rho} = \frac{r \cos \psi - R}{\sqrt{r^2 + R - 2r\, R_e \cos \psi}} \tag{4.105}$$

---

* for a spherical earth

This latter equation can be used to determine visibility of a satellite from a station as follows.

If $\ell_z > 0$ the satellite is visible.

If $\ell_z > \cos(90 - \epsilon_M)$ the satellite is visible above an elevation mask of ϵ_M.

This discussion has, therefore, established the relationships which exist between the orbit and visibility at a station. Obviously, the modeling can be made more precise. However, for most preliminary applications, the added complexity is unjustified.

2.4.6 Lighting

2.4.6.1 Introduction

Lighting constraints may be imposed during the design of a mission for a number of reasons; for example,

a. Thermal/environmental control

b. Navigation

c. Subsatellite illumination requirements

d. Electrical power supply (solar cells)

e. Scientific experiments

However, the lighting parameter of primary interest is whether the vehicle is in sunlight or darkness at a particular time; in addition, the times of entrance into and exit from the earth shadow are of interest if these are periods of darkness during an orbit since these times define the illumination duration. Also of interest may be the orientation of the earth-sun line with respect to the orbit plane.

2.4.6.2 Eclipse Geometry

A schematic of the earth shadow geometry is presented in Figure 4-10*. This figure shows the umbra (the region of complete eclipse of the sun by the earth) and the penumbra (the region of partial eclipse, i.e., a portion of the sun's disk is always visible).

---

* The affect of atmospheric refraction will not be modeled.

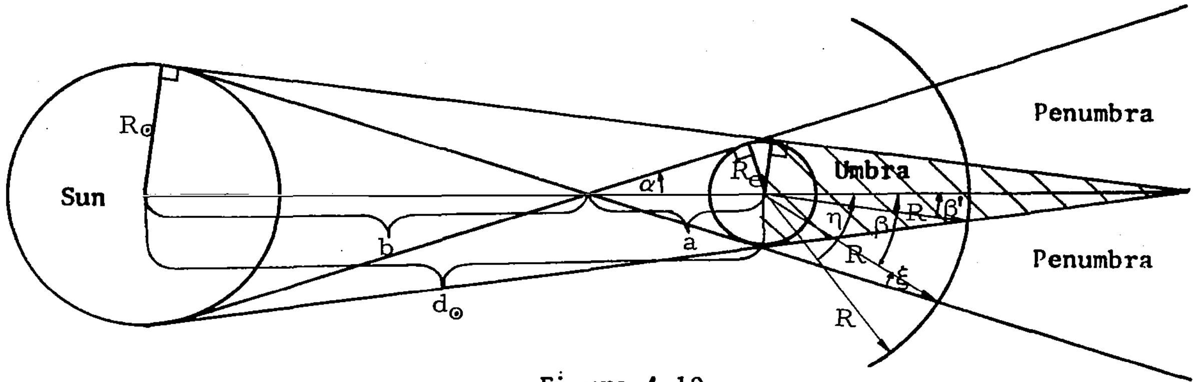

Figure 4-10

This figure allows computation of the angular size of the earth's shadow at a radius (R) to be performed as follows:

2.4.6.2.1 Penumbra

From Figure 4-11 it can be seen that

$$\sin \alpha = \frac{R_e}{a} = \frac{R_{\odot}}{b} \tag{4.106}$$

and

$$d_{\odot} = a + b \tag{4.107}$$

Thus, equations (4.106) and (4.107) can be solved yielding

$$a = \frac{R_e \, d_{\odot}}{R_{\odot} + R_e} \tag{4.108}$$

$$\alpha = \sin^{-1}\left(\frac{R_e}{a}\right) \qquad 0 < \alpha < 90^\circ \tag{4.109}$$

Then

$$\xi = \sin^{-1}\left(\frac{a \sin \alpha}{R}\right) \tag{4.110}$$

and

$$180 - \beta = 180 - (\alpha + \xi) \tag{4.111}$$

giving the penumbra angular size at R.

$$\beta = \alpha + \xi \tag{4.112}$$

2.4.6.2.2 Umbra

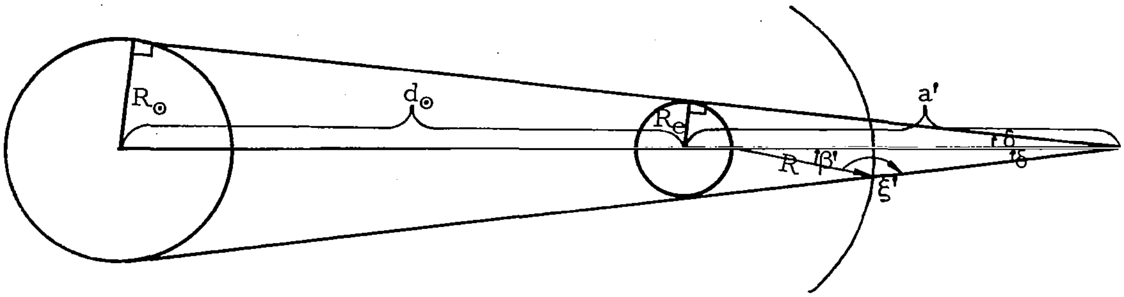

Figure 4-11

From Figure 4-11 it can be seen that

$$\sin \delta = \frac{R_e}{a'} = \frac{R_\odot}{a' + d_\odot} \tag{4.113}$$

giving

$$a' = \frac{R_e \, d_\odot}{R_\odot - R_e} \tag{4.114}$$

and

$$\delta = \sin^{-1}\left(\frac{R_e}{a'}\right) \tag{4.115}$$

Thus,

$$\xi' = \sin^{-1}\left(\frac{a' \sin \delta}{R}\right) \tag{4.116}$$

and the angular size of the umbra at R is

$$\beta' = 180 - (\delta + \xi') \tag{4.117}$$

2.4.6.2.3 Shadow Discriminant

If $\overline{S}$ is a unit vector in the direction of the sun and $\overline{R}$ is the position vector of the satellite as in Figure 4-12, then

$$\cos(180 - \eta) = \frac{\overline{R} \cdot \overline{S}}{|\overline{R}|}$$

or

$$\eta = \cos^{-1}\left(- \frac{\overline{R} \cdot \overline{S}}{|\overline{R}|}\right) \tag{4.118}$$

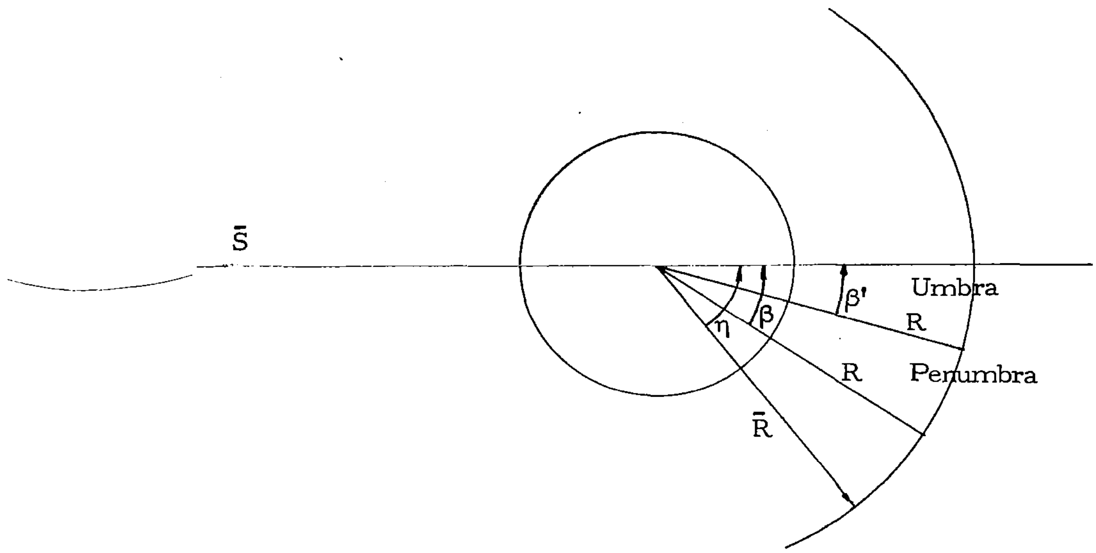

Figure 4-12

Thus, the lighting conditions of the vehicle at $\bar{R}$ can be determine from the following criteria

$\eta > \beta$	Vehicle in full sunlight
$\beta > \eta > \beta'$	Vehicle in penumbra
$\beta < \beta'$	Vehicle in umbra (i.e., completely eclipsed)

if the effect of atmospheric refraction on the shadow dimensions can be neglected in the analysis.

2.4.6.3 Relation to Orbits

Consider a low eccentricity earth orbit defined by the elements a, e, i, Ω, ω, and time of perifocal passage. Assume the ecliptic as the reference plane and the vernal equinox as the reference direction. The geometry of the orbit passage through the shadow is represented in Figure 4-13.

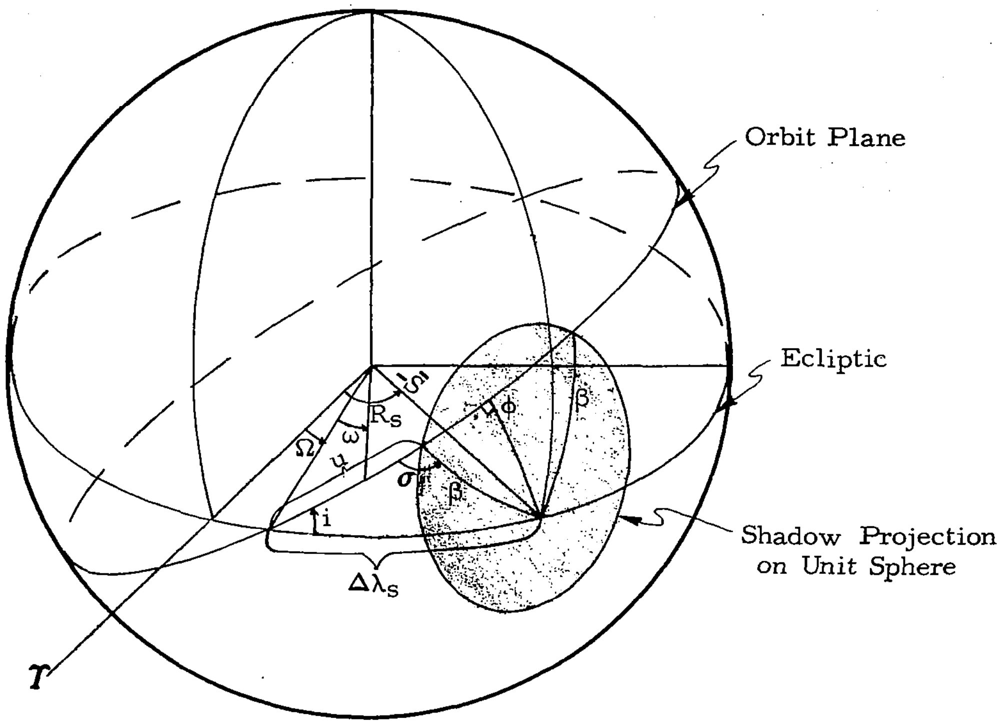

Figure 4-13

The shaded region in the diagram is the projection of the shadow onto the unit sphere. The angular radius β of the spherical segment is symbolic and can be either the size of the shadow at radius R for entrance into the penumbra or the size of the shadow for entrance into the umbra (β or β' of the previous section). However, for either case, entrance into the shadow can be determined from the following

$$\phi = \sin^{-1}(\sin \Delta\lambda_s \sin i) \qquad 0 < \phi < 90° \qquad (4.119)$$

where

$$\Delta\lambda_s = \lambda_s - \Omega \qquad (4.120)$$

$$\lambda_s = \lambda_\odot + 180 \qquad (4.121)$$

Then for

$\phi > \beta$ the orbit does not pass through the shadow

$\phi < \beta$ the orbit passes through the shadow.

If the orbit passes through the shadow, the time of entrance and exit can be determined from Figure 4-13 once the spherical triangle $(u, \beta, \Delta\lambda_s)$ is known. This solution, in turn, requires the computation of σ

$$\sigma = \sin^{-1}\left(\frac{\sin \Delta\lambda_s \sin i}{\sin \beta}\right) \tag{4.122}$$

Two solutions are obtained for σ from equation (4.122) corresponding to entrance into and exit from the shadow. Let σ_i, $i = 1, 2$, signify the two values of σ; then, the arguments of latitude corresponding to the two values of σ can be found from Napier's analogies giving

$$u_i = 2 \tan^{-1}\left\{\frac{\tan\left(\frac{\Delta\lambda - \beta}{2}\right)\sin\left(\frac{\sigma_i + i}{2}\right)}{\sin\left(\frac{\sigma - i}{2}\right)}\right\} \tag{4.123}$$

Thus, the true anomalies of entrance and exit are

$$\theta_i = u_i - \omega \qquad i = 1, 2 \tag{4.124}$$

where the smaller value of θ_i will correspond to entrance into the shadow and the larger to exit. The time since perifocal passage of entrance into and exit from the shadow may then be found from

$$E_i = \cos^{-1}\left(\frac{\cos \theta_i + e}{1 + e \cos \theta}\right) \qquad i = 1, 2 \tag{4.125}$$

where quadrant adjustments for E are made by inspection of θ, and

$$M_i = E_i - e \sin E_i \qquad i = 1, 2 \tag{4.126}$$

Then the times of entry and exit are

$$T_i = \frac{M_i}{\sqrt{\mu}} a^{3/2} \qquad i = 1, 2 \tag{4.127}$$

2.4.6.4 Shadow Ellipse Approximation

The previous analysis presented a technique whereby penumbral and umbral lighting conditions for circular or near circular orbits can be computed.*

* The restriction to circularity arises from the fact that the arc β was used to define both limits of the shadow. In general, noncircular orbits would be characterized by distinct values of β for entrance and exit from the shadow.

However, for orbits within an altitude of one earth radius, lighting conditions may be computed, assuming a cylindrical earth shadow and the results will be accurate to within an order of 1 percent of the orbital period. The following analysis outlines the technique for the cylindrical shadow approach.

If the shadow is assumed to be cylindrical, the intersection of the orbit plane and the shadow will form a semi-ellipse which can be constructed once the angle between the earth-sun line and the orbit plane is known. This angle can be easily computed from the earth-sun vector and the vehicle position and velocity vectors ($\overline{R}$ and $\overline{V}$) at some time T as follows.

The unit vector normal to the orbit plane is given by

$$\overline{W} = \frac{\overline{R} \times \overline{V}}{|\overline{R} \times \overline{V}|} \tag{4.128}$$

Thus, the angle (ψ) between the orbit plane and the sun vector ($\overline{S}$) can be computed as

$$\cos(90 - \psi) = \overline{W} \cdot \overline{S}$$

or

$$\psi = 90° - \cos^{-1}(\overline{W} \cdot \overline{S}) \tag{4.129}$$

But from Figure 4-14, it can be seen that the semi-major axis of the shadow ellipse is given by

$$a_s = \frac{R_e}{\sin \psi} \tag{4.130}$$

and the semi-major axis

$$b_s = R_e$$

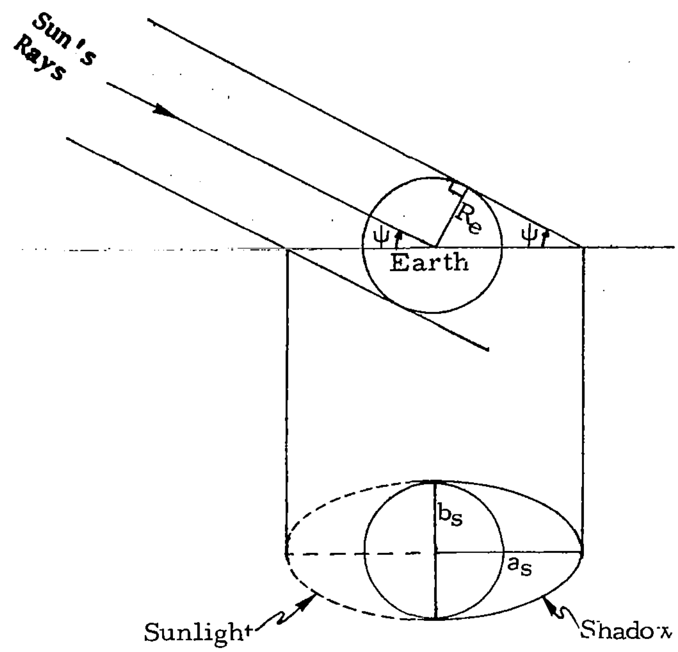

Figure 4-14

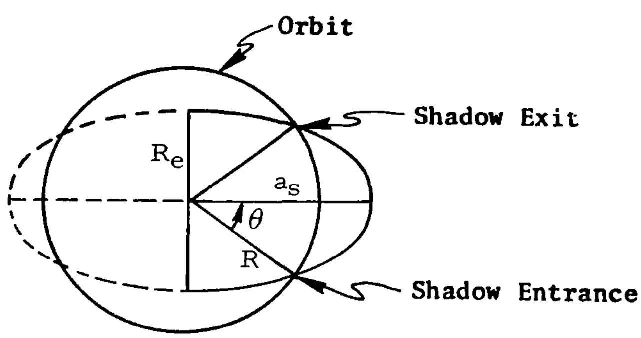

Figure 4-15

Now, from Figure 4-15 it can be seen that the duration in the shadow is the time for passage of the satellite through an angle of 2θ*where

$$\theta = \sin^{-1}\left(\frac{R_e}{R}\sqrt{\frac{a_s^2 - R^2}{a_s^2 - R_e^2}}\right) \tag{4.131}$$

The time in the shadow is then

$$\Delta t = 2\theta/n \tag{4.132}$$

---

* Again circular orbits or very special elliptic orbits are assumed.

where

$$n = \frac{\sqrt{\mu}}{a^{3/2}} \tag{4.133}$$

The shadow ellipse technique can also be applied to elliptical orbits. See Figure 4-16.

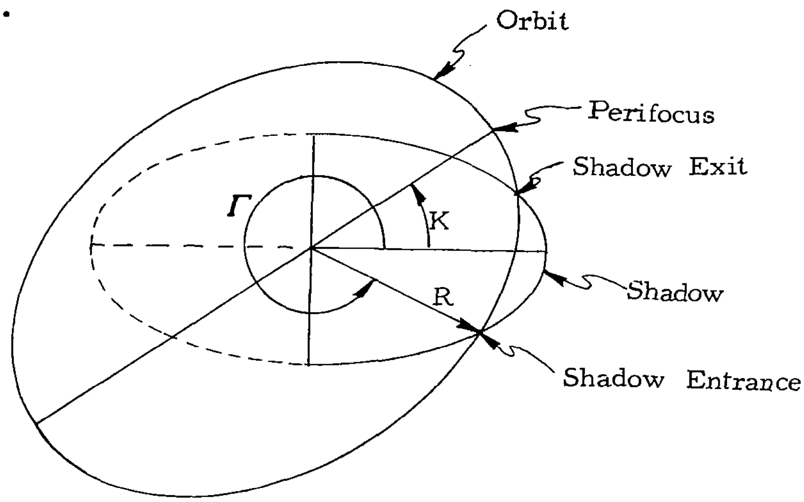

Figure 4-16

To compute the lighting conditions in the elliptical orbit, it is necessary to compute the intersections of the shadow ellipse and the elliptical orbit. This computation can be accomplished from the polar equation of the shadow ellipse

$$R = \frac{a_s^2 \, R_e^2}{a_s^2 \sin^2\Gamma + R_e^2 \cos^2\Gamma} \tag{4.134}$$

and the orbit equation

$$R = \frac{a(1 - e^2)}{1 + e \cos(\Gamma - K)} \tag{4.135}$$

The solution of (4.134) and (4.135) yields a fourth degree equation which can be solved for the intersections. Various techniques and approximations for solutions have been given in References 21, 23, and others. The solution is lengthy and will not be given here.

2.4.6.5 Continuous Exposure to Sun

The previous analyses assumed restricted two-body motion around a spherical earth. Since the earth is actually an oblate spheroid, perturbations will occur which continuously change the orbital elements, most notably a rotation of its node and argument of perigee. However, by proper orientation of the orbit, it is possible to cause the line of nodes to rotate .986 degrees per day so as to produce a nearly constant orbit plane orientation with respect to the sun as the earth moves in its orbit about the sun. Furthermore, by proper choice of orbit inclination and node a satellite will remain entirely in sunlight during an orbit. Therefore, it is possible to design an orbit which will remain entirely in sunlight throughout its lifetime. The relationships governing the orbit selection for continuous exposure to the sun are given below.

For a nodal precession of .986 deg/day

$$\cos i_{eq} = \frac{.986}{3\pi\ J_2} \left(\frac{P}{R_e}\right)^2 \tag{4.136}$$

where i_{eq} is the inclination of the orbit to the earth equator and is between 90° and 180° (i.e., retrograde). Thus by orienting the orbit so that its node is initially 90° from the earth-sun line and trading inclination and altitude through the use of equation (4.136), a continuously sunlight orbit can be designed.

2.4.7 Radiation

2.4.7.1 Van Allen Belts

The Van Allen Belts are intense regions of charged particles trapped in the earth's magnetic field; these radiation regions are generally divided into two belts, an inner Van Allen Belt and an outer Van Allen Belt. The inner belt is composed primarily of high energy protons while the outer belt consists mainly of electrons. The belts form a toroidal-like solid around the earth which is symmetrical about the magnetic equator. (See Figure 4-17 [from Reference 2] for the general shape of a portion of the belt.) This magnetic equator approximates a great circle inclined to the geographic equator by about 13° with the ascending node at geographic longitude of about 20°E. Anomalies in the earth's magnetic field cause the magnetic equator to deviate from a great circle. Figure 4-18 (from Reference 2) illustrates the geographic latitude and longitude of the magnetic equator and the great circle which is sometimes used to approximate it.

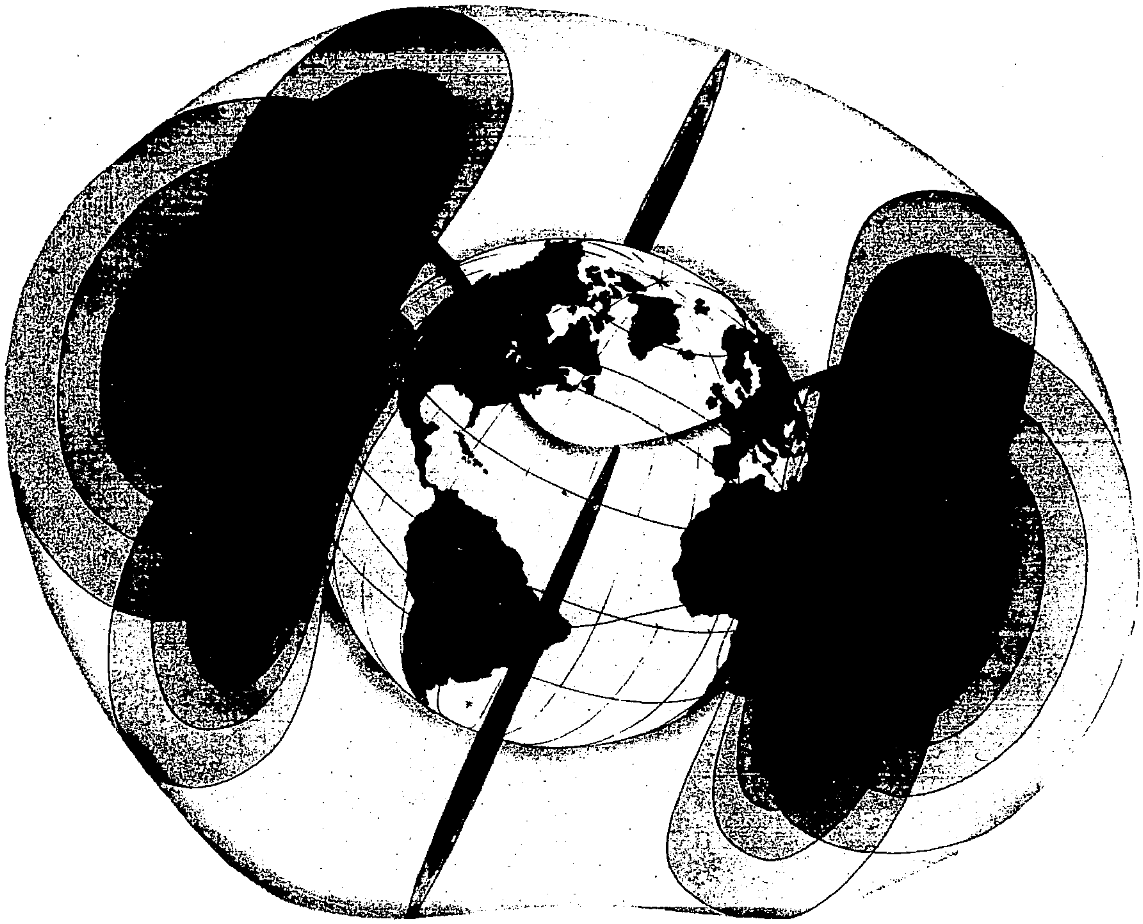

Inner Van Allen Belt

Figure 4-17

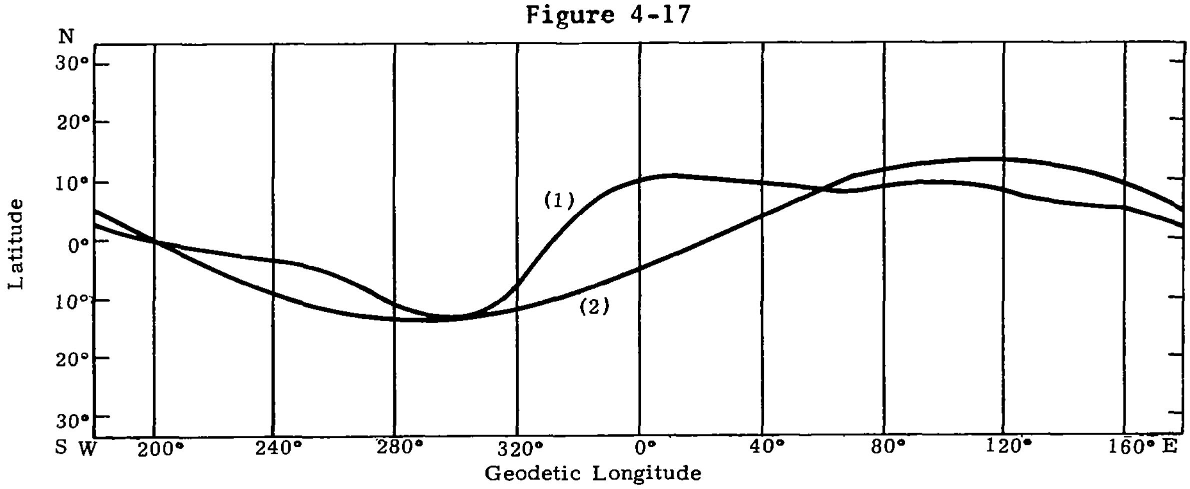

Magnetic Dip Equator (1) from USN Hydrographic Office, 1955 and Geocentric Magnetic Equator (2) Inclined 13° to the Equator at Longitude 290°

Figure 4-18

The inner belt begins at about 500 KM altitude and the outer belt extends to more than 40,000 KM altitude. Peak intensities are reached in the inner radiation belt at an altitude of about 4000 KM over the magnetic equator. In the outer belt two peak areas exist, one at about 10,000 KM altitude and the other at about 14,000 KM altitude both over the magnetic equator.

The space environment under 1000 KM altitude is generally considered safe enough to establish stable orbits for the various types of space vehicles though it is noted that the recent tendency to revise upward the radiation tolerance level will result in a corresponding increase in the maximum altitude. However, it is still desirable to minimize exposure to the radiation environment when passing through the belts for lunar, planetary, or high altitude earth orbit (e.g., synchronous satellite) mission; this objective is generally satisfied with the natural shielding provided by the spacecraft structure provided the belts are traversed at as high a velocity as possible. Near parabolic and hyperbolic velocities will keep the dosage to a completely acceptable level. In the way of contrast, however, future missions might involve low thrust vehicles which would spend many hours, even days, spiraling away from the earth; these missions could meet with very significant radiation problems. Figure 4-19 indicates the relative intensities of electrons and nrotons within the belt.

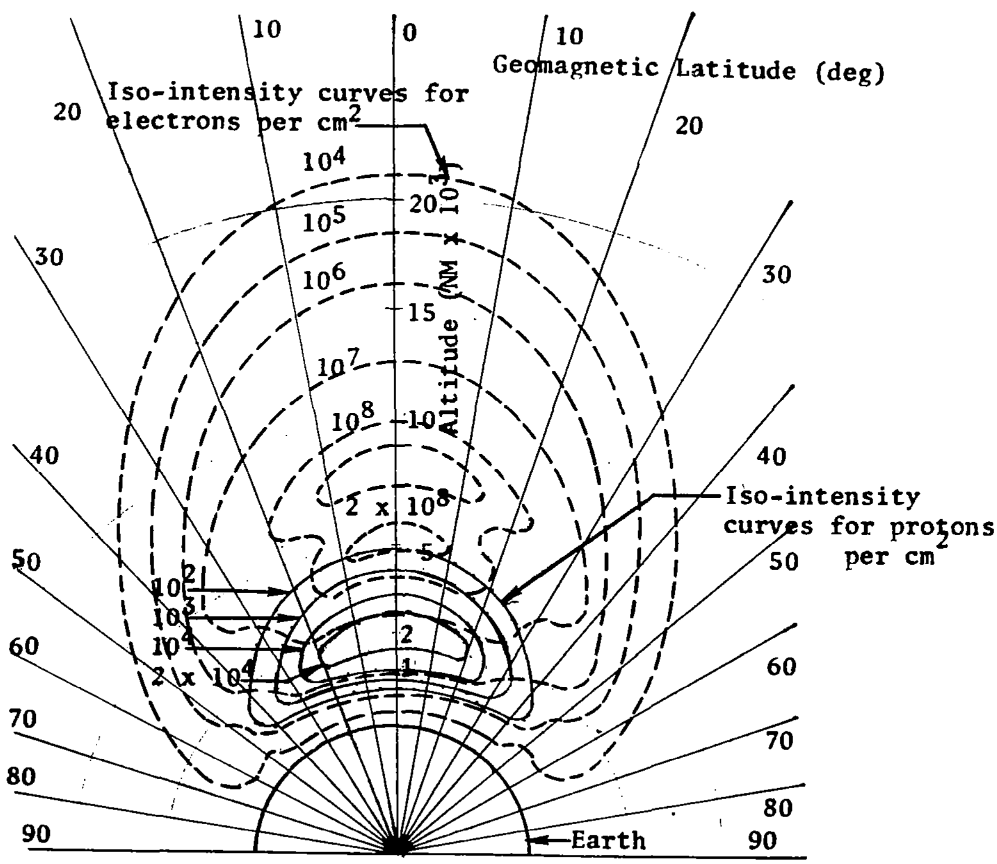

Figure 4-19

2.4.7.2 Solar Flare Radiation

Solar flares or solar bursts present an unpredictable hazard to space missions. A solar flare is basically an eruption on the surface of the sun which ejects particles, mostly protons into space around the sun for great distances. Of course, most flares do not result in flare particles reaching the vicinity of the earth. However, to date no successful methods have been developed which will predict when flares will occur or result in particles reaching the earth,though it has been observed that there is an 11 year cycle of sunspot activity which will predict generally the peak flare periods. During the 1958 peak period more than 3100 flares occurred while during the minimum period of 1954 only 16 occurred. While there is substantial difference in the frequency of occurrence of solar flares from a minimum to a peak period there is no acceptable way of predicting the individual flares.

The radiation dosage due to solar flares reaches lethal levels for an unshielded astronaut in space. However, solar flare radiation is rather effectively shielded by small amounts of absorbers. For example, in the Apollo program, the procedure in the event of a solar proton event during the cislunar portion of the mission is to point the aft end of the spacecraft in the direction of the approaching flare particles. This procedure places the propellant tanks and the major portion of the spacecraft structure between the astronauts and the approaching radiation and should afford adequate protection for the crew during the hour or so duration of the proton event.

For near earth orbital missions, under 1000 KM altitude, the earth's magnetic field effectively shields the latitudes within about 50° of the magnetic equation from solar flare radiation.

2.5 DEORBIT

2.5.1 Introduction

Deorbit is one of the most crucial phases of an orbital mission since the deorbit maneuver must result in a trajectory which will satisfy precise entry conditions on which the survival of the payload or crew may depend. However, the deorbit maneuver is subject to extreme time constraints to assure that landing in the selected recovery area results. Further, the maneuver should be economical in the use of propellants and simple to perform to ensure reliability. In the following sections the deorbit problem will be analyzed and formulated in an effort to aid in the understanding of mission relationships to the deorbit maneuver.

2.5.2 General Deorbit Maneuver

The deorbit maneuver is, in its broadest sense, a maneuver which places the spacecraft on a trajectory which will intersect the earth's atmosphere at a given altitude and usually with a prescribed flight path angle. In some cases, the velocity is also given and limits may be placed on the velocity and/or the flight path angle. The altitude at which the terminal conditions are specified is termed the entry altitude and is generally chosen so that atmospheric drag is considered negligible; the entry altitude usually accepted for low earth orbit deorbits is 300,000 feet while, for comparison, entry altitude for an Apollo lunar return trajectory is generally taken at 400,000 feet. The entry flight path angle and velocity constraints are highly dependent on the vehicle configuration parameters such as lift over drag and heat shield design.

In this section the deorbit maneuver required to satisfy a given set of entry constraints will be examined from an impulsive viewpoint. Optimization of the maneuver, timing considerations, and deorbit via an intermediate orbit will be considered in subsequent sections.

If entry velocity (V_e), flight path angle (γ_e), and altitude (h_e) are specified, the deorbit maneuver for deorbits from any point in earth orbit (defined by altitude, h_o) is completely defined since the angular momentum (H_D) of the descent trajectory is given by

$$H_D = (R_e + h_e)V_e \cos \gamma_e \tag{5.1}$$

(where R_e is the radius of the earth)and since the energy per unit mass is related to the semi-major axis (a_D) of the descent orbit

$$a_D = \frac{\mu\, r_e}{2\mu - r_e\, V_e^2} \tag{5.2}$$

where $r_e = R_e + h_e$

μ = (GM) earth gravitational constant

Thus, the velocity in the descent trajectory (V_D) after retrofire can then be determined by

$$V_D = \sqrt{\mu\left(\frac{2}{R_e + h_o} - \frac{1}{a_D}\right)} \qquad (5.3)$$

and the flight path angle (γ_D) after retro as determined from the angular momentum (H_D) of the descent ellipse is

$$\gamma_D = \cos^{-1}\left[\frac{H_D}{(R_e + h_o)V_D}\right] \qquad -90° \leq \gamma_D \leq 0 \qquad (5.4)$$

Now, from Figure 5-1 it can be seen that the delta-V requirement is given by

$$\Delta V = [V_o^2 + V_D^2 - 2V_o\, V_D \cos \Delta\gamma]^{1/2} \qquad (5.5)$$

where $\Delta\gamma = \gamma_D - \gamma_o$

R_o = vehicle position vector at retro

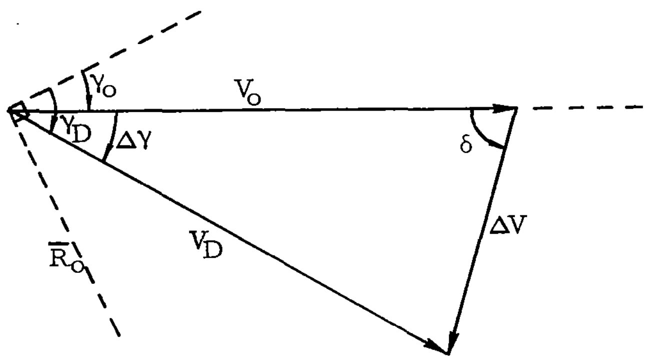

Figure 5-1

Finally, the thrust vector direction parameter (δ) with respect to the pre-retro velocity vector can be computed from

$$\delta = \sin^{-1}\left(\frac{V_D \sin\Delta\gamma}{\Delta V}\right) \qquad (5.6)$$

The angular range covered during the descent from deorbit to entry can be found after first noting the eccentricity (e_D) of the descent trajectory is related to the energy and angular momentum by

$$p_D = \frac{H_D^2}{\mu} \qquad (5.7)$$

and

$$e_D = \sqrt{1 - \frac{p_D}{a_D}} \tag{5.8}$$

Now, the true anomaly (θ_D) of the vehicle in the descent trajectory at the deorbit point can be obtained from

$$\cos \theta_D = \frac{p_D - (R_e + h_o)}{e_D(R_e + h_o)} \tag{5.9}$$

and

$$\sin \theta_D = \frac{p_D \tan \gamma_D}{e_D(R_e + h_o)} \tag{5.10}$$

so that,

$$\theta_D = \tan^{-1}\left(\frac{\sin \theta_D}{\cos \theta_D}\right) \tag{5.11}$$

In a similar manner, the true anomaly at entry (θ_E) can be found from equations (5.9), (5.10), and (5.11) by substituting entry parameters giving

$$\cos \theta_E = \frac{p_D - (R_e + h_e)}{e_D(R_e + h_e)} \tag{5.12}$$

$$\sin \theta_E = \frac{p_D \tan \gamma_E}{e_D(R_e + h_e)} \tag{5.13}$$

Then

$$\theta_E = \tan^{-1}\left(\frac{\sin \theta_E}{\cos \theta_E}\right) \tag{5.14}$$

Therefore, the angular range (ρ) from deorbit to entry is given by

$$\rho = \theta_E - \theta_D \tag{5.15}$$

The time from deorbit to entry is computed from the eccentric anomalies at deorbit and entry (E_D and E_E, respectively) as defined from

$$\sin E_{D,E} = \frac{\sqrt{1 - e_D^2}\,\sin \theta_{D,E}}{1 + e_D \cos \theta_{D,E}} \tag{5.16}$$

$$\cos E_{D,E} = \frac{e_D + \cos \theta_{D,E}}{1 + e_D \cos \theta_{D,E}} \tag{5.17}$$

$$E_{D,E} = \tan^{-1}\left(\frac{\sin E_{D,E}}{\cos E_{D,E}}\right) \tag{5.18}$$

Then the mean anomaly (M) at each point is

$$M_D = E_D - e_D \sin E_D \tag{5.19}$$

$$M_E = E_E - e_D \sin E_E \tag{5.20}$$

giving the time (ΔT_E) from deorbit to entry

$$\Delta T_E = \frac{M_E - M_D}{\sqrt{\mu}} (a_D)^{3/2} \tag{5.21}$$

The deorbit maneuver described will place the vehicle on a trajectory which will satisfy the given entry constraints. However, in order to deorbit and land at a predetermined site the descent trajectory range (ρ) and time (ΔT_E) along with the earth orbit parameters must be factored into a timing analysis such as will be described in section 2.5.4. This is also true of the minimum energy deorbit discussion which follows.

2.5.3 Minimum Energy/Time Deorbit

In many instances for low altitude earth orbits, depending on vehicle characteristics, entry parameter constraints are not very restrictive. For example, in some cases if the entry angle is specified, it may be possible to tolerate a large range of entry velocities or vice versa. In such cases, nominalization of the deorbit maneuver is possible in order to minimize deorbit delta-V or time from deorbit to entry, etc. The following discussion presents the technique for determining the minimum delta-V deorbit maneuver for coplanar deorbits from a circular orbit to a specified entry altitude and flight path angle. This discussion is also applicable to deorbits from apogee or perigee of an elliptical but, in general, final orbital ejection to entry is made from a low altitude circular orbit.

After the deorbit maneuver, the descent trajectory can be described by the conservation of angular momentum equation

$$r_o V_o \cos \gamma_o = r_E V_E \cos \gamma_E \tag{5.22}$$

and the energy equation

$$V_o^2 - \frac{2\mu}{r_o} = V_E^2 - \frac{2\mu}{r_E} \tag{5.23}$$

where γ = flight path angle

r = vehicle radius

V = vehicle velocity magnitude

subscript o refers to just after deorbit

subscript E refers to entry

However, for convenience, the velocities in (5.22) and (5.23) will be normalized with respect to the local circular velocity by multiplying and dividing by

$$V_c = \sqrt{\frac{\mu}{r_c}} \tag{5.24}$$

Squaring equation (5.22) and normalizing the velocities gives

$$r_o\, b_o \cos^2\gamma_o = r_E\, b_E \cos^2\gamma_E \tag{5.25}$$

where

$$b_o = \left(\frac{V_o}{V_{co}}\right)^2$$

$$b_E = \left(\frac{V_E}{V_{CE}}\right)^2 \quad .$$

Thus, equation (5.23) becomes

$$\frac{r_E}{r_o} = \frac{b_E - 2}{b_o - 2} = R \tag{5.26}$$

or

$$b_E = R(b_o - 2) + 2 \tag{5.27}$$

Substitition of (5.27) into (5.25) now yields

$$r_o\, b_o \cos^2\gamma_o = r_E \cos^2\gamma_E\, [R(b_o - 2) + 2] \tag{5.28}$$

which can be written

$$b_o[\cos^2\gamma_o - R^2 \cos^2\gamma_E] = (2R \cos^2\gamma_E)(1 - R) \tag{5.29}$$

and solved for $\cos\gamma_o$ as

$$\cos\gamma_o = \sqrt{\frac{B}{b_o} + A} \tag{5.30}$$

where

$$A = R^2 \cos^2\gamma_E$$

$$B = (2R\cos^2\gamma_E)(1 - R)$$

But, from Figure 5-2 it can be seen that for an arbitrary deorbit maneuver from a circular orbit

$$\Delta V^2 = V_o^{\,2} + V^2 - 2V_o\, V \cos\gamma_o \tag{5.31}$$

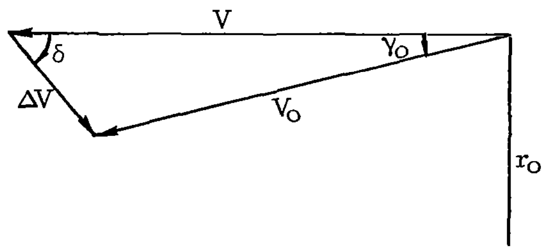

Figure 5-2

or normalizing

$$\left(\frac{\Delta V}{V_{co}}\right)^2 = b + b_o - 2\sqrt{b\, b_o}\, \cos\gamma_o \tag{5.32}$$

where

$$b = \left(\frac{V}{V_c}\right)^2$$

Now, substituting equation (5.30) into (5.32)

$$\left(\frac{\Delta V}{V_c}\right)^2 = F = b + b_o - 2\sqrt{B\, b + A\, b_o\, b} \tag{5.33}$$

and differentiating with respect to b_o yields

$$\frac{dF}{db_o} = 1 - \frac{1}{\sqrt{Bb + Ab_o b}} \tag{5.34}$$

Thus, the minimum delta-V can be obtained by employing the condition

$$\frac{dF}{db_o} = 0 \tag{5.35}$$

and solving for b_o as

$$b_o = \frac{A^2 b - B}{A} \tag{5.36}$$

Now, substituting (5.36) into (5.33) yields

$$\left(\frac{\Delta V}{V_c}\right)^2_{min} = b(1 - A) - \frac{B}{A} \tag{5.37}$$

The direction of the thrust can be determined by considering the expression for an arbitrary deorbit maneuver. This equation can be written as

$$b_o = b + \left(\frac{\Delta V}{V_c}\right)^2 - 2\sqrt{b}\,\frac{\Delta V}{V_c}\cos\delta \tag{5.38}$$

Then, by substituting (5.36) and (5.37) into (5.38) and solving for δ

$$\cos\delta = (1 - A)\left[\frac{b}{b(1 - A) - B/A}\right]^{1/2} \qquad 0 < \delta < 180° \tag{5.39}$$

Equations (5.37) and (5.39) define the minimum delta-V and the thrust direction for deorbits from a circular earth orbit to a specified entry flight path angle and altitude. The resulting entry velocity can be easily determined from equations (5.27) and (5.36).

2.5.4 Deorbit Timing

The deorbit maneuvers described in the previous sections are designed to transfer the vehicle from earth orbit onto a trajectory profile which will intersect the earth's atmosphere under prescribed conditions. Deorbit, however, implies landing at some preselected location on the rotating earth. Therefore, the timing of the deorbit maneuver, in order to provide proper impact location, becomes of primary interest. The descent trajectory consists of three phases:

the finite burn, the coast to the entry interface, and the entry trajectory. However, the burn duration for deorbits from low altitude circular orbits is sufficiently short that it can be assumed that the maneuvers are impulsive; further, the atmospheric trajectory will be discussed in section 2.6. Thus, attention can turn to the coast arc.

The opportunities for deorbit and impact at a specified landing site can be computed with the aid of Figure 5-3 as follows.

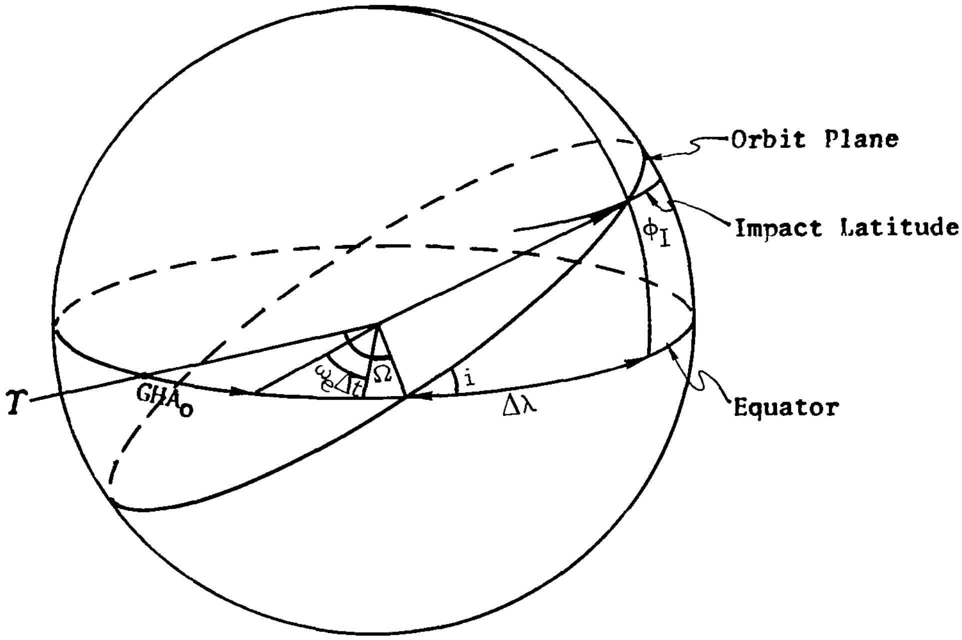

Figure 5-3

Figure 5-3 shows that for the landing site to lie in the orbit plane the longitude of the intersection point of the orbit plane and the latitude minor circle (λ') must be equal to the landing site longitude (λ_I). That is,

$$\lambda_I = \lambda' = \Omega - (GHA_o + \omega_e \Delta t - 2\pi m) + \Delta\lambda \qquad (5.40)$$

where

$\Omega = \Omega_o + n\dot{\Omega}$

Ω_o = right ascension of the node at t_o

t_o = epoch from which deorbit opportunities are being computed (most conveniently taken at a time of nodal crossing)

$\dot{\Omega} = -3\pi J_2\left(\frac{R_E}{p}\right)^2 \cos i$ (nodal regression per revolution, see section 2.4.2)

n = number of revolutions since t_o (not necessarily an integer)

GHA_o = Greenwich Hour Angle of the vernal equinox at t_o

ω_e = earth's rotational rate

Δt = time since t_o

m = integer, number of completed days since t_o

$\Delta\lambda = \sin^{-1}\left(\frac{\tan \phi_I}{\tan i}\right)$ southerly approachs

$= \pi - \sin^{-1}\left(\frac{\tan \phi_I}{\tan i}\right)$ northerly approachs

ϕ_I = landing site latitude

λ_I = landing site longitude

But, equation (5.40) can be rearranged to give the times since t_o that the landing site is in the orbit plane as

$$\Delta t = \frac{\Omega_o + n\,\dot{\Omega} - GHA_o + 2\pi \quad m + \Delta\lambda}{\omega_e} \tag{5.41}$$

and the time in orbit from t_o to impact can be written

$$\Delta t = n\,P_o + t_D \tag{5.42}$$

where

P_o = the nodal period of revolution over an oblate earth

$$\simeq \frac{2\pi}{\sqrt{\mu}}\, a^{3/2} \left\{ 1 - \frac{3}{2}\frac{J_2 R_e^2}{a^2}\left(\frac{7\cos^2 i - 1}{4}\right) \right\}$$

n = number of revolutions since t_o (not necessarily an integer)

t_D = time from deorbit to impact

Thus, equations (5.41) and (5.42) can be solved for n, the revolution number and fraction thereof, to assure that the landing site would be in the orbit plane at touchdown.

$$n = \frac{\Omega_o - GHA_o + 2\pi \quad m + \Delta\lambda - \omega_e\, t_D}{\omega_e\, P_o - \dot{\Omega}} \tag{5.43}$$

As can be seen from examination of equations (5.40) through (5.43) and Figure 5-3, there are two opportunities per day in which the landing site will be in the orbit plane at touchdown.* (One opportunity corresponds to a northerly approach and the other to a southerly approach.) Though equation (5.43) defines positions in orbit (with respect to the vehicle position at t_o) at which, if deorbit was initiated, the landing site would be in the orbit plane at touchdown, it does not define the deorbit trajectory range. This range from the deorbit position to the landing site may not be compatible for every opportunity.

After computing the values of n for which the landing site is in the orbit plane at touchdown, another set of computations is required to determine which deorbit opportunities are acceptable or compatible with the descent trajectory for a particular case. This computation may require an iteration procedure in which the deorbit maneuver is altered slightly to obtain a descent trajectory range and time from which a successful landing may be accomplished within the variable range capabilities of the entry vehicle.** The technique for the final evaluation of the deorbit opportunities is as follows.

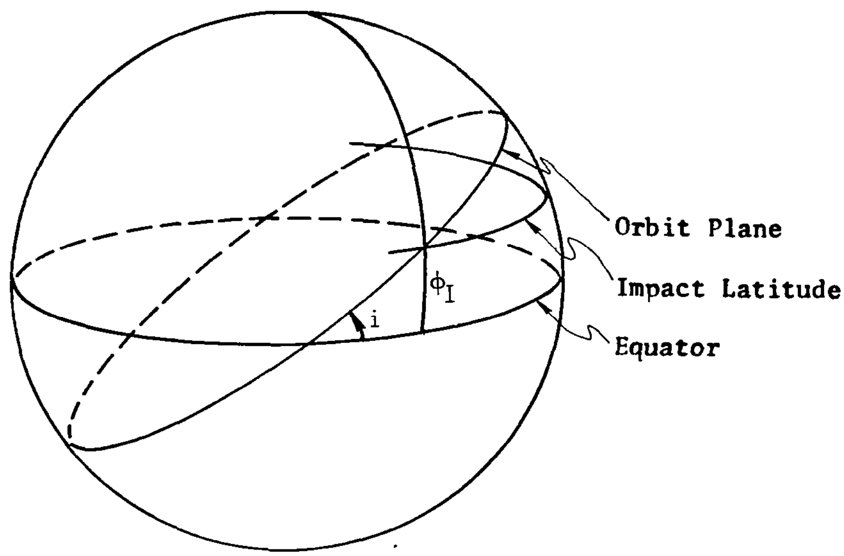

Figure 5-4

From Figure 5-4 it can be seen that the number of revolutions (n') required for the vehicle to be over the landing site if the vehicle is at the ascending node at t_o is

$$n' = N + \frac{1}{2\pi} \sin^{-1}\left(\frac{\sin \phi_I}{\sin i}\right) \tag{5.44}$$

for approaches from the south, or

---

* assuming that the orbit inclination is grater than the latitude of the landing site.

**A deorbit window can be defined in exactly the same manner employed in the discussion of the launch window for rendezvous if lateral maneuverability is considered. This window will greatly simplify the recovery problem.

$$n' = N + \frac{1}{2\pi}\left[\pi - \sin^{-1}\left(\frac{\sin \phi_I}{\sin i}\right)\right]$$

for approaches from the north, where

N = in integer number of revolutions

ϕ_I = landing site latitude

i = orbit inclination to the equator plane

Therefore, the deorbit maneuver must be initiated prior to n' by an angular range (ρ) equal to the total descent trajectory range from retro to touchdown. That is, in order to impact the landing site the following relationship must hold

$$n = n' - \rho \pm \sigma \tag{5.45}$$

where σ is an in-plane range tolerance which may be absorbed by entry vehicle maneuverability depending on the maneuverability characteristics of the entry vehicle. Equations (5.43) and (5.44) provide opportunities which, though not mathematically precise, are well within the tolerance implied in σ.

2.5.5 Deorbit Via Intermediate Orbit

Although it is possible to deorbit from elliptical or high altitude earth orbits directly, the crucial nature of the deorbit maneuver is simplified if it is made from a low altitude circular or near circular orbit. The use of an intermediate parking orbit is also useful for reasons of phasing for landing at a given site and for tracking station coverage during the deorbit maneuver. Further increase in the flexibility is realized if the possibility of making a small plane change during the maneuver into the intermediate orbit is considered; however, plane changes are costly from a performance standpoint, and the same affect can be produced using an intermediate orbit. Thus, plane changes employing thrust are generally not considered.*

The transfer from the initial to the parking orbit may be accomplished with a Hohmann type trajectory initiated at apogee or perigee of the initial orbit. However, because constraints may exist for such items as tracking station coverage at initiation or completion of the trajectory trajectory, a more generalized transfer technique will be discussed. (See Figure 5.5)

---

* Abort is an exception.

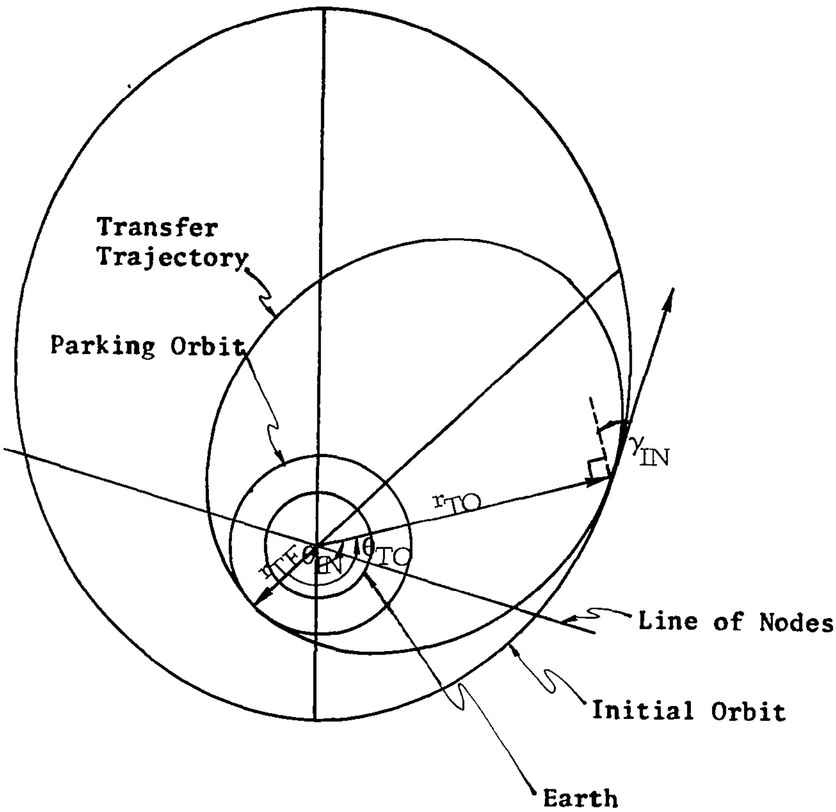

Figure 5-5

Assuming that, because of tracking coverage by a particular station or for some other reason, the location at which the maneuver is to be initiated can be defined by true anomaly (θ_{IN}), the departure point radius is given by

$$r_{TO} = \frac{p_{IN}}{1 + e_{IN} \cos \theta_{IN}} \tag{5.46}$$

where

p_{IN} = semi-latus rectum of initial orbit

r_{TO} = departure point radius

e_{IN} = eccentricity of initial orbit

θ_{IN} = true anomaly in initial orbit of departure point

Second, assuming that, for delta-V efficiency, the transfer ellipse is tangent to the initial ellipse at the departure point, the condition

$$\gamma_{TO} = \gamma_{IN}$$

is imposed (where

γ_{TO} = flight path angle at departure point in transfer orbit

γ_{IN} = flight path angle at departure point in initial orbit).

But since the flight path angle at the departure point in the initial orbit is given by

$$\cos \gamma_{IN} = \left[\frac{a_{IN}^2(1 - e_{IN}^2)}{r_{TO}(2a_{IN} - r_{TO})}\right]^{1/2} \tag{5.47}$$

$$\sin \gamma_{IN} = \frac{e_{IN} \sin \theta_{IN}}{\sqrt{1 + 2e_{IN} \cos \theta_{IN} + e_{IN}^2}} \tag{5.48}$$

$$\gamma_{IN} = \tan^{-1}\left(\frac{\sin \gamma_{IN}}{\cos \gamma_{IN}}\right) \tag{5.49}$$

this angle is a known function of the variable θ_{IN}.

Now, from the conservation of angular momentum (assuming parking orbit insertion occurs at perigee of the transfer orbit)

$$r_{TO} V_{TO} \cos \gamma_{IN} = r_{TF} V_{TF} \tag{5.50}$$

Then since

$$V_{TO}^2 = \mu\left(\frac{2}{r_{TO}} - \frac{1}{a_T}\right) \tag{5.51}$$

$$V_{TF}^2 = \mu\left(\frac{2}{r_{TF}} - \frac{1}{a_T}\right) \tag{5.52}$$

the semi-major axis of the transfer ellipse can be expressed by

$$a_T = \frac{r_{TF}^2 - r_{TO}^2 \cos^2\gamma_{IN}}{2(r_{TF} - r_{TO} \cos^2 \gamma_{IN})} \tag{5.53}$$

Finally, the velocity in the initial orbit at the departure point is

$$V_{IN} = \left[\mu\left(\frac{2}{r_{TO}} - \frac{1}{a_{IN}}\right)\right]^{1/2} \tag{5.54}$$

and the velocity at departure in the transfer orbit is

$$V_{TO} = \left[\mu\left(\frac{2}{r_{TO}} - \frac{1}{a_T}\right)\right]^{1/2} \tag{5.55}$$

so that the delta-V required to insert into the transfer orbit is

$$\Delta V = V_{IN} - V_{TO} \tag{5.56}$$

To this point, it has been assumed that the true anomaly (θ_{TO}) in the transfer orbit of the departure point was known. This variable can be computed from

$$e_T = 1 - \frac{r_{TF}}{a_T} \tag{5.57}$$

$$p_T = a_T(1 - e_T^2) \tag{5.58}$$

$$\cos\theta_{TO} = \frac{p_T - r_{TO}}{e_T\ r_{TO}} \tag{5.59}$$

$$\sin\theta_{TO} = \frac{p_T \tan\gamma_{IN}}{e_T\ r_{TO}} \tag{5.60}$$

$$\theta_{TO} = \tan^{-1}\left(\frac{\sin\theta_{TO}}{\cos\theta_{TO}}\right) \tag{5.61}$$

Thus, the transfer central angle (β) is

$$\beta = 2\pi - \theta_{TO} \tag{5.62}$$

and the corresponding transfer time is computed from

$$\cos E_{TO} = \frac{a_T - r_{TO}}{a_T\ e_T} \tag{5.63}$$

$$\sin E_{TO} = \frac{\sqrt{1 - e_T}\ \sin\theta_{TO}}{1 + e_T\cos\theta_{TO}} \tag{5.64}$$

$$E_{TO} = \tan^{-1}\left(\frac{\sin E_{TO}}{\cos E_{TO}}\right) \tag{5.65}$$

$$M_{TO} = E_{TO} - e_T \sin E_{TO} \tag{5.65}$$

$$T_T = \frac{2\cdot\pi - M_{TO}}{\sqrt{\mu}} (a_T)^{3/2} \tag{5.66}$$

where

E_{TO} = eccentric anomaly in the transfer orbit at departure

M_{TO} = mean anomaly in the transfer orbit at departure

T_T = transfer time from departure to parking orbit insertion

The circular parking orbit velocity (V_{co}) is obtained from

$$V_{co} = \sqrt{\frac{\mu}{r_{TF}}} \tag{5.67}$$

and the velocity at parking orbit insertion in the transfer ellipse is given by

$$V_{TF} = \left[\mu\left(\frac{2}{r_{TF}} - \frac{1}{a_T}\right)\right]^{1/2} \tag{5.68}$$

so that the delta-V required for parking orbit insertion is

$$\Delta V = V_{TF} - V_{co} \tag{5.69}$$

After insertion into the low altitude circular orbit the techniques of sections 2.5.2, 2.5.3, and 2.5.4 can be applied for the final deorbit to impact. Note that in the process of introducing this orbit an additional degree of freedom* has been introduced. Thus, when an analysis is performed, optimization of this degree of freedom is required.

---

* If the intermediate orbit were elliptic there would be yet another degree of freedom even under the assumption that injection occurred at $\theta_{TF} = 0$.

2.6 ENTRY TRAJECTORIES

2.6.1 Introduction

Every mission for which physical recovery or survival at the earth's surface is desired must consider carefully the atmospheric entry phase since the presence of an atmosphere presents severe design and guidance problems for the descent vehicle. The severity of the problem can be visualized by considering a vehicle in a low earth orbit. For example, a vehicle in a 200 mile altitude circular orbit possesses a kinetic energy of about 13,000 BTU/lb which is over half the energy required to vaporize carbon which requires about 25,000 BTU/lb,and carbon has one of the highest heats of vaporization known. Thus if all of the potential and kinetic energy were converted to thermal energy, the total would be more than sufficient to completely vaporize most structural materials. Fortunately, however, through the mechanism of gas-dynamic drag the bodies initial energy is transformed into thermal energy in the air around the body and only part of this energy(dependent on the characteristics of flow around the body) is transformed to the bodies surface as heat.

The preceding discussion points out one of the major entry trajectory interfaces, namely the tradeoff between the heat load/rate capabilities of the vehicle and the trajectory. The other major factor which affects the survival of the vehicle and its payload is the deceleration level during the entry trajectory. Deceleration forces are experienced by the vehicle as its velocity is reduced by drag experienced along the entry trajectory. This deceleration,as was the vehicle heating, is a function of the vehicle configuration and the entry trajectory.

The factors mentioned, vehicle heating and deceleration, interface primarily with the actual survival of the vehicle and/or its payload. Other factors which interface with recovery of the vehicle after landing are the entry trajectory range and time to touchdown and the lateral maneuver capabilities. Therefore, these factors and their relationships to the trajectory and to the vehicle configuration will also be discussed along with the trade-off of mission constraints and trajectory capabilities.

2.6.2 Entry Dynamics

The equations of motion for a vehicle moving in an atmosphere as a function of the vehicles initial velocity, the drag and lift characteristics, and the mass-area ratio can be written (see Figure 6-1) as

$$-\frac{du}{dt} = -g \sin\gamma + \frac{C_D A_C}{m}\frac{\rho}{2}u^2 \tag{6.1}$$

$$\frac{u}{\cos\gamma}\frac{d\gamma}{dt} = -g - \frac{u^2}{r} - \frac{C_L A_C}{m}\frac{\rho}{2}\frac{u^2}{\cos\gamma} \tag{6.2}$$

where

u = velocity

g = gravitational acceleration

γ = flight path angle

C_D = gas dynamic drag coefficient

A_C = cross-sectional frontal area

m = mass

ρ = atmospheric density

r = radius

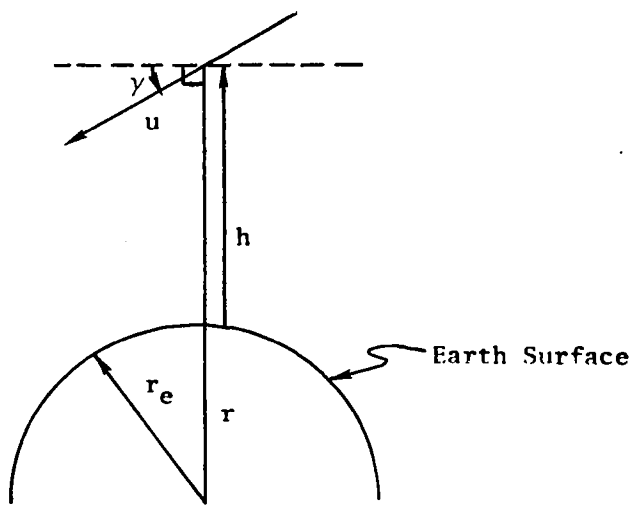

Figure 6-1

Though these equations [(6.1) and (6.2)] can be solved numerically for any prescribed atmosphere, they can be solved analytically only under certain approximations for some types of entry.

However, for purposes of this report, it will be assumed that the general relationships between the parameters are of more interest than is the precision. Accordingly, the analytic approach will be followed. In this approach, the atmospheric density is described by an isothermal atmosphere in hydrostatic equilibrium model as

$$\rho = \rho_o e^{-\alpha h} \tag{6.3}$$

where

ρ_o = sea level density

h = altitude

$$\alpha = -\frac{1}{\rho}\frac{d\rho}{dh} = \frac{Mg}{RT}$$

M = molecular weight

g = gravitational acceleration

R = universal gas constant

T = absolute temperature

Although it is recognized that the atmosphere is dynamic and is not isothermal, equation (6.3) gives a reasonable density distribution below 400,000 ft and is sufficient for preliminary entry calculations.

In the following sections solutions of equations (6.1) and (6.2) under various assumptions which correspond to various types of entry will be discussed.

2.6.2.1 Direct Entry

Direct entry implies a relatively steep atmospheric entry of a non-lifting body. The path is essentially linear through the atmosphere during the major deceleration. The assumptions corresponding to this type of entry are:

1. A constant flight path angle (γ)

2. A constant drag coefficient (C_D)

3. A small gravitational force compared to the drag force

Under these assumptions, an analytic solution of (6.1) and (6.2) can be obtained for variations in altitude and velocity with time. Equation (6.1) becomes

$$\frac{du}{dt} = -\frac{C_D\ AC}{m}\frac{\rho_o}{2}\ \sigma\ u^2 \qquad (6.4)$$

where

$$\sigma = \frac{\rho}{\rho_o}$$

Then the atmospheric density variation as given in equation (6.3) becomes

$$\frac{d\sigma}{dt} = \alpha \sigma u \sin \gamma \tag{6.5}$$

when from Figure 6-2

$$dh = u \sin \gamma \, dt$$

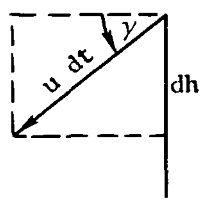

Figure 6-2

Now, eliminating time between equations (6.4) and (6.5) yields

$$\frac{du}{d\sigma} = - \frac{C_D A_C}{m \sin \gamma} \frac{\rho_o}{2\sigma} u \tag{6.6}$$

But this equation can be integrated between the initial entry point (where $\sigma = 0$ and the entry velocity is u_i) and some point in the atmosphere to yield

$$\frac{u}{u_i} = e^{- \frac{C_D A_C}{m \sin \gamma} \frac{\rho_o}{2\alpha} \sigma} \tag{6.7}$$

which gives the velocity variation as a function of altitude.

Then, the deceleration at any point during entry experienced by the vehicle can be obtained from equations (6.4) and (6.7). Rewriting (6.7)

$$- \frac{C_D A_C \rho_o}{2m} \sigma = \alpha \sin \gamma \ln\left(\frac{u}{u_i}\right) \tag{6.8}$$

Substituting into equation (6.4), and normalizing the velocity by (u_i), the deceleration (-du/dt) is given by

$$\left(- \frac{du}{dt}\right) = \alpha u_i^2 \sin\gamma \left(\frac{u}{u_i}\right)^2 \ln\left(\frac{u}{u_i}\right) \tag{6.9}$$

An expression for the maximum deceleration level is obtained by differentiating equation (6.9) and equating the result to zero.

$$\dot{u}\ \alpha \sin \gamma \left[1 + 2\ \ell n\left(\frac{u}{u_i}\right)\right] = 0 \qquad (6.10)$$

But, since the term u α sin γ is nonzero at the maximum deceleration point

$$\ell n\left(\frac{u}{u_i}\right) = -\frac{1}{2} \qquad (6.11)$$

This relationship gives the velocity at maximum deceleration as

$$\frac{\dot{u}}{u_i} = \frac{1}{\sqrt{e}} \qquad (6.12)$$

For equation (6.12) to hold, the exponential term in equation (6.7) becomes

$$\frac{C_D\ A_C\ \rho_o}{m\ \sin\ \gamma\ 2\alpha}\ \sigma = \frac{1}{2} \qquad (6.13)$$

The resulting peak deceleration value is therefore

$$\left(-\frac{du}{dt}\right)_{max} = \frac{\alpha\ u_i^2\ \sin\ \gamma}{2e} \qquad (6.14)$$

These expressions give good agreement with numerical solutions, according to Reference (1), for entry angles greater than about 5° and for near orbital entry velocities throughout the period where the major deceleration occurs. The equations also give good approximations for long range (over 500 miles) ballistic missile or sounding rocket analysis.

2.6.2.2 Lifting Entry (Equilibrium Glide Path)

The opposite extreme from the direct entry discussed in the previous section is the lifting entry; such trajectories are flown by a lifting vehicle on an equilibrium glide path. An equilibrium glide is one in which the gravitational force is balanced at every point by the gas dynamic lift force and by the centrifugal force due to curvature of the path. For this case, the flight path angle is small and slowly changing; thus, the equations of motion [(6.1) and (6.2)] can be solved analytically by making assumptions based on the small, slowly changing flight path angle.

$\sin \gamma \ll 1$

$\cos \approx 1.0$

$\frac{d\gamma}{dt} \approx 0.0$

$g \sin \gamma \ll \frac{du}{dt}$

Under these assumptions, equations (6.1) and (6.2) become

$$\frac{du}{dt} = - \frac{C_D \ AC}{m} \frac{\rho_o}{2} \sigma \quad u^2 \tag{6.15}$$

$$\frac{C_L \ A_C}{m} \frac{\rho o}{2} \quad \sigma \ u^2 = g - \frac{u^2}{r} \tag{6.16}$$

The velocity can be obtained directly from (6.16) as a function of radius.

$$\frac{u}{u_o} = \frac{1}{\sqrt{1 + \alpha \ r \frac{L}{D} \frac{C_D \ A_C}{m} \frac{\rho o}{2} \sigma}} \tag{6.17}$$

where

u_o = circular orbit velocity = $\sqrt{gr}$

C_L = L/D C_D

L = lift

D = drag

Thus, the deceleration at any point can be found by substituting (6.17) into (6.15) to obtain

$$- \frac{du}{dt} = \frac{g \left[1 - \left(\frac{u}{u_o} \right)^2 \right]}{L/D} \tag{6.18}$$

or

$$- \frac{du}{dt} = \frac{g}{\frac{L}{D} + \frac{1}{\alpha\ r\ \frac{C_D\ A_C \rho_o}{m\ 2\alpha}\ \sigma}} \tag{6.19}$$

In the equilibrium glide case, no peak deceleration is experienced; rather the deceleration increases continuously during the glide asymptotically approaching the value

$$\left(- \frac{du}{dt}\right)_{max} = \frac{g}{L/D} \tag{6.20}$$

as the velocity increases.

The flight path angle during descent can be found from (6.15) and (6.16) by first differentiating (6.16)to obtain

$$\frac{d\sigma}{du} = - \frac{\frac{2}{r} + \frac{2\ C_L\ A_C}{m} \frac{\rho_o}{2}\ \sigma}{\frac{C_L\ A_C}{m} \frac{\rho_o}{2}\ u} \tag{6.21}$$

Then, combining equations (6.21) and (6.15) to obtain $(d\sigma/dt)$ and equating to equation (6.5), an expression for the flight path angle can be obtained as

$$\sin\gamma = \frac{2}{\alpha\ r\ \frac{L}{D} \left(\frac{u}{u_o}\right)^2} \tag{6.22}$$

or

$$\sin\gamma = \frac{2\left(1 + \alpha\ r\ \frac{L}{D}\ \frac{C_D\ A_C}{m} \frac{\rho_o}{2}\ \sigma\right)}{\alpha\ r \left(\frac{L}{D}\right)}$$

Utilizing this expression for the flight path angle, the distance traveled in the glide path can be obtained by considering the incremental distance (dX) traveled in the interval of time dt is given by

$$dX = u\ dt \quad * \tag{6.23}$$

---

* Since $\gamma(t) \approx 0$, the motion is nearly rectilinear.

but from equation (6.5)

$$u\ dt = \frac{d\sigma}{\alpha\ \sigma\ \sin\gamma} \tag{6.24}$$

so that the distance traveled from the initial point X_i to point X is given by the integral

$$\int_{X_i}^{X} dX = \int_{\sigma_i}^{\sigma} = \frac{1}{2}\frac{L}{D} r \int_{\sigma_i}^{\sigma} \frac{d\sigma}{\left(1 + \alpha\ r\ \frac{L}{D}\frac{C_D\ AC}{m}\frac{\rho_o}{2\alpha}\sigma\right)} \tag{6.25}$$

Integration gives

$$X - X_i = \frac{1}{2}\frac{L}{D} r\ \ell n \frac{\sigma\ \sin\gamma_i}{\sigma_i\ \sin\gamma} \tag{6.26}$$

which since the radius r changes very little compared to the distance $(X - X_i)$ enables the expression for the angular range ρ to be written

$$\rho = \frac{X - X_i}{r} = \frac{1}{2}\frac{L}{D}\ \ell n \frac{\sigma\ \sin\gamma_i}{\sigma_i\ \sin\gamma} \tag{6.27}$$

The final parameter of interest is the time variation with altitude or velocity which can be obtained directly by integration of equation (6.18) giving

$$t - t_i = \frac{u_o\left(\frac{L}{D}\right)}{2g}\ \ell n \frac{\left(1 + \frac{u_i}{u_o}\right)\left(1 - \frac{u}{u_o}\right)}{\left(1 - \frac{u_i}{u_o}\right)\left(1 + \frac{u}{u_o}\right)} \tag{6.28}$$

2.6.2.3 General Case of Shallow Entry

The analytic solutions of equations (6.1) and (6.2) presented in the previous sections are limited to either relatively steep entries ($\gamma > 5°$) of a non-lifting body or to the case of a lifting entry on an equilibrium glide path (L/D > 1). For other classes of entry, such approximate analytical solutions are generally not possible. However, many numerical techniques have been developed for the solution of equations (6.1) and (6.2). As an example, a solution for shallow entries of both simple drag and lifting bodies developed by Chapman (Reference 1) will be presented. Chapman's solution basically involves the reduction of equations (6.1) and (6.2) to a single second order non-linear differential equation in terms of the general parameters.

$$\bar{u} = \frac{u\ \cos\gamma}{u_o} \tag{6.29}$$

and

$$Z = \frac{\rho o}{2\alpha} \frac{C_D \; A_C}{m} \sqrt{\alpha \; r} \;\; \sigma \;\; \bar{u}$$

with the assumptions

1. spherical, non-rotating planet and atmosphere
2. exponential variation in atmospheric density with altitude (equation [6.3])
3. $dr/r \ll d\bar{u}/\bar{u}$
4. In the case of lifting bodies, the horizontal component of lift is small compared to the horizontal component of drag. ($L \sin \gamma \ll D \cos \gamma$)

Proceeding, equations (6.1) and (6.2) are reduced to

$$\bar{u}\, Z \; - Z' + \frac{Z}{u} = \frac{1 - \bar{u}^2}{\bar{u}\; Z} \; \cos^4\gamma \; - \sqrt{\alpha \; r}\, \frac{L}{D} \cos^3\gamma \tag{6.30}$$

Thus, if a substitution

$$\Gamma = \frac{Z}{\bar{u}} = \frac{\rho o}{2\alpha} \frac{C_D \; A_C}{m} \; \sqrt{\alpha r} \;\; \sigma . \tag{6.31}$$

is introduced in order to clearly separate the generalized altitude and velocity, equation (6.30) becomes

$$\bar{u}^2\Gamma'' + \bar{u}\; \Gamma = \frac{1 - \bar{u}^2}{\bar{u}^2 \; \Gamma} \cos^4\gamma \;\; - \sqrt{\alpha \; r}\, \frac{L}{D} \cos^3\gamma \tag{6.32}$$

Equation (6.32) is then solved numerically on a digital computer. The numerical solutions of (6.32) can also be used to obtain range and descent time. Differentiation and manipulation of equations (6.29) and (6.31) result in the integral for angular range

$$\frac{X_2 - X_i}{r} = \frac{1}{\sqrt{\alpha \; r}} \int_{\bar{u}_2}^{\bar{u}_1} \frac{\cos \gamma}{\bar{u}\; \Gamma} \; d\bar{u} \tag{6.33}$$

and for time

$$t_2 - t_1 = \frac{1}{\sqrt{g \; \alpha}} \int_{\bar{u}_2}^{\bar{u}_1} \frac{\cos \gamma}{\bar{u}^2 \; \Gamma} \; d\bar{u} \tag{6.34}$$

2.6.2.4 Maneuverability

As missions become more advanced and corresponding sophistication of entry vehicles is achieved, significant increases in efficiency and crew safety can be realized by maneuverability of the entry vehicle since lateral maneuverability and range control can be used to compensate for entry uncertainties and dynamic atmosphere effects to enable a more precise landing at a predetermined site. However, maneuverability of a vehicle can be considered on several levels of sophistication covering the spectrum from simple pre-entry L/D adjustments to a complex glide-landing vehicle which could be flown to the landing site after the initial deceleration.

To illustrate the parameters involved in the maneuverability of a vehicle, the equations of motion including a lateral motion term available if the vehicle is banked during entry are presented below. (Vehicle banking during entry is a method whereby some range control as well as lateral control is achieved. Range control by banking is performed by employing alternate banking arcs to achieve an S-shaped trajectory during descent.) These equations of motion are equivalent to equations (6.1) and (6.2) under the substitution

$$ds = u\ dt \tag{6.35}$$

$$M\ u \frac{du}{ds} = -\ D - m\ g \sin \gamma$$

$$m\ u^2 \frac{d\gamma}{ds} = L - m \cos \gamma \left(g - \frac{u^2}{r}\right) \tag{6.36}$$

$$m\ u^2 \frac{d\psi}{ds} = Y$$

where

ψ = out of plane angle

Y = side force normal to L and D

s = entry arc length

Now, if the vehicle possesses a constant aero lift-drag ratio $(L/D)_o$

$$\frac{L}{D} = \left(\frac{L}{D}\right)_o \cos \phi$$

and

$$\frac{Y}{D} = \left(\frac{L}{D}\right)_o \sin \phi \tag{6.37}$$

The equations (6.36) can be solved under the constraint imposed by equation (6.37) by numerical methods and in some cases by analytical approximation techniques similar to those developed in earlier sections.

2.6.3 Entry Heating

As mentioned before, the heat load during entry is one of the parameters on which the very survival of the vehicle and/or its payload depends. Two heating parameters are of interest: one is the rate at which heat is transferred to the entering body and the other is the total heat load accumulated by the vehicle during the entry. The vehicle entry heating is a function of the vehicle's configuration, its thermodynamic properties and the entry trajectory being flown.

The relationship between the trajectory parameters discussed in previous sections and the vehicle heating can be seen in the approximate relationship for laminar heat transfer rate per unit frontal area given in Reference 1 as

$$\frac{q}{A_C} \approx \frac{3}{2}\sqrt{\frac{M_\infty}{R\,e_{d_\infty}}}\ \rho\ u^3 \qquad (6.38)$$

or

$$\frac{q}{A_C} \approx \frac{3}{2}\ \frac{\rho_{SL}\ u_i^3}{\left[\left(\frac{R\,e_{d_\infty}}{M_\infty\ d}\right)_{SL} d\right]^{1/2}}\ \sqrt{\sigma}\left(\frac{u}{u_i}\right)^3$$

where

q = heat transfer rate

A_C = cross-sectional frontal area

d = body diameter or thickness

$\left(\frac{R\,e_{d_\infty}}{M_\infty\ d}\right)_{SL}$ = the Reynold's number per unit length per Mach number at sea level $\approx 7.0 \times 10^6\ ft^{-1}$ for earth atmosphere

ρ = atmospheric density

u = velocity

ρ_{SL} = atmospheric density at sea level

u_i = entry velocity

$\sigma = \rho/\rho_{SL}$

Equation (6.38) is adequate for heat rate distribution over blunt axisymetric noses and blunt two-dimensional surfaces. However, it is noted that turbulant heating rates are roughly an order of magnitude higher than laminar values in equation (6.38).

Equation (6.38) can be used to generate safe thermal flight corridors as shown in Figure 6-3.

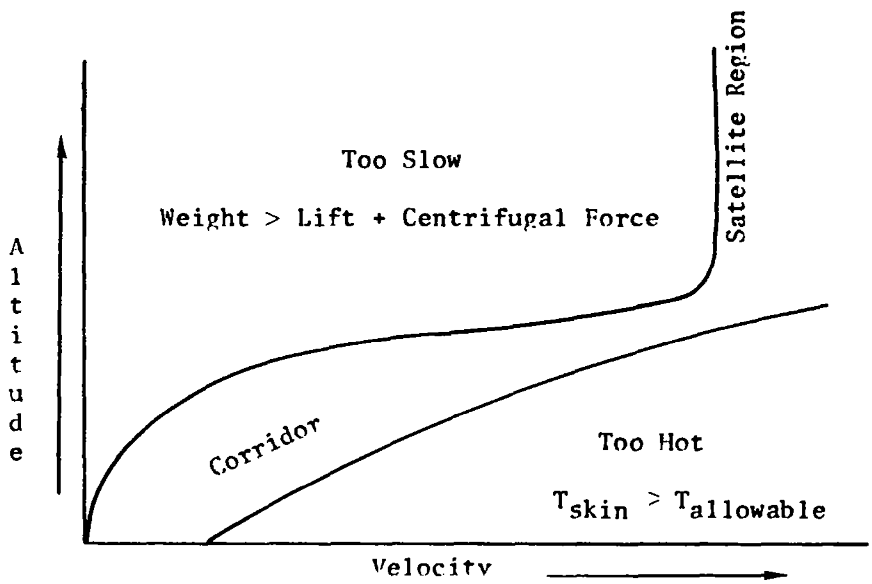

Figure 6-3

The corridor in Figure 6-3 delineates the region of the altitude-velocity plane where continuous flight is possible by virtue of the dynamic pressure being great enough to support lifting flight and yet the heating rates are enough to allow economic surface cooling.

The relationships obtained for various types of entry in previous sections may be used in conjunction with equation (6.38) to define various heating parameters. For direct entry, evaluation of equation (6.38) and equation (6.7) indicate that the maximum heating rate occurs when

$$\frac{u}{u_i} = e^{-1/6}$$

$$\frac{\rho_o}{2\alpha} \sigma \frac{C_D A_C}{m \sin \gamma} = \frac{1}{6}$$

Thus, the maximum heating rate is given by

$$\frac{q}{A_C}\bigg|_{max} = \frac{.371\ \rho_{SL}\ u_i^3\ \sqrt{\sin\gamma}}{\sqrt{\left(\frac{R\ e_{d_\infty}}{M_\infty\ d}\right)_{SL}}\ d\ \sqrt{\frac{C_D\ A_C}{m}\ \frac{\rho_o}{2\alpha}}} \tag{6.39}$$

and the heating rate as a function of time is

$$\frac{q}{q_{max}} = 4.05\ \sqrt{\frac{\rho_o}{2\alpha}\ \sigma\ \frac{C_D\ A_C}{m\ \sin\gamma}}\ \exp\left[-3\ \frac{\rho_o}{2\alpha}\ \sigma\ \frac{C_D\ A_C}{m\ \sin\gamma}\right] \tag{6.40}$$

Now, the total heat load can be obtained by integration of the heat rate over the time of heating as

$$\frac{q}{A_C} = 3\sqrt{\pi/2}\ \ u_i^3\ \frac{\sqrt{\frac{\rho_o}{2\alpha}}}{\sqrt{\left(\frac{R\ e_{d_\infty}}{M_\infty\ d}\right)_{SL}}\ d\ \sqrt{\frac{C_D\ A_C}{m}\ \sin\gamma}} \tag{6.41}$$

Similar relationships can be determine for the other types of entry discussed in previous sections.

3.0 RECOMMENDED PROCEDURES

3.1 INTRODUCTION

A broad scope of mission constraints and their relationship to trajectories was discussed in section 2.0, without regard for potential incompatibilities between individual constraints. In general, simplifying assumptions were purposely introduced such that the mission constraint and trajectory interfaces could be readily identified. A more general treatment of the individual concepts discussed in section 2.0 exists in the references, section 4.0, and probably is warranted for the generation of actual trade-off data.

The subsequent discussion of methodology for applying the results of section 2.0 to the trajectory selection process is necessarily general. However, some basic concepts in methodology, which are independent of the type of mission, will be discussed.

3.2 METHODOLOGY

The first step in defining the mission profile is to assign priorities to the mission constraints. The spatial orbit phase constraints generally affect mission objectives most directly so they generally receive the highest priority. Launch and entry constraints are not completely independent of the spatial phase, however, since launch constraints define the orbital inclinations which are achievable without plane changes and orbital altitude versus payload limitations, etc. In any event, it should be possible to order the mission constraints by priority or at least in priority groups (e.g., high priority, desirable, low priority, flexible, etc.).

The mission oriented constraints define the general nature of the orbit; i.e., they determine whether the orbit should be near earth, high altitude, synchronous, equatorial, polar, elliptical, etc. Then the launch and insertion technique should be considered to determine the degree of compatibility with the mission and with the launch trajectory constraints.

The evaluations mentioned can usually be performed with relatively minor analysis. The result is an initial guess in the mission design iteration scheme. After development of the "initial guess" mission profile, the techniques and relationships developed and presented in section 2.0 are used to converge on the final mission profile. Some obvious tradeoffs and optimizations can usually be made prior to generation of parametric data since the proposed profile can be examined to assure that the orbits are near circular where desired (assuming minimum allowable altitudes) that the inclinations are restricted to launch azimuth capabilities, that rendezvous compatible orbits are produced for rendezvous missions if possible, etc.

The next phase in the mission design is to generate mission constraint and trajectory interface parametric data. Section 2.0 presents relationships from which the data could be generated. The requirements for parametric data depend on the constraint priority since tradeoff analysis of parametric data for higher priority constraints may result in compromises which violate lower priority constraints.

Many publications [for example Reference (2)] contain extensive presentations of parametric data relating trajectory profiles to commonly used mission constraints. By utilizing such published data the generation of parametric data for any given mission can be minimized or even limited to final refinements of the mission.

The complete definition of a preliminary mission profile may require compromise of the mission constraints. Thus, after a preliminary mission profile has been defined using relationships such as thos defined in this report, refinements and final definition of the mission is performed by precision trajectory techniques. Figure 7-1 presents a flow diagram of the methodology discussed above.

MISSION DESIGN METHODOLOGY

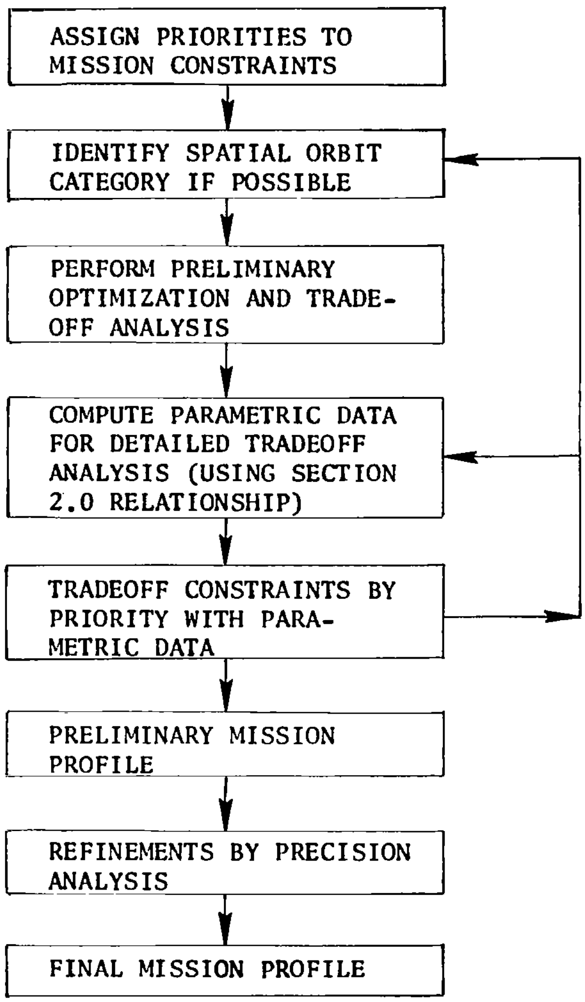

Figure 7-1

4.0 REFERENCES

1. Handbook of Astronautical Engineering, H. H. Koelle Editor, McGraw-Hill, New York, N. Y., 1961.

2. Orbital Flight Handbook, NASA SP-33, Martin Co. for George C. Marshall Space Flight Center, Parts 1, 2, and 3, NASA Office of Scientific and Technical Information, 1963.

3. Dew, J.K., "Minimum ΔV From Arbitrary Apogee to a Specific Entry Flight Path Angle and Entry Radius," NAA Internal Letter 101-012-65-069, June 29, 1965.

4. Vargo, L.G., et al., "Observation Satellite Orbits," American Rocket Society Journal, January 1962.

5. Crickmay, C.J., "Optimizing the Geographical Location of Satellite Tracking Stations," American Rocket Society Journal, January 1962.

6. Vette, James I., Models of the Trapped Radiation Environment, NASA SP-3024, NASA Scientific and Technical Information Division, 1966.

7. Napolin, A.L., "Task 4.1.7 Final Report," NAA Internal Letter 092-241-66-48, July 1966.

8. Arsenault, Jeannine, et al., Earth Satellite Ephemerides by General Perturbation, Aeronutronics Corp., Technical Report U-970, August 25, 1960.

9. Ladner, J.E. and Ragsdale, G.C., Earth Orbital Satellite Lifetime, NASA Technical Note TN D-1995, January 1964.

10. Hanson, James, N. and Fairweather, Stephan H., "Nodal Rotation for Continuous Exposure of an Earth Satellite to the Sun," American Rocket Society Journal, May 1961.

11. Strune, Otto, Elementary Astronomy, New York and Oxford Press, 1959.

12. Stern, T.E., "Effects of the Rotation of a Planetary Atmosphere on the Orbit of a Close Satellite," American Rocket Society Journal, Vol. 29, pp. 777 - 782, 1959.

13. El'Yasberg, P.E., "Dependence of Secular Variations of Orbit Elements on Air Resistance," American Rocket Society Journal, Vol. 30, pp. 672 - 675, 1960.

14. Galman, B.A., "Minimum Energy Deorbit," Journal of Spacecraft and Rockets, July 1966.

15. Holloway, P.F., "Return From Orbit to the Continental United States," Journal of Spacecraft and Rockets, December 1966.

16. Alexander, J.D., "Project Apollo - Proposed Concentric Orbit Technique for LEM Rendezvous With CSM," NASA-MSC Internal Note No. 65-FM-92, July 23, 1965.

17. Blum, Ronald, "Re-Entry Trajectories: Flat Earth Approximation," American Rocket Society Journal, April 1962.

18. Straly, W.H., "The Phasing Technique in Rendezvous," American Rocket Society, April 1962.

19. Kidd, A.T. and Soule, P.W., "Terminal Maneuvers for Satellite Ascent Rendezvous," American Rocket Society, January 1962.

20. Billik, B.H., "Satellite Lifetimes," American Rocket Society Journal, December 1962.

21. Escobal, P.R., "Orbital Entrance and Exit From the Shadow of the Earth," American Rocket Society Journal, December 1962.

22. Koskela, P., Nicola, L., and Walters, L.G., "Station Coordinates From Satellite Observations," American Rocket Society Journal, February 1962.

23. Cunningham, F.G., "Calculation of the Eclipse Factor for Elliptical Satellite Orbits," American Rocket Society Journal, September 1962.

24. Mangad, M. and Schwartz, M.D., The Calculus of Variations and Modern Applications, NAA S&ID, SID 65-1200-4, February 1966.

25. Bieber, R.E., "Relative Influence of Atmospheric Properties on Launch Vehicle Design," Journal of Spacecraft and Rockets," February 1967.

26. Bate, R.R. and Johnson, R.W., "Emperical Formulas for Ballistic Re-Entry Trajectories," American Rocket Society Journal, December 1962.

27. Same as 24.

28. McIntyre, J.E., The Pontryagin Maximum Principle, NAA S&ID, SID 65-1200-7, 13 May 1966.

29. Abbott,A.S. and McIntyre, J.E., Dynamic Programming, NAA S&ID, SID 66-1678-2, 15 November 1966.

30. Bender, D.F. and Blackford, A.L., Relative Motion - Guidance Equations for Terminal Rendezvous, NAA S&ID, SID 66-1678-4.

31. Kampos, B., General Perturbations Theory, NAA S&ID, SID 66-1678-1, 1 December 1966.